Lift & drag analysis of a 3D synthetic dragonfly wing

A thesis

submitted in fulfilment

of the requirements for the degree

of

Master of Engineering

at

The University of Canterbury

by

SRUJAN RAJ DHANDU

2016

Table of content

Acknowledgements

Foremost, I would like to express my sincere gratitude to my advisor Prof. Mark Jermy for the continuous support of my Masters research, for his patience, motivation, enthusiasm, and immense knowledge. His guidance helped me in all the time of research and writing of this thesis. I could not have imagined having a better advisor and mentor for my masters research.

My sincere thanks also goes to Duncan Shaw, for photographing the dragonfly specimen. Secondly I would like to thank Julian Murphy, Gerry Kirk, Patrick Geoghegan and David Read for contributing their valuable time in various stages of my project.

I thank my fellow lab mates Cletus Adams, Natalia Kabaliuk and Kevin Clemens for the stimulating discussions and suggestions throughout the project.

Last but not the least, I would like to thank my family and my friends for supporting me throughout my time.

Abstract

A 3D dragonfly wing is developed by using the Autodesk point cloud methodology, which takes several high definition (HD) pictures of the wing and uploads them into the software which computes all the spatial points and to give a rough matrix of the external structure. The structure is further modified by using Mesh mixer and printed in 3D of Acrylonitrile butadiene styrene (ABS) material.

Initially a bending and torsion stiffness test is carried out by cantilevering the wing onto a U shaped frame, where the increasing weights are suspended on the wing tip end to calculate the deflection upon loading at different room temperatures. Keeping the Reynolds and Strouhal numbers constant, a flapping mechanism is designed consisting of two smart servo motors connected to the wing root with a fixtures designed to give the wing four axis degrees of freedom (DOF) maintaining the centre line axis. The servos are programmed by using Arduino Nano board and the whole mechanism is fixed onto two load cells on an apparatus which is connected to a LabView® programme for collecting the data. The data from the load cells is taken and investigated in MatLab® by using Fourier analysis.

The maximum deflection of the wing tip as per the literature review is in the range of 3-12 mm depending on the loads acting on the wing during flight. For this thesis the average deflection of the wing tip during the experiment upon applied loading is to be about 3-10 mm. It varies with the forces acting on it and also expected to change for another sample of the model wing which can be produced using flexible

PVC which has different properties. These deflection values are used to determine the amount of force acting on the wing tip during the bottom end of the flap cycle. The torsional deflection of the wing during flight was assumed to be 20 degrees. Where as in the torsional stiffness experiment it is more than 10 degrees for the ABS structure. The values obtained during the experiment is lower compared to the value from the previous literature due to the rigidity of the material. It varies with the forces acting on it and also expected to change for another sample of the model wing which can be produced using flexible PVC which has different properties.

The flapping experiment is carried out for various flapping and torsional angles using a flapping test rig. The data is studied for the extraction of the forces acting on the wing and is assumed to give more information on the stable and unstable aerodynamics of the dragonfly wing. It is observed that when the phase difference is changed from 0° to 270° the lift generated value is raised from 0.4N to 0.6N. C_L-max is determined as 0.55 and is maximum when the phase difference between the flapping angle, torsion angle is maintained as 270°. It is reducing for lower phase differences of 90° and 0°. For two consecutive experiments with a 180° phase difference C_L-max is remaining constant at flapping angle of 60°,90° while frequency and torsion angle are maintained constant. The C_D is observed to be consistently low and reaching maximum of 0.125 within the experiments.
This research values can be used as a source for developing a flapping unmanned aerial vehicle (UAV).

List of abbreviations

ABS	Acrylonitrile butadiene styrene
AOA	Angle of Attack
DOS	Degrees of freedom
FDM	Fused Deposition Modelling
HD	High definition
LLDPE	Linear Low Density Polyethylene
SCA	support cleaning apparatus
UAV	unmanned aerial vehicle
vs	versus
MRI	Magnetic Resonance Imaging

List of figures

List of tables

List of graphs

1 Introduction

Man has always dreamt of flying since the beginning of time. By studying birds, we have been able to understand the mechanics of flight and apply those in the design of aircraft that are being used today.

In recent times, the development of miniature flying drones has given rise to the necessity of studying insects rather than birds as they fly at lower Reynolds number. Since then manoeuvrability is a requirement at such close quarters. Dragonflies are in particular a suitable option since they are able to manoeuvre in all dimensions with ease.

To understand the flow over the dragonfly wings, the initial step is taken to develop a 3D dragonfly wing and test it for its structural parameters and to develop a flapping mechanism which can replicate the flapping motion during a stable hovering flight.

2 Theoretical basics

2.1 Dragonfly

Dragonflies have fascinated scientists for most of this century. They have dominating flying characteristics which can help reaching speeds up to 60mph for which it took 300 million years for them to adapt. A dragonfly is also capable of cutting corners at high speeds, hover and glide which is possible by individual flapping of its two pairs of wings. The dragonfly has two pairs of wings that operate asynchronously. To do this one pair of the wings stand in a forward position with respect to the other. Two opposing muscle groups move the wings to ascend the two frontal wings and descend the back pair of wings. The muscles are tied to levers inside the body. While one group of muscles pull up a pair of wings by contracting, the other muscle group opens the other pair by relaxing.[1]

[1] Yahya 2002: 17, 20.

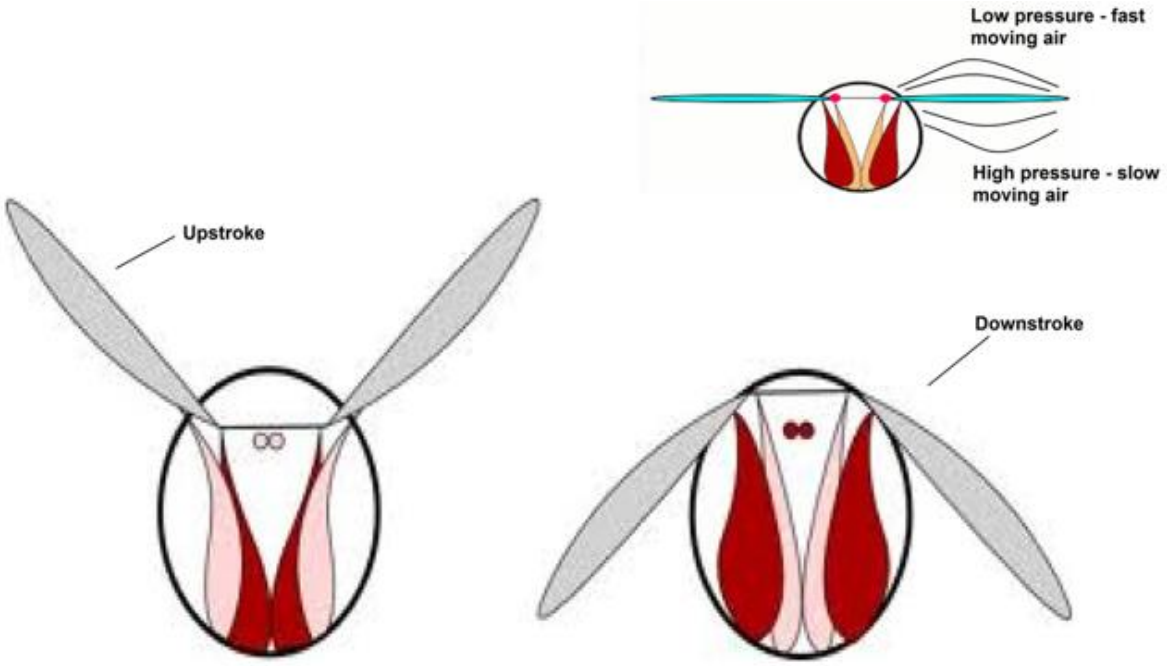

Figure 1: Dragonfly muscle movement[2]

Dragonflies are powerful and agile fliers, capable of migrating across oceans, moving in any direction, and changing direction suddenly. In flight, the adult dragonfly can propel itself in six directions: upward, downward, forward, backward, to the left and to the right. They have four different styles of flight. A number of flying modes are used, that includes counter stroking with forewings beating 180° out of phase with the hind wings which is used for hovering and slow flight.[3] Figure 2 shows a dragonfly (*Uropetela*) specimen which is used as a source for the 3D model wing construction.

[2] http://theflightofbirdsandinsects.weebly.com/uploads/3/0/6/6/30665567/7329723_orig.png.
[3] Silsby, Jill. Dragonflies of the World. Csiro publishing, 2001.27-32.

Figure 2: Dragonfly specimen[4]

[4] Authors own resource.

2.2 Structure of a dragonfly wing

Dragonfly wings are not smooth or simple cambered surfaces. They have a corrugated cross section camber. This corrugated design is an important factor in the ultra-light construction of the wing structure.[5] A dragonfly wing structure is made up of two components mainly, veins and membrane. The skeletal structure is made up of veins and there is a thin film layer on top and bottom known as membrane. The membrane is made up of Chitin, which is a material that is soft on inside and hard on outside. Chitin is also found in different insects and spiders, which is not elastic and helps in the growth of the body of the insects and flies.[6] The chitin in its natural form is translucent and can be from varying thicknesses which helped in the construction of the extremely thin dragon fly wing whereas the veins are made up of cuticles, which consists of nerves and trachea surrounded by upper and lower cuticles. They harden during the growth of a dragonfly. The compartment between the wing veins is called a cell. The area of each cell is generally about 1sq-mm. The biggest among the cells is the *Pterostigma* which is located at the leading edge of the fore wing. It is darker in colour and stands out from all other cells. Due to its mass contribution, the *Pterostigma* tends to raise the flying speed by causing favourable, inertial, pitching moments during the acceleration phases of wing flapping. It is predicted that in one species of dragonflies (*Odonata*) this cell helps in 10-25% of increase in critical gliding speeds and also acts like a counter weight for wing

[5] Kesel, Antonia B. "Aerodynamic characteristics of dragonfly wing sections compared with technical aerofoils." *Journal of Experimental Biology* 203.20 (2000): 3125-3135.
[6] Kreuz, P., W. Arnold, and A. B. Kesel. "Acoustic microscopic analysis of the biological structure of insect wing membranes with emphasis on their waxy surface." *Annals of biomedical engineering* 29.12 (2001): 1054-1058.

flapping.[7] The current 3D model wing does not contain "*Pterostigma*", which is not highlighted and its properties are not considered, due to much less information being available to prove that the *Pterostigma* in specimen *Uropetala* gives an increase in critical gliding speeds. Figure 3 shows a microscopic structure of a dragonfly wing which consists of corrugated cell pattern. The microscopic spikes on the structure are studied by previous researchers and found that it reduces the drag coefficient to the negligible value because the generation of the vortex on the wing are suppressed by the spike projections. Due to the negligible value, it is not considered in this wing development.

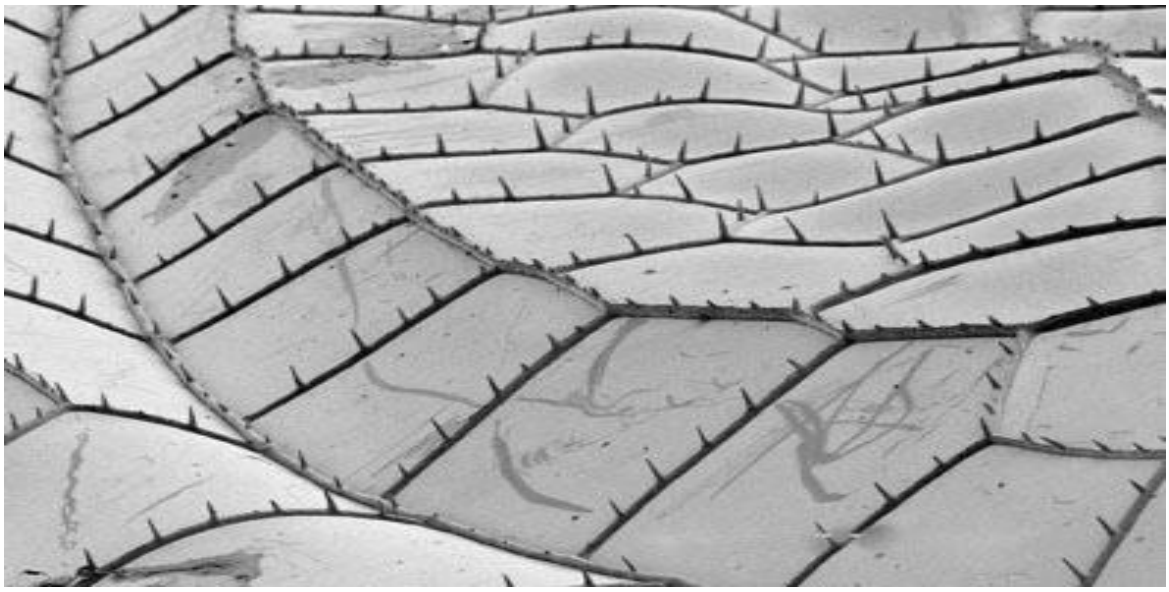

Figure 3: Microscopic structure of a dragonfly wing[8]

[7]Kreuz, P., W. Arnold, and A. B. Kesel. "Acoustic microscopic analysis of the biological structure of insect wing membranes with emphasis on their waxy surface." *Annals of biomedical engineering* 29.12 (2001): 1054-1058.
[8] http://scienceblogs.com/bioephemera/wp-content/blogs.dir/263/files/2012/04/i-182a4868c656367ae4778c96019c1424-Paulson1.jpg.

Figure 4 shows a half dragonfly with a body and its two right wings. The *Pterostigma* of the right fore-wing is highlighted in the figure.

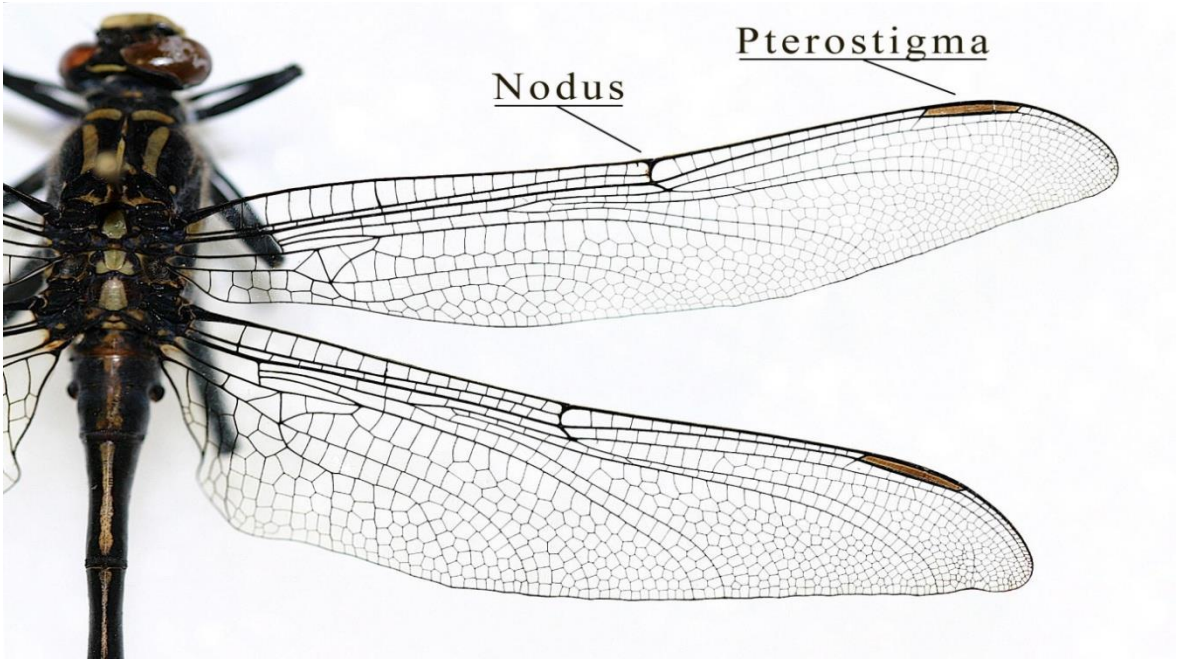

Figure 4: *Pterostigma* in a dragonfly wing[9]

The membrane of a dragonfly wing is like a thin film which connects two veins of the structure. A dragonfly wing consists of two layers of membrane, one on top and the other on the bottom. Structural veins are sandwiched between these membrane layers. The membrane layers help in strengthening the skeletal structure.

[9] http://bioweb.uwlax.edu/bio203/s2007/cocchiol_matt/Anisoptera.htm.

2.3 Material properties of a Dragonfly wing

Nano-indentation tests of the wing membranes were carried out by F. Song in 2007 using a continuous stiffness method and Young's modulus value of the membrane is determined from the experiment as 1.5 GPA. The stiffness is calculated as 3.5 GPA for the model wing. The average gross thickness of wing membrane is 2.8 +/- 0.3 μm. In table 1 it is shown how the material properties for a dragonfly wing are determined by F. Song in 2007:[10]

Properties	Value
Young's modulus of wing membrane	1.5 GPA
Mass of the wing	3.4mg
Area	1sq-mm
Poisons Ratio	0.4
Average Gross thickness of wing membrane	2.8+/-0.3µm
Hardness	0.14 GPA
Average vein stiffness	6 GPA
Membrane stiffness	3.75 GPA

Table 1: Material properties of a dragonfly wing[11]

2.4 Literature review and current research objectives

Since years many people have studied dragonflies and proposed different theories for its structure, aerodynamics and parameters. For example, a high speed cinematography for a range of dragonflies was first described by Magnan in 1934, who took films of tethered dragonflies at 3200 frames/sec and measured their stroke amplitude and wing beat frequencies.[12]

[10] Song, F., et al. "Microstructure and Nano mechanical properties of the wing membrane of dragonfly." Materials Science and Engineering: A 457.1 (2007): 254-260.
[11] Song, F., et al. "Microstructure and Nano mechanical properties of the wing membrane of dragonfly." Materials Science and Engineering: A 457.1 (2007): 254-260.
[12] Magnan, A. (1934). La Locomotion chez les Animaux. I. Le Vol des Insectes. Paris: Hermann et Cie.

The free hovering flight of *Aeshnajuncea* was filmed in the field by Norberg in 1975.[13] He described how this dragonfly hovered with a horizontal body and a steeply inclined stroke plane. Figure 5 shows a dragonfly hovering stroke plane A schematic diagram of the coordinate system for a dragonfly wing, where α is the torsional angle and β is the flapping angle.

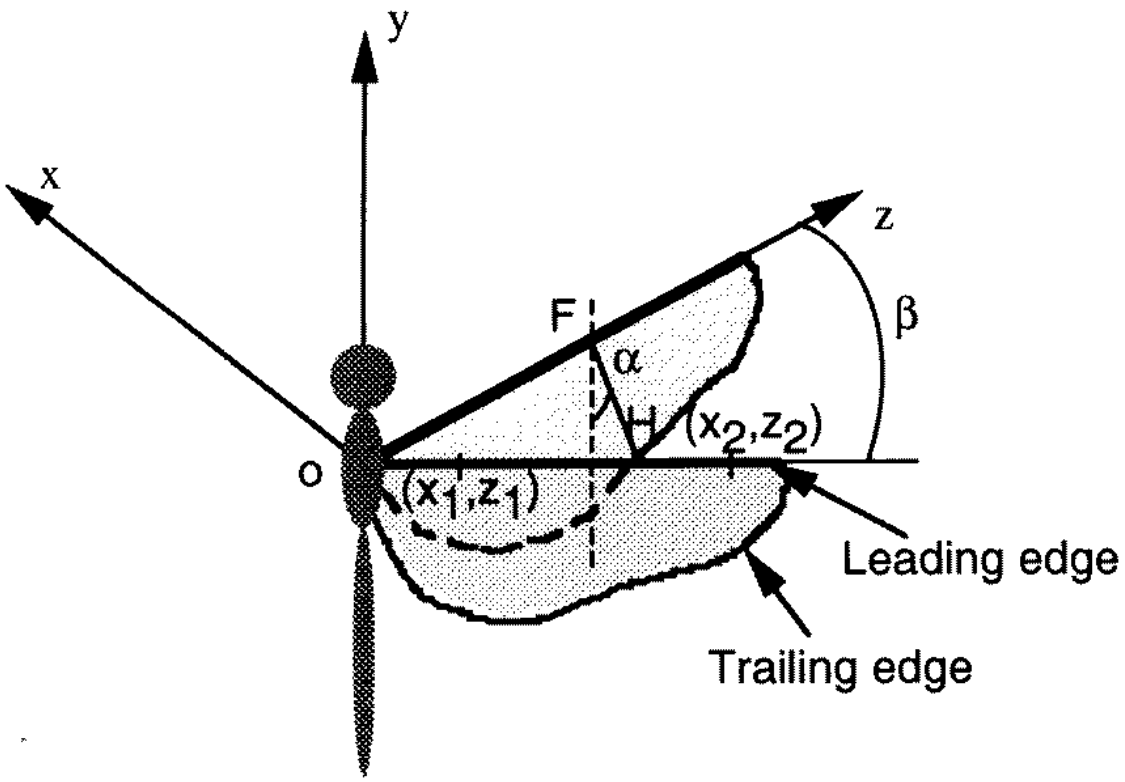

Figure 5: Dragonfly flapping and torsional angle[14]

[13] Norberg, R. Åke. "Hovering flight of the dragonfly Aeschnajuncea L., kinematics and aerodynamics." *Swimming and flying in nature*. Springer US, 1975. 763-781.

[14] Zeng, Lijiang, Hirokazu Matsumoto, and Keiji Kawachi. "A fringe shadow method for measuring flapping angle and torsional angle of a dragonfly wing." *Measurement Science and Technology* 7.5 (1996): 776.

This orientation required even greater lift, because weight Z support is only possible on the down stroke. This is in contrast to insects hovering with a 'normal' horizontal stroke plane, where lift on both the morphological up- and down strokes can be used for weight support.[15]

Dragonflies typically fly with their wings beating out of phase, or counter stroking. It has been suggested that beating their wings in phase, or parallel stroking, may produce higher aerodynamic forces and so may be used for high-lift situations such as rapid accelerations or tandem flying with a mate.[16]

Based on the basic flying characteristics of a dragonfly the company Techjet.com has developed a miniature four winged *Ornithopter* drone UAV for aerial photography, interactive gaming, autonomous patrolling for security and surveillance.

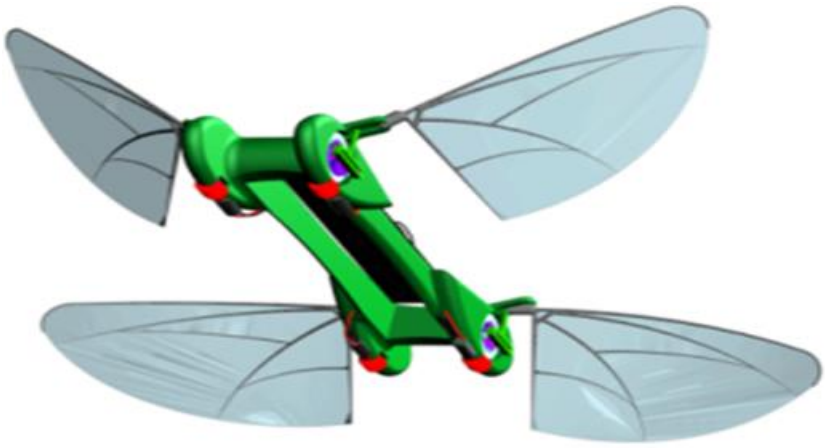

Figure 6: Techjet Robotic dragonfly[17]

[15] Wakeling, J. M., and C. P. Ellington. "Dragonfly flight. II. Velocities, accelerations and kinematics of flapping flight." *Journal of experimental biology* 200.3 (1997): 557-582.
[16] Rüppell, G. "Kinematic analysis of symmetrical flight manoeuvres of Odonata." *Journal of Experimental Biology* 144.1 (1989): 13-42.
[17] https://techject.com/wp-content/uploads/2013/11/Picture11.png.

Next to the model of Techjet.com the company Delfly developed another model called Delfly micro and macro. These are flapping micro aerial vehicles that resemble a light robotic fly which are developed by the inspiration from the flapping flight of flies.

Figure 7: Delfly micro and macro[18]

In this project we focus on 3D structural function of dragonfly wings, as their venation pattern has remained similar during the evolution. *Protodonata* are the ancestors of the present dragonflies. Approximately 325-350 million years old fossils of very large dragonfly ancestors of the *Protodonata* are found in Upper Carboniferous rocks; these had wingspans up to about 750mm (30 in). Their wings are similar enough to modern dragonflies, suggesting the comparable flight capabilities.[19] Figure 8 shows

[18] http://www.delfly.nl/images/delfly12.jpg.
[19] Carpenter, Frank M. "Early insect life." *Psyche* 54.2 (1947): 65-85.

an ancient 350 million years old fossil of *Protodonata* which had a wingspan of 750mm.

Figure 8: Protodonata fossil[20]

[20] https://upload.wikimedia.org/wikipedia/commons/2/26/Meganeura_fossil_1.JPG

Till now no individual 3D wing of contemporary dragonfly wing has been designed or developed to understand the forces generated and acting upon it. With an objective to understand the force generation of a scaled up flapping wing during hovering the following objectives were listed out in the beginning:

- Design and development of a scaled up 3D dragon fly wing
- Designing of test rigs for the flapping
- Calculating various structural and aerodynamic parameters
- High speed video analysis for the torsion and bending of the wing during flapping
- Gaining the knowledge of the dynamics from the kinematics of dragonflies

Underpinning these objectives is desire to understand the aerodynamic characteristics of a contemporary dragonfly wing and to contribute the research knowledge for the further development of the dragonfly based Macro UAV and drones. This thesis describes how the research objectives are achieved.

2.5 Bending and torsional stiffness

The corrugated structure of the dragonfly wing spars possesses great resistance to bending, but are compliant in torsion. Twisting of the leading or trailing edge results in torsion and relative movement of the remaining spars. As result camber will automatically change and sets in the wing as it twists. In flight the aerodynamic forces produced during the wing strokes will result in bending and twisting changing the camber that will help improve the aerodynamic efficiency. This chapter explains how

the bending and torsional stiffness values are determined for the dragonfly 3D model wing.

Bending stiffness

The bending stiffness 'K_b' is the resistance of a member against bending deformation. It is a function of elastic modulus 'E', the area moment of inertia 'I' of the beam cross-section about the axis of interest, length of the beam and beam boundary condition. Bending stiffness of a structure can analytically be derived from the equation of structure deflection when it is applied by a force.

$$K_b = \frac{P}{W}$$

In the above equation 'P' stands for applied force and 'W' (W=δ) for deflection.[21] Figure 9 shows the deflection of a cantilever beam when a load is applied on it.

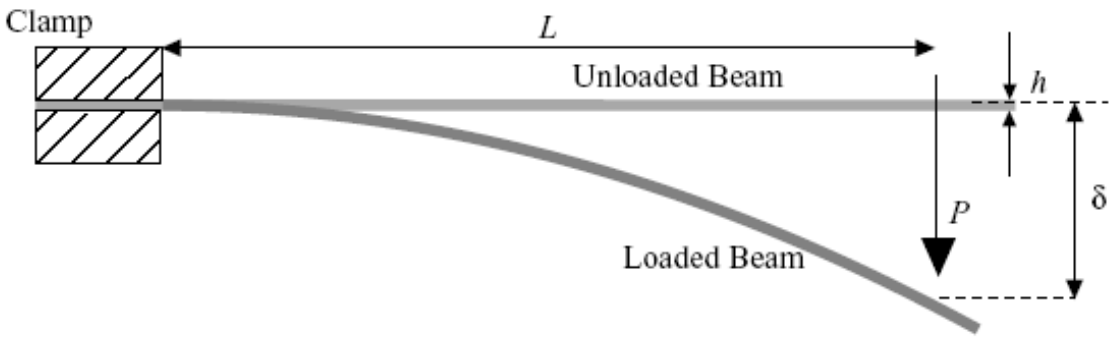

Figure 9: Bending of a cantilever beam[22]

[21] http://www.wisegeek.com/what-is-beam-stiffness.htm.
[22] http://www.doitpoms.ac.uk/tlplib/thermal-expansion/images/cantilever.gif.

Torsional stiffness

Torsional stiffness 'K_t' is the measure of the amount of torque that a structure can sustain during its rotation in a mechanical system. The torsional stiffness of a structure can analytically be derived from the below equation.

$$K_t = \frac{P}{\theta}$$

In the above equation 'P' stands for applied force and 'Ɵ' for angular deflection.[23] In figure 10 the angular deflection of a cantilever beam is shown when a load P is applied on it.

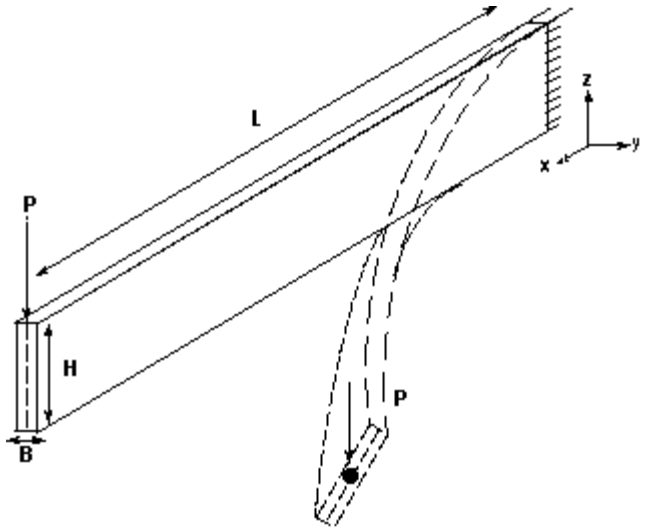

Figure 10: Torsion of a cantilever beam[24]

[23] http://www.doitpoms.ac.uk/tlplib/beam_bending/twisting.php.
[24] http://www.ansys.stuba.sk/html/guide_55../graphics/GADV26.gif.

The bending and torsional stiffness experiments are to be carried out on the 3D printed model wing structure to determine the values of deflection upon loading and compare it with the values in the literature.

2.6 3D printing

3D printing or additive manufacturing is a process of making three dimensional solid objects from a digital file. The creation of a 3D printed object is achieved using additive processes. In an additive process an object is created by laying down successive layers of material until the entire object is created. Each of these layers can be seen as a thinly sliced horizontal cross-section of the eventual object.[25]

A commonly used technology in this process is Fused Deposition Modelling (FDM) The FDM technology works using a plastic filament or metal wire which is unwound from a coil and supplying material to an extrusion nozzle which can turn the flow on and off. The nozzle is heated to melt the material and can be moved in both horizontal and vertical directions by a numerically controlled mechanism, directly controlled by a computer-aided manufacturing software package. The model or object is produced by extruding melted material to form layers as the material hardens immediately after extrusion from the nozzle. This technology is most widely used with two plastic filament material types: Acrylonitrile Butadiene Styrene and Polylactic acid but many other materials are available ranging in properties from conductive, flexible etc. The software that comes with this technology automatically generates

[25] http://web.stratasys.com/APJ-ANZ-PPC-2015_PPC_ANZ_3DABC_WP_LP_v2.html?cid=70113000002F3w6&utm_ad=3D+Printer&utm_source=google&utm_term=3d%20printer&utm_campaign=AU+-+Search+-+3D&utm_medium=cpc&utm_content=sUUQbwN8X_dc|pcrid|90915388441|pkw|3d%20printer|pmt|p|.

support structures if required. The machine dispenses two materials, one for the model and one for a disposable support structure.[26]

The below figure shows the layering of the molten material through the heated extrusion nozzle. The printing filament from the spool is passed through the heating chamber in the extrusion head which moves in different directions over the printing bed. The molten filament is dropped down in several layers vertically over the printing platform. These successive layers printed onto the platform form a complete shape of the desired 3D model.

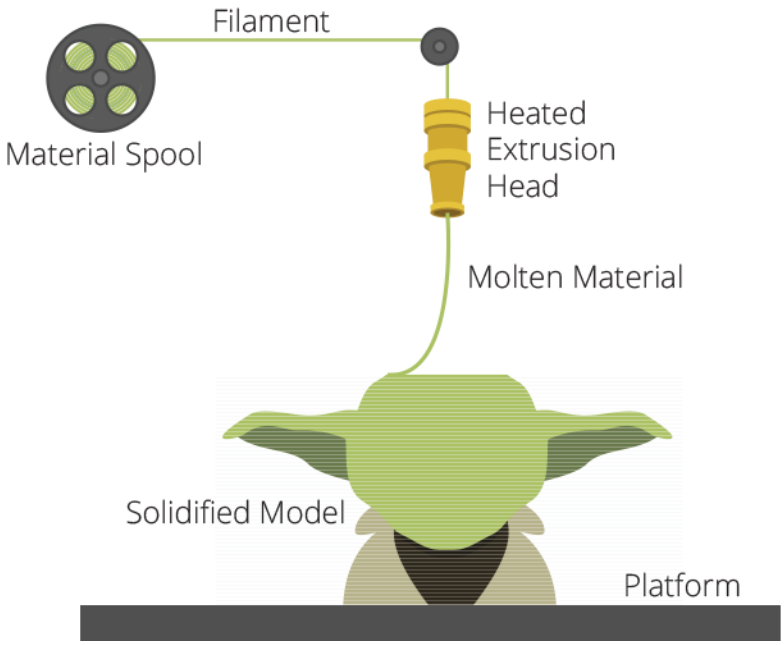

Figure 11: Layering of the melted material from the extrusion nozzle[27]

[26] http://web.stratasys.com/APJ-ANZ-PPC-2015_PPC_ANZ_3DABC_WP_LP_v2.html?cid=70113000002F3w6&utm_ad=3D+Printer&utm_source=google&utm_term=3d%20printer&utm_campaign=AU+-+Search+-+3D&utm_medium=cpc&utm_content=sUUQbwN8X_dc|pcrid|90915388441|pkw|3d%20printer|pmt|p|.
[27] http://3dprintingindustry.com/3d-printing-basics-free-beginners-guide/processes.

2.7 Vacuum forming

Vacuum forming is defined as a simplified form of thermoforming, where a sheet of plastic is heated to a forming temperature, stretched onto a mould surface and forced against the mould by suction of air from vacuum. This method is very efficient on the thermoplastics and transparent materials.[28] Figure 12 shows the sequence drawing of the vacuum forming process which consists of simple six step process.

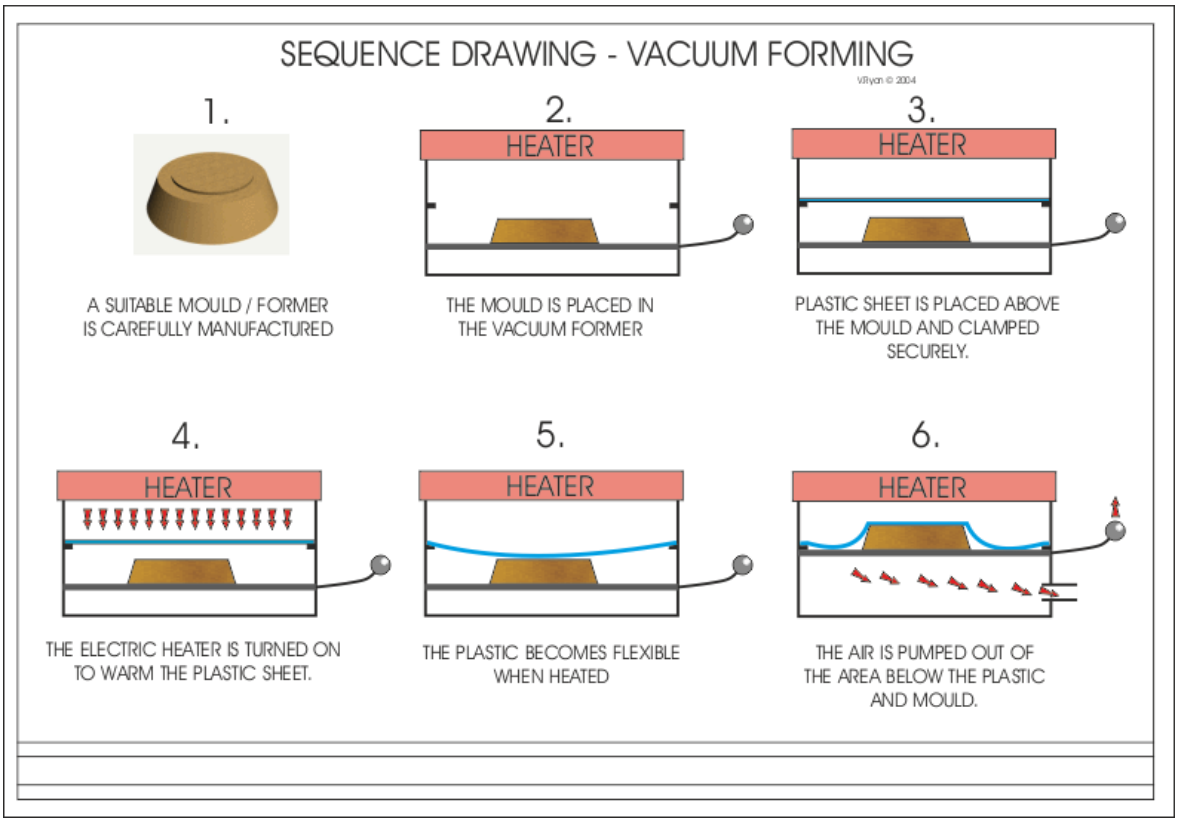

Figure 12: Vacuum forming process[29]

[28] http://www.technologystudent.com/equip1/vacform1.htm.
[29] http://www.technologystudent.com/equip1/vacform1.htm.

2.8 Photogrammetry

Photogrammetry is the science of making measurements from photographs, especially for recovering the exact positions of surface points. Moreover, it may be used to recover the motion pathways of designated reference points located on any moving object, on its components and in the immediately adjacent environment. Photogrammetry feeds the measurements from remote sensing and the results of imagery analysis into computational models in an attempt to successively estimate, with increasing accuracy, the actual, 3-D relative motions within the researched field.[30]

Photogrammetric methods

Photogrammetry uses many disciplines, which including optics and projective geometry. The data model in figure 13 shows the type of information that can go into and come out of photogrammetric methods. 3-D coordinates define the locations of object points in the 3D space. The image co-ordinates define the locations of the object points' images on the film or an electronic imaging device.[31]The exterior orientation of a camera sets its location in space and its view direction whereas the inner orientation specifies the geometric parameters of the imaging process. This is primarily the focal length of the lens, but can also include the description of lens distortions. Further additional observations play an important role: With scale bars,

[30]http://www.mat.uc.pt/~gil/downloads/IntroPhoto.pdf
[31]http://www.mat.uc.pt/~gil/downloads/IntroPhoto.pdf

basically a known distance of two points in space, or known fix points, the connection to the basic measuring units is created.[32]

Figure 13 shows the Georg Wiora's data model of photogrammetry. It explains the four main variables of photogrammetric method according to Georg's data model each of the four main variables can be an input or an output of a photogrammetric method.

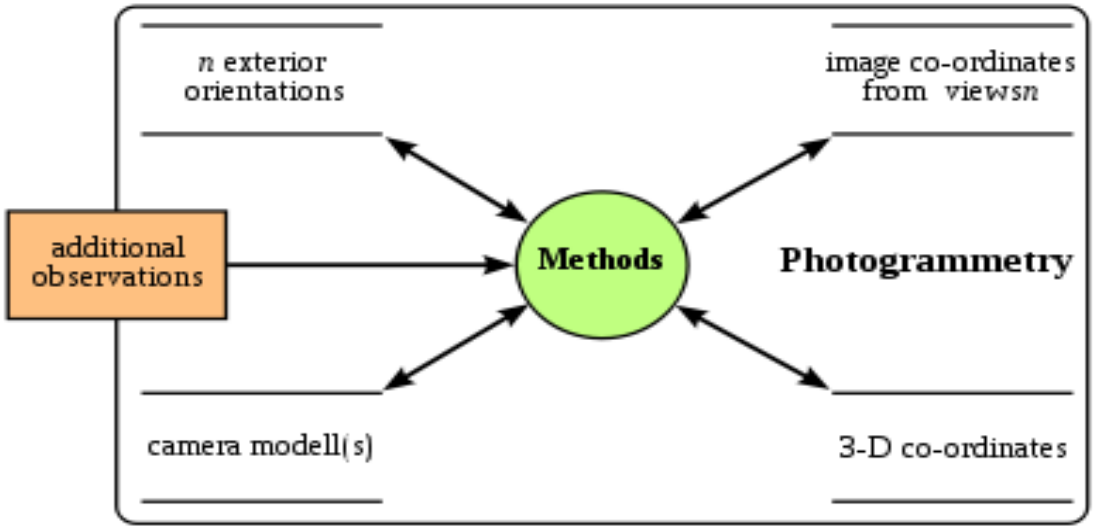

Figure 13: Photogrammetry methods[33]

[32] http://www.mat.uc.pt/~gil/downloads/IntroPhoto.pdf.
[33] http://www.geometh.ethz.ch/uav_g/proceedings/hudzietz_presentation.

3 Empirical analysis

3.1 Design and development of a 3D Dragonfly forewing

The major objective of this project is to design and develop a 3D dragonfly wing with all its corrugations and details. Several methods were predicted to design a 3D dragon fly wing. Among them the photogrammetric software Autodesk 123D Catch is used. This chapter explains the design, development and manufacturing process of the 3D wing.

3.1.1 Photographing of a dragonfly specimen

An *Uropetela* dragonfly which was caught in 1982 near the Waimak river by the senior post-grad students of the Forestry department of University of Canterbury and was preserved using the curing technique where the fly is left in acetone filled airtight box for 3-10 days and then dried for 2-3 days. The preserved specimen is taken and placed on a single thin stem of radius 2mm. The stem is placed on a white background with two masking flash lights for HD photography. 43 HD photographs of 4,368 × 2,912 (12.8 megapixels) resolution from various angles covering a total 360° in loop sequential using small increments are taken using Canon 5D camera. Care is taken that for every single shot the background remains the same with the specimen undisturbed. The distance of the specimen from the camera lens is also maintained precisely to preserve the distance between the points in every image. This prevents the overlapping of the image points and triangles when all the images are collated together in the cloud.

3.1.2 Image processing of a dragonfly wing

The initial step for the image processing is to arrange the photos in a sequential order. When the images are arranged in order they are uploaded into a software called Autodesk 123D catch profile load page. The HD images loaded on the profile are automatically uploaded on the Autodesk cloud server where each and every photo is stitched together by selecting various points from every single image. After the stitching all the images in a sequential order the cloud server returns the rough 3D graphic image onto the profile. Figure 14 shows the Autodesk graphical view of the arrangements of various HD images stitched together and in a sequential 360° loop to form a 3D stitched image after processing it in the cloud server.

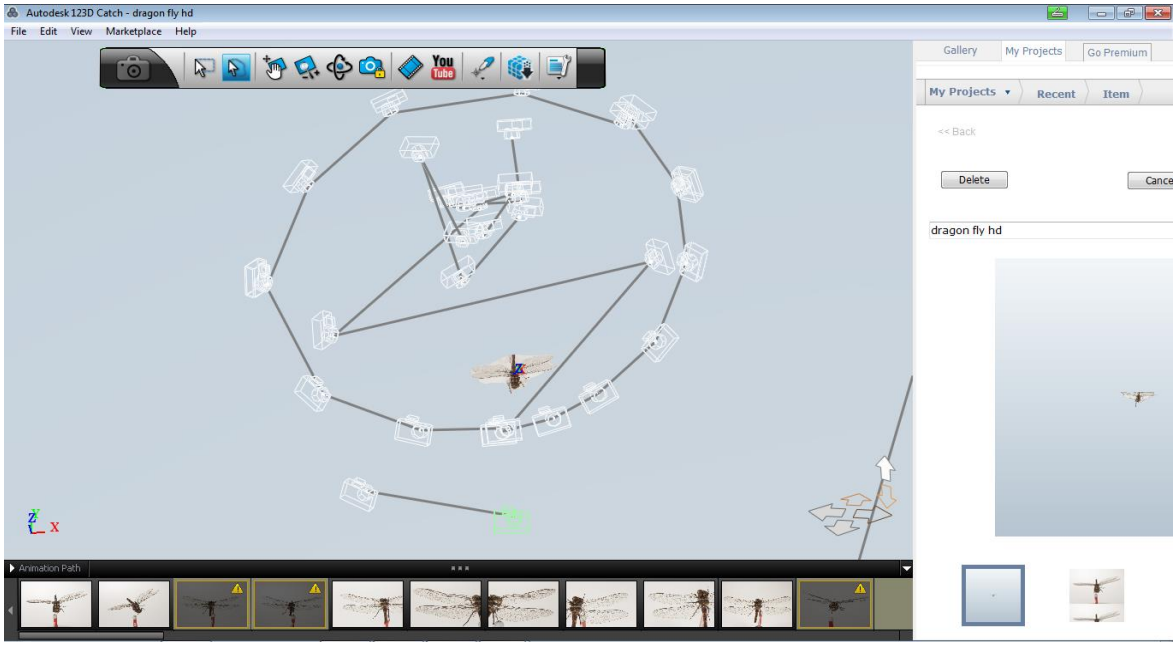

Figure 14: Graphical view of photographing a dragonfly specimen in 360° in Autodesk[34]

[34] Authors own resource.

By using the acquired 3D graphic model, now it is possible to transfer it into the graphic modifying tool known as Mesh Mixer®-2.9.3[35]for further modification. Mesh Mixer is a design software which supports a wide variety of 3D-design tasks. Many 3D tools were modified so as to make it user friendly. It uses an unstructured high resolution triangle mesh algorithm rather than using compact data structures with many degrees of freedom. Due to its capability of geometrical processing with many degrees of freedom, it is used to slice and modify the graphical model to analyse the cross section.

3.1.3 Wing structure modification

For the wing structure modification, a software called Mesh mixer® is used. The 3D stitched graphical structure is loaded into the software where it first takes a complete solid with an outline of the shape.

Figure 15 shows the stitched outline 3D shape. The various colours on the surface of the 3D graphic model represent the sections over the surface in three different planes. It can also be described by the various colours, each one representing one of the slices into which the whole model can be cut into for analysis.

[35] http://www.meshmixer.com/.

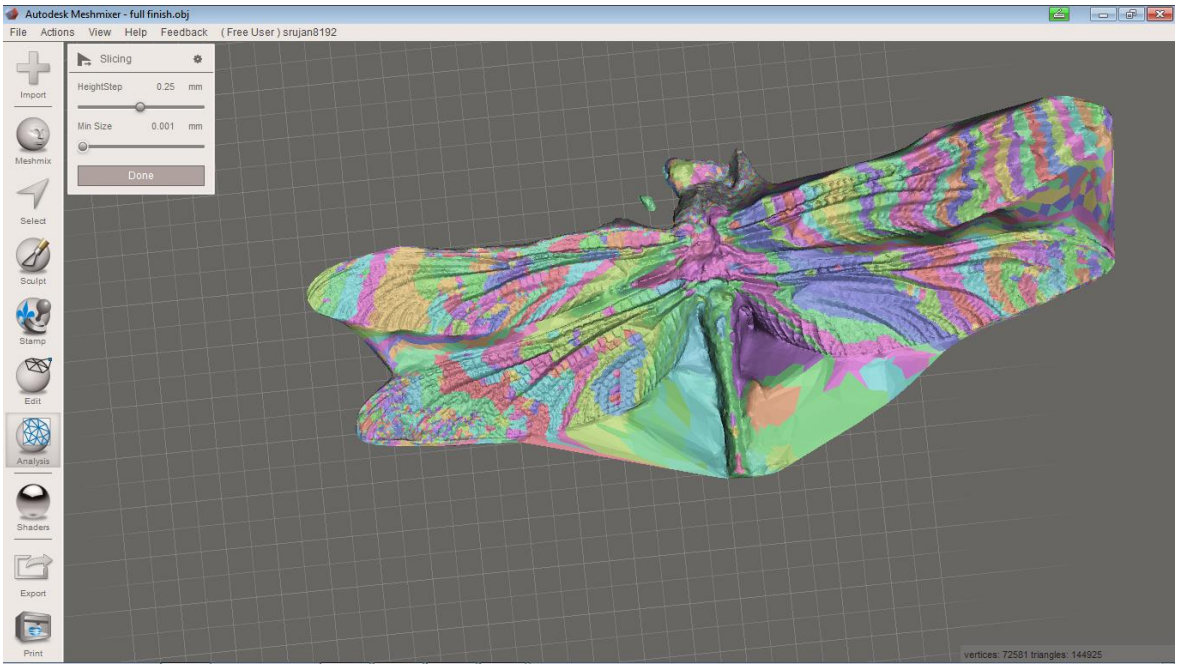

Figure 15: Initial solid outline shape of the 3D stitch[36]

3.1.4 Forewing separation from the stitched structure

As per the objective of the project mentioned earlier the forewing of the 3D graphical structure is separated using the slicing method. In the slicing method the complete structure is examined for its strength. This strength analysis helps in maintaining the strength of the wing structure during the surface modification where every single cell on the wing surface is modified according to its parameters. It also prevents the defects in the internal structure of the wing during manufacturing either by casting or 3D printing.

[36] Authors own resource.

Figure 16 shows the overall strength of the 3D graphical structure that gives an idea of which sections are fragile after 3D printing. The different colours point out where the 3D model has its strengths or weaknesses. All parts showing green are the strong parts of the model and do not need further editing. According to this the yellow parts demonstrate the medium strong and the red parts the weak positions of the model. In figure 16 the weaker parts are the head and the tail depicted in red colour coding but the wings which are of the interest for this thesis at this point is still depicted in green colour giving the access to take it to the next step. The red coloured areas can also be strengthened by modifying their triangular mesh. This analysis assumes the object as a solid model. Any hollow spaces that exist within the structure are not considered by the software during the analysis. It clearly shows that except the head and tail areas the rest of the structure, including the wings, is strong and can be processed for further slicing.

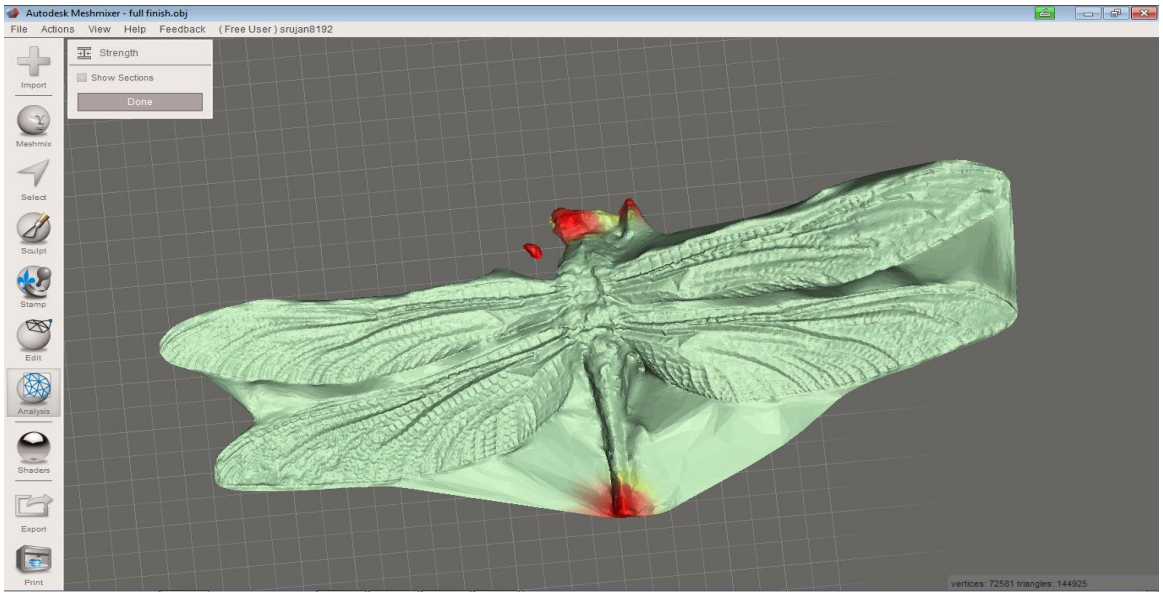

Figure 16: Strength analysis of the 3D model[37]

[37] Authors own resource.

Colour coding for the Strength analysis:

GREEN	**---**	**STRONG**
YELLOW	**---**	**MEDIUM**
RED	**---**	**WEAK**

After the strength analysis of the whole dragonfly, the 3D left forewing is sliced from the structure. During this slicing care is taken that cells from root to tip within the wing are not disturbed. Even though the whole structure consists of triangles, all the edges and corrugations are well preserved without any damage during slicing. The initial step after slicing is to reanalyse the whole wing for its slicing planes as it gives a chance for further slicing if necessary.

Figure 17 shows the separated wing that has been sliced from the complete structure of the dragonfly. The various colours on the wing in figure 17 depict as to which the number of slices the wing can be further sliced into if necessary without weakening the remaining area. The contours shown in the figure are based upon the horizontal plane passed through the wing instead they appear to be non-linear due to the corrugated cross section of the wing.

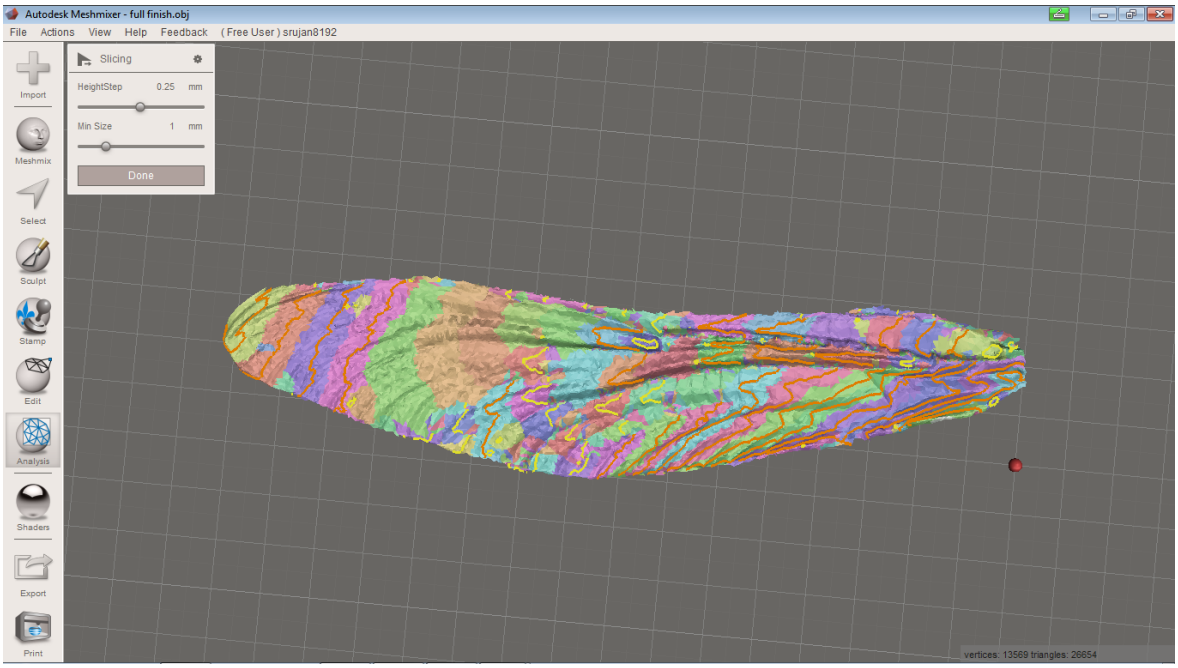

Figure 17: Individual plane analysis of the wing structure for slicing[38]

After separating the left forewing of the body the structure of the forewing needs to be analysed in detail for its strength. As before the software points out strengths and weaknesses by using different colouring again. As shown in figure 18 it is only one part of the wing coloured in red and yellow. This part needs further attention and modification. The whole graphical structure is made up of triangular mesh. In the modification process each and every cell boundary is selected and the triangular mesh between the boundaries is smoothened and cropped as per the dimensions if the cells of the real wing. At the weaker areas the triangular mesh between the boundaries of the cell is not smoothened before cropping so as to give a support to the boundaries of the cell. The cells near the weaker areas are not cropped according to the dimensions to maintain the strength of the structure.

[38] Authors own resource.

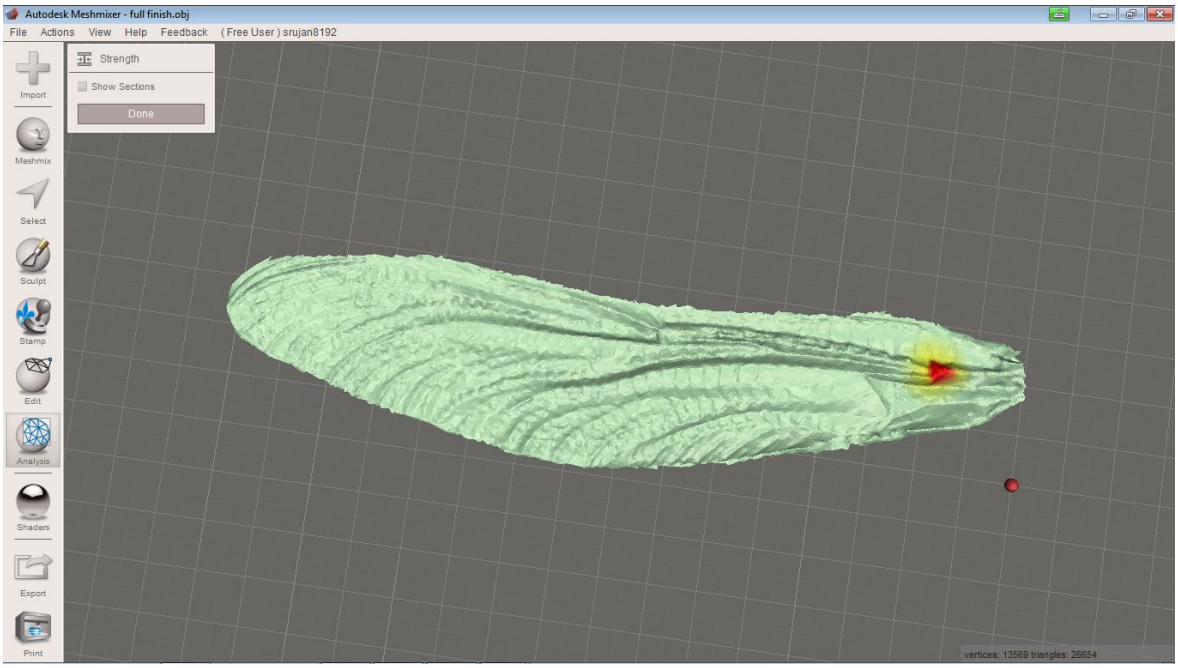

Figure 18: Strength analysis of the wing structure[39]

In the next stage the general structure can be elaborated. Figure 19 shows how the leading edge row of cells is being crafted accordingly. To make sure the model is still strong enough to withstand additional modifications a strength analysis is carried out again. Now the weak part of the wing changed to the upper middle part and the root of the wing. These parts need to be examined after the next stage.

[39] Authors own resource.

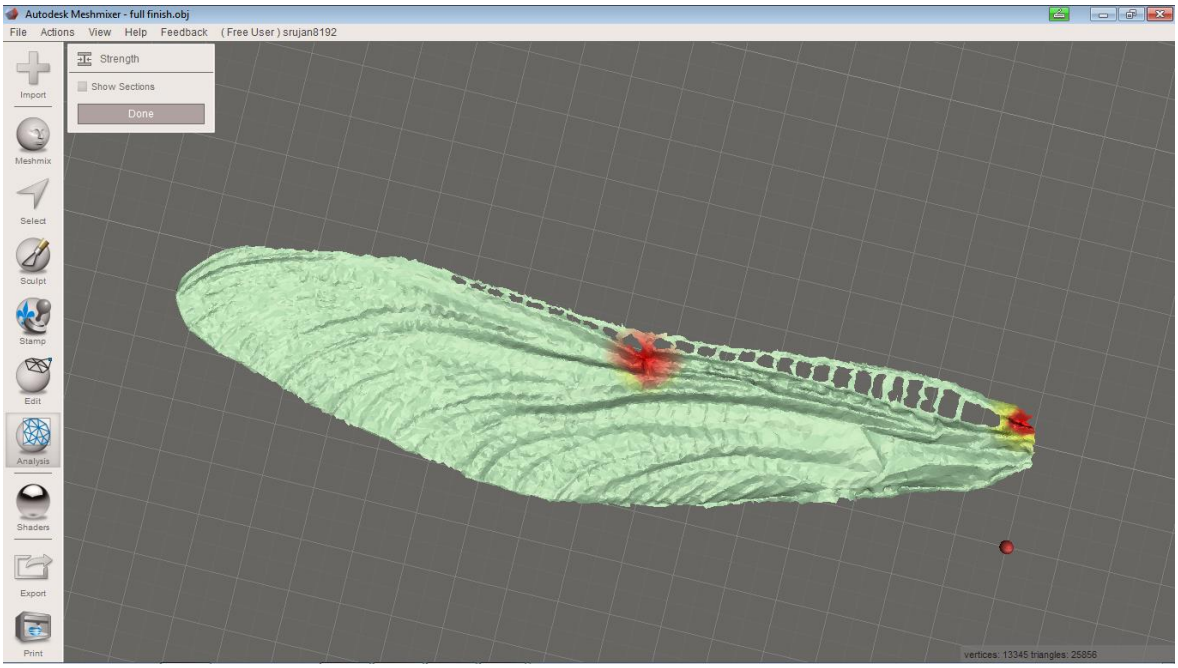

Figure 19: Stage 1 strength analysis of the structure during surface modification[40]

By adding a triangular meshing near the cells, that are concerning the weaker area, figure 20 points out that the weaker area in the upper middle of the forewing could be changed into a strong part. The weaker area of the root depicted in red-yellow is still untouched as it is considered as the strong base for wing structure. It will be modified as per the requirement after all the other cells within the structure are modified.

[40] Authors own resource.

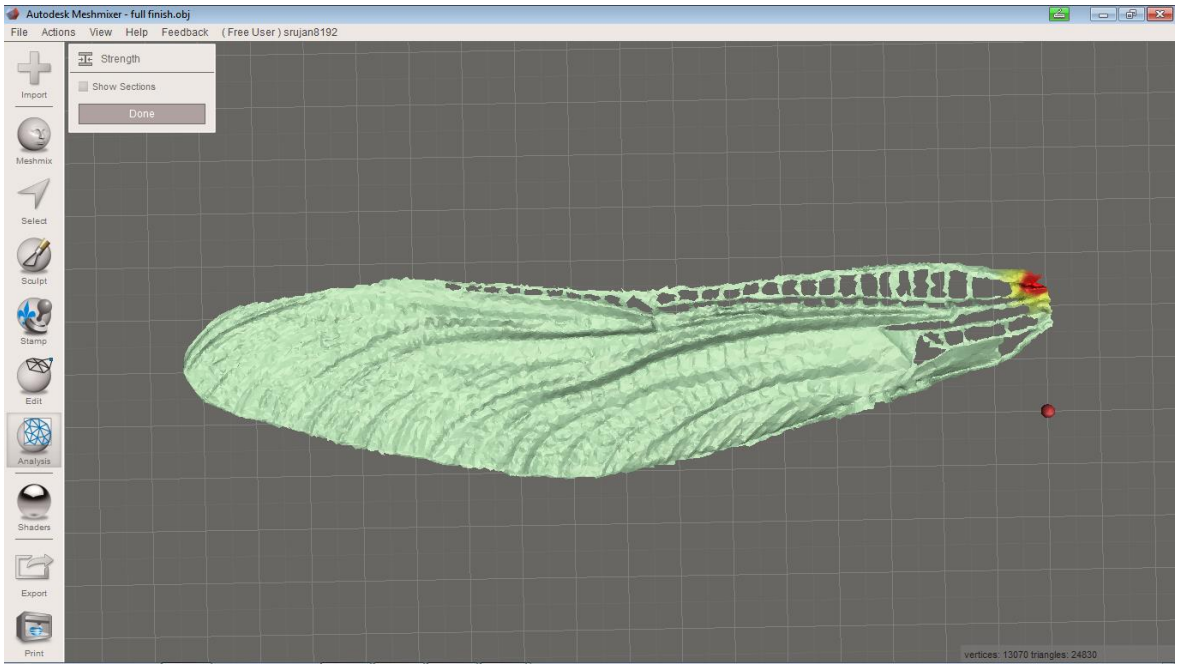

Figure 20: Stage 2 strength analysis of the structure during surface modification[41]

The modification process is continued for the next three stages and the following strength analysis results are shown in the following figures.

[41]Authors own resource.

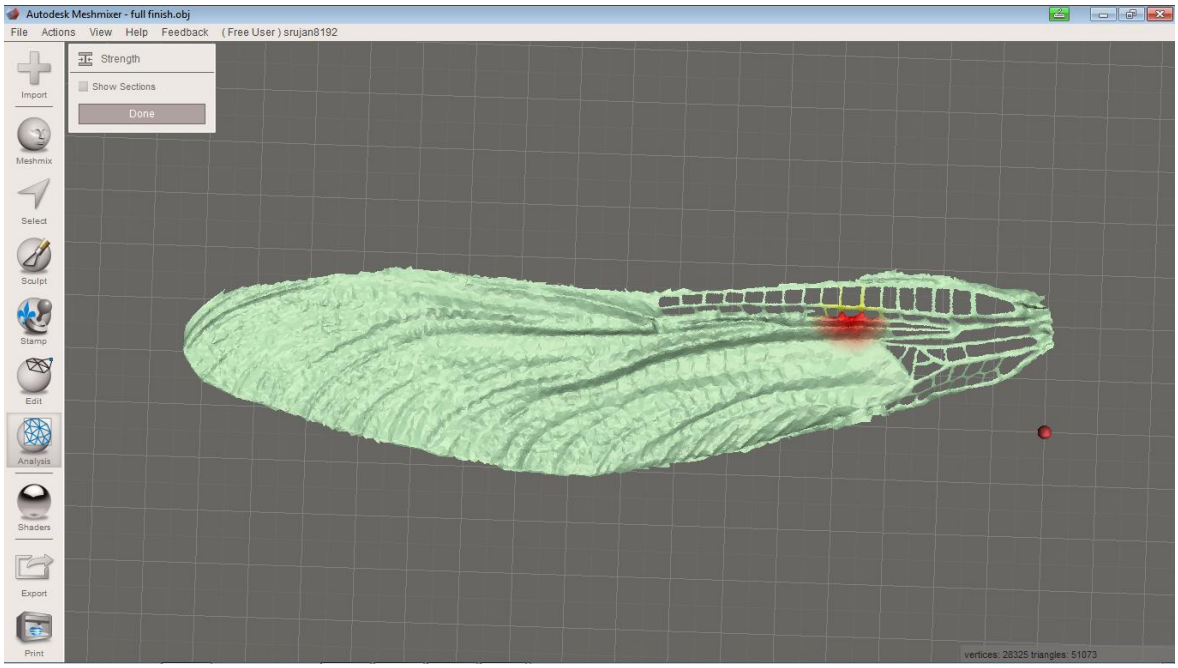

Figure 21: Stage 3 strength analysis of the structure during surface modification[42]

Figure 22 points out the strength analysis of the structure at stage 4. During the crafting procedure the strength analysis figures depict that the weaker areas tend to change for every stage. At this point the individual cells of the structure are crafted in a pattern of root to tip so as to leaving extra triangular meshes around the weaker structure to strengthen them.

[42] Authors own resource.

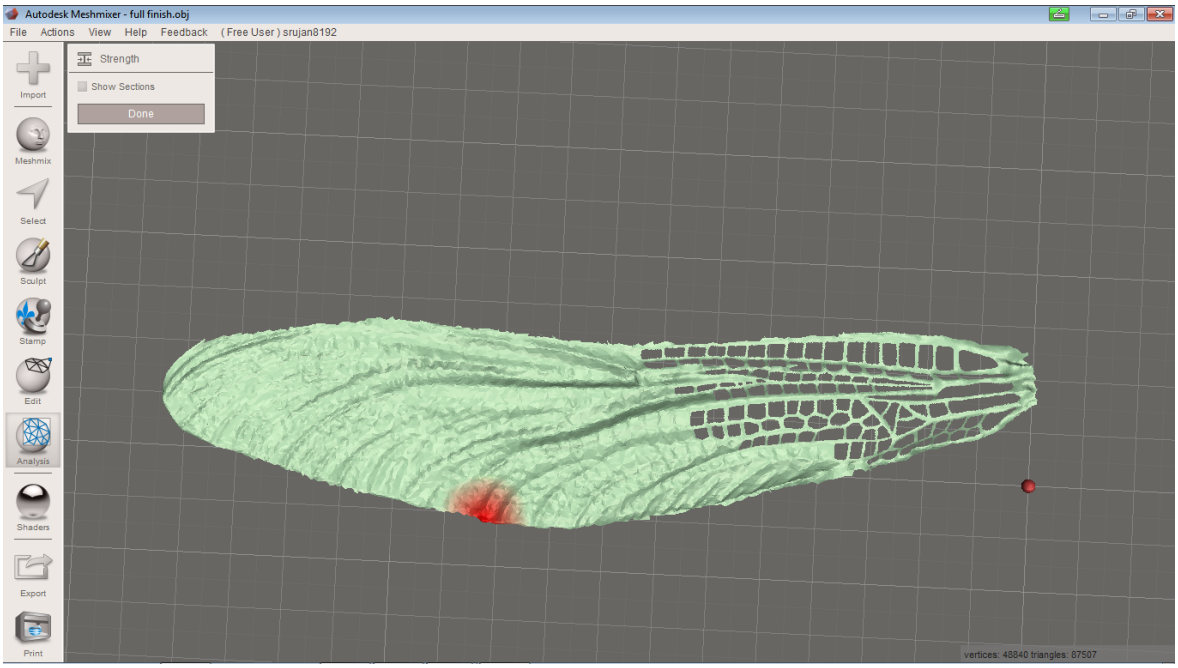

Figure 22: Stage 4 strength analysis of the structure during surface modification[43]

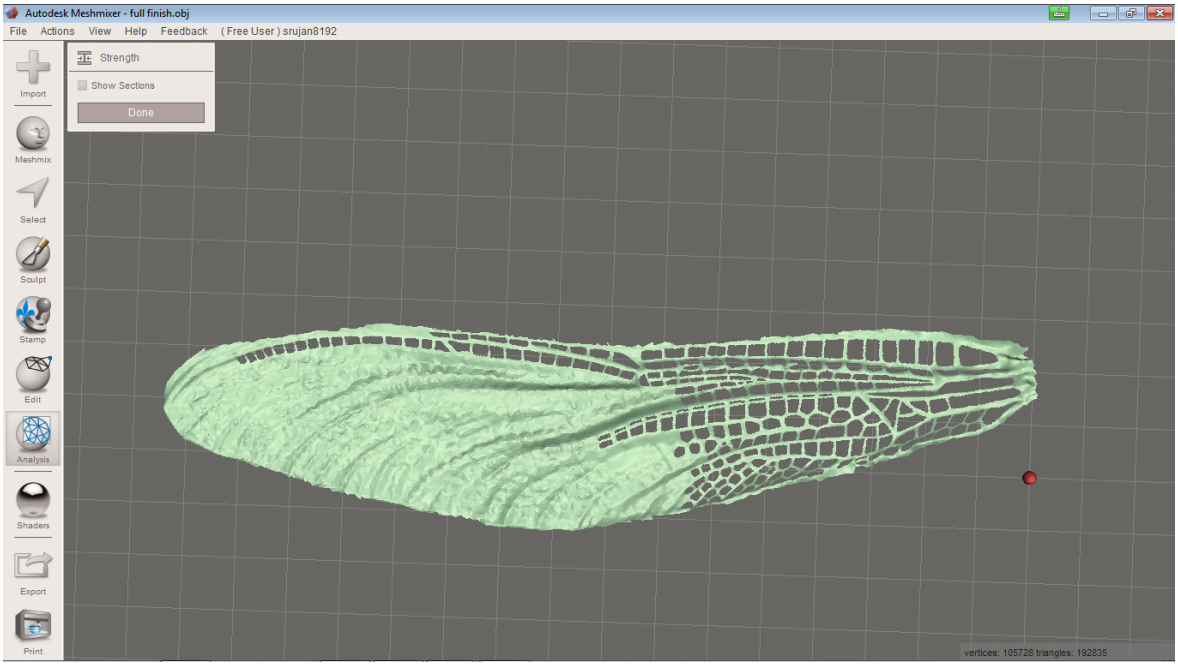

Figure 23: Stage 5 strength analysis of the structure during surface modification[44]

[43] Authors own resource.
[44] Authors own resource.

After eliminating all flaws of the wing, the structure has its final structure as shown in Figure 24. The structure now is completely green without any red or yellow colourization, which means that the final structure is strong enough to process it to the next stage of development which is to convert the 3D graphic model into 3D solid model.

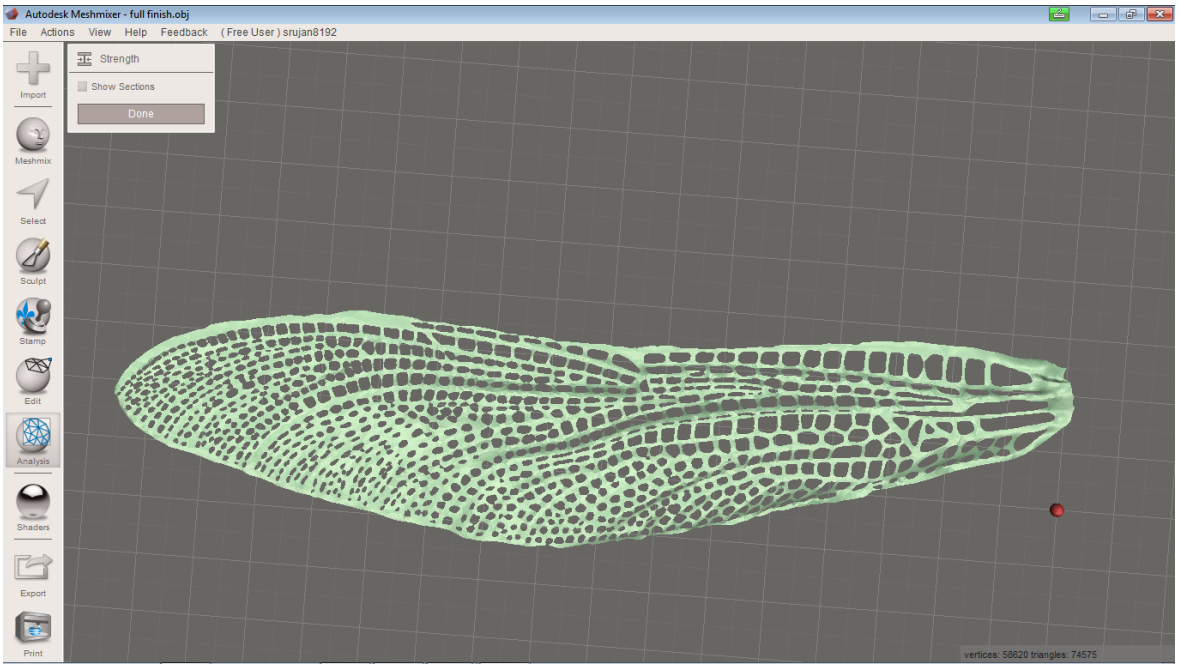

Figure 24: Final stage strength analysis of the structure during surface modification[45]

[45] Authors own resource.

3.2 Construction of a 3D model wing

3.2.1 Scaling of the wing

Due to the limitations of the Mesh mixer design tool which is not capable to convert a graphic 3D model to a solid 3D model it is necessary to transfer the .stl file from Mesh mixer into Solid works. As per the objective of the project the next step is to upscale the wing which means to increase the span of the wing by 4.48 times of the original size. The used scaling ratio of the wing of 1:4.48 is calculated by taking into consideration the limitations of manufacturing or producing the wing.

Physical dimensions of the wing

Wing Type	Length (span) in mm	Width (chord) in mm
Real Wing	66	12
Model Wing	296	53.7

Table 2: Physical dimensions of the wing[46]

Scaling Ratio

	Span	Chord
Scaling Ratio	296 : 66	53.7 : 12
	4.48 : 1	4.48 : 1

Table 3: Scaling Ratio[47]

[46] Authors own resource.
[47] Authors own resource.

The method opted for producing the wing is a 3D printing using the Stratasys 3D HDM printer which has an orienting bed of height of 350mm.

Figure 25 shows the changes that have been made in the dimensions of the span wise length from 66mm to 296mm. The width of the chord is also changed from 12.0mm to 53.7mm. After scaling the 3D wing model to the desired ratio, it is re-tested for its strength. The re-test shows that the model is now full green coloured and strong enough to proceed for further steps.

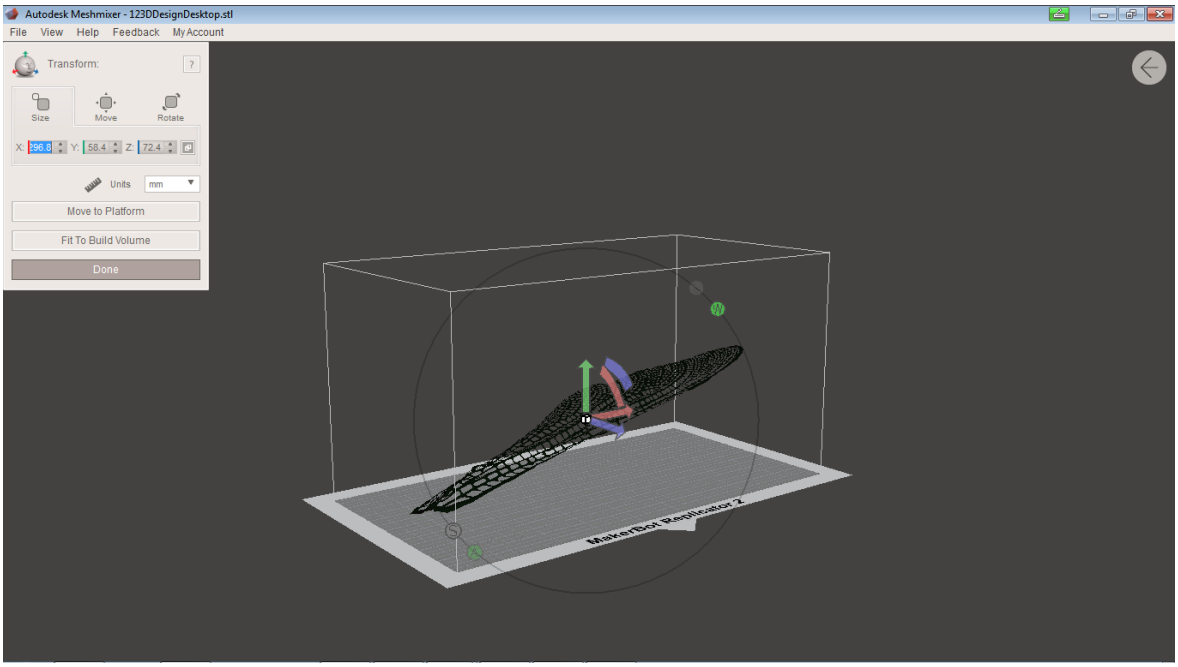

Figure 25: Scaling of 3D wing in Mesh mixer[48]

[48] Authors own resource.

3.2.2 Support design for the wing structure

The wing model cannot be directly printed in the 3D printer, as it has no base to start the printing layers and due to the vertical projection of the structure it needs the support framing to hold in onto the base as well as for the printing support material, which is later removed after printing.

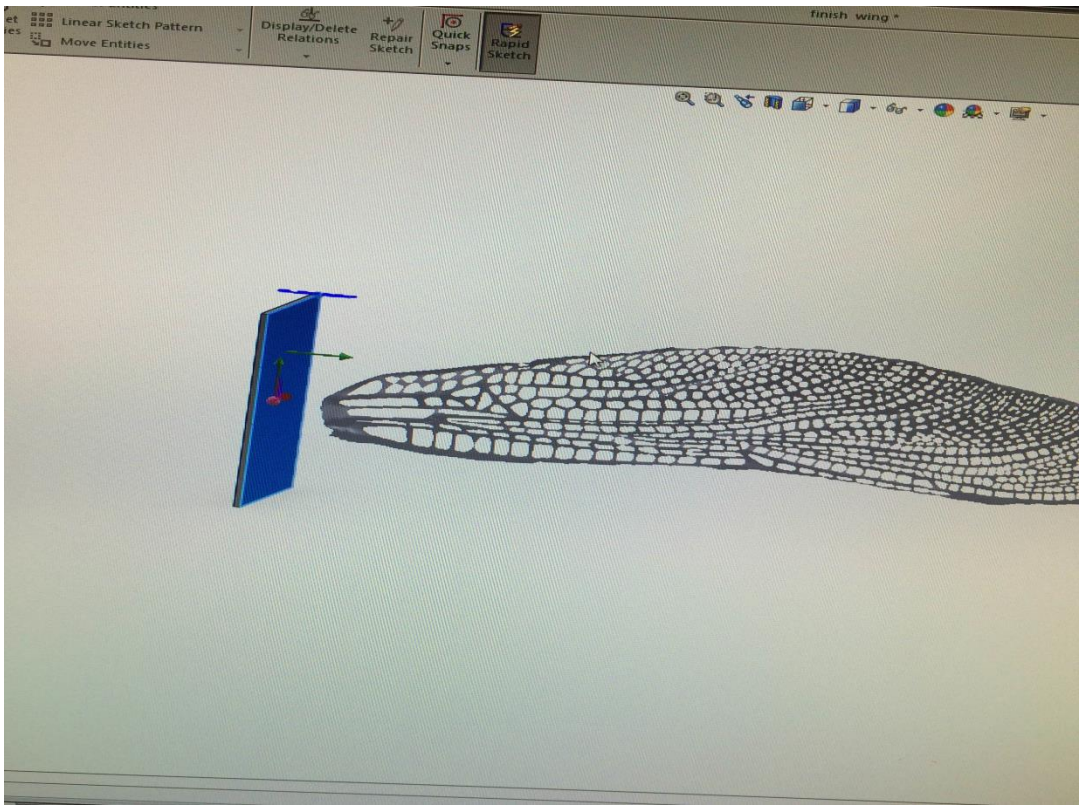

Figure 26: Attaching a base to the 3D wing[49]

[49] Authors own resource.

The initial step is to attach a rectangular base which fits onto the base of the printer. A horizontal base is designed with a width of 80mm and a length of 100mm and it is extruded outwards for 10mm. During the extrusion of the base, two layers are made and the top layer is attached to the root of the wing as shown in the below figure:

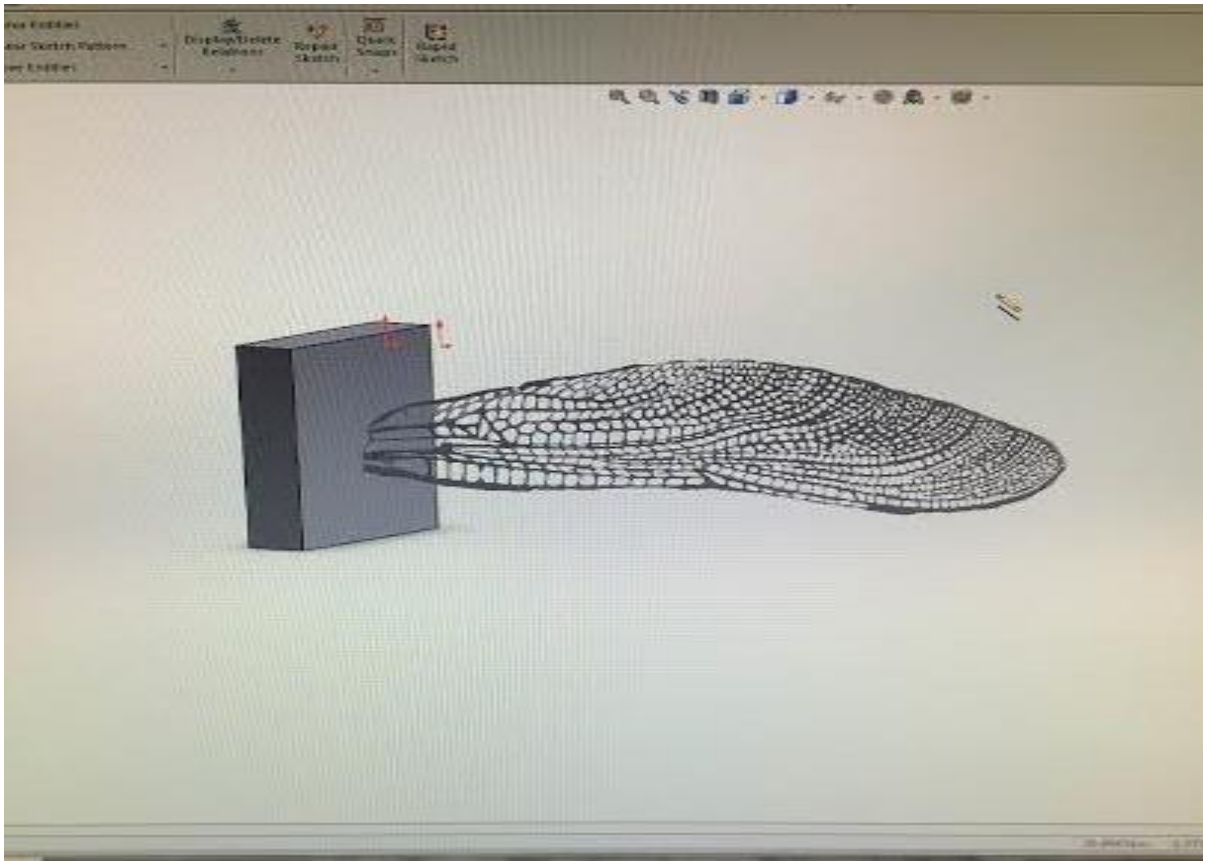

Figure 27: Image showing the square base attached to the wing root[50]

[50] Authors own resource.

Three support beams of square cross section in a triangular pattern are extruded from the base and attached to the wing structure in 3 different points. The cross section of the end attachment point at the wing is designed as rectangular for detaching it easily during the after process of the printing.

In figure 28 it is shown how the finished support frame for the 3D wing structure looks like. These three supports are attached to the 3D model wing rigidly in an alignment so that the extrusion head nozzle stays linear without any misalignments' while printing, which may result in excess costs for printing another sample model.

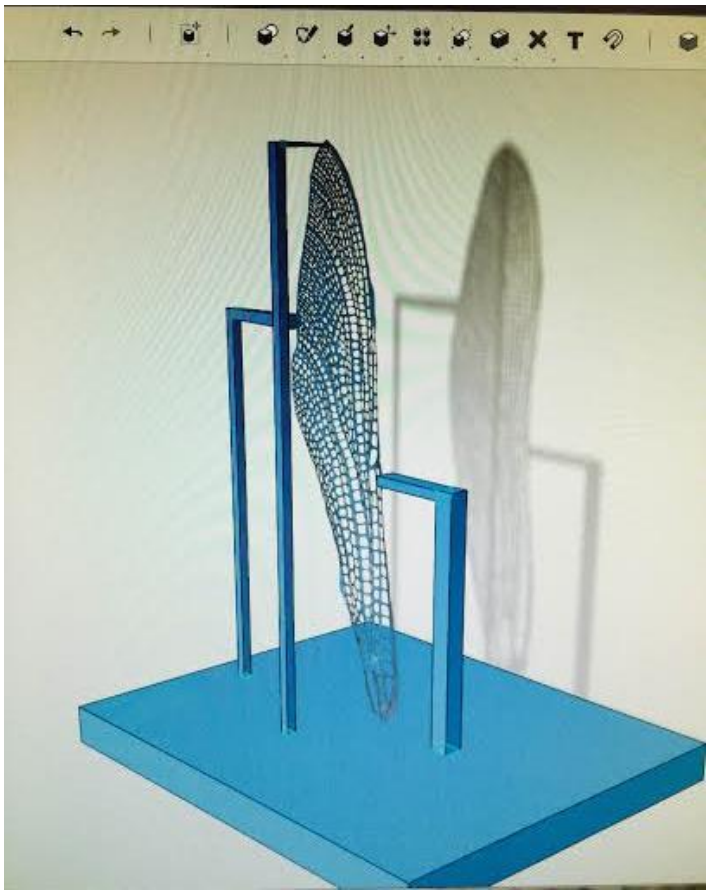

Figure 28: Image showing the supports attached to the 3D wing[51]

[51] Authors own resource.

3.2.3 3D printing of a dragonfly wing

The 3D wing is printed by the Stratasys® 3D printer that utilises FDM technology. The material chosen for printing is Acrylonitrile Butadiene Styrene as it is economical and easy to handle in the after process. As the printing is a very complicated process it took 28 hours to be done. The objective of this initial 3D printing is to investigate the faults in the initial printed model. Figure 29shows the first 3D printed dragonfly forewing which is still attached to the support beams. The printing support material is removed by dissolving it in alkaline inside support cleaning apparatus (SCA). Support beams are detached using a hot wire technique, in which the beam layers are carefully sliced using the thin heated copper wire. As the fumes emitted from the hot wire method of slicing are dangerous to inhale, face masks, gloves and protective gear are used while handling the 3D wing. In the below figure 29 at the 70% of the span length of the model wing the surface has an imperfection crated during the 3D printing. This is caused due to the printer head misalignment which has gone out of registration and needed a replacement. The imperfection is around 1mm deep and as it is a misalignment of a single layer, this is easily fixed by manual modification in which the misaligned layer is heated and is pressed back into place using forceps. This modification had no effect on the structure of the wing.

Figure 29: Final 3D printed wing[52]

3.2.4 Membrane Construction

The membrane of a dragonfly wing is like an ultrathin film which connects two veins of the structure. A dragonfly wing consists of two layers of membrane, one on top and the other on the bottom. Structural veins are sandwiched between this membrane layers. The membrane layers help in strengthening the skeletal structure. From the previous chapter, the Young's modulus of the membrane is calculated as 1.5 GPA and stiffness is 3.5 GPA for the model wing. The average gross thickness

[52] Authors own resource.

of the wing membrane is 2.8 +/- 0.3 μm. This chapter explains how a membrane is attached onto the skeletal 3D model wing.

Based upon the values of the material properties of the membrane for a real wing, the closest match is a Linear Low Density Polyethylene (LLDPE). The Membrane for the skeletal structure is fixed onto it using the vacuum forming method. A forming bench is made up of a hollow wooden frame of dimensions 450mm×450mm×450mm. A flat wooden sheet of 5mm thickness is fixed inside the frame at a height of 50mm from the bottom. Several 3mm diameter holes are drilled all over the sheet for the suction air to pass through. Near the bottom of the frame at right angles to the wooden sheet a 30mm diameter hole is drilled for fixing the suction pipe.

As the material used of forming is very thin and of lower density, a low voltage heating element is attached at the top of the forming bench. This low voltage heating element helps in heating up the material to a forming temperature without melting and it also helps in preventing the deformation of the wing structure due to high temperatures. During the process of vacuum forming, at first the model wing surface is made completely dry to prevent any moisture interaction between the membrane and the surface. A high voltage suction pump is mounted to the bottom of the forming bench to suck air from the forming chamber, creating a vacuum.

The model wing is placed at the centre of the forming chamber. There on a 0.3mm thick sheet of LLDPE is heated to a forming temperature by the heating element and

slowly lowered onto one side of the wing with a suction. This suction creates a vacuum and due to the temperature of the membrane material, it sticks onto one side of the wing. An additional heat is applied to remove any air pockets created. The excess material remaining is trimmed out with extra care. Same procedure is followed for the bottom layer membrane fixing. After attaching the top and bottom layers of the membrane, the whole setup is not disturbed for two hours for complete curing. The final product obtained is a 3D dragonfly wing structure with a membrane. Extra care is taken while handling the model wing as the temperature of the membrane is hot after forming. Figure 30 shows the 3D wing structure with the membrane attached onto it. The membrane can be seen as the glossy film over the skeletal structure.

Figure 30: 3D wing structure with membrane[53]

3.2.5 Servo flapping mechanism

Dragonflies flap their wings independently of each other. There is always a phase difference between the fore and hind wing flapping. To calculate the aerodynamic

[53] Authors own resource.

forces generated during flapping, a flapping mechanism is designed and developed taking into consideration sinusoidal flapping motion and flapping amplitude of 100°. Dragonflies also twist their wings during the flapping to direct the vortices and the airflow from one wing to another to improve efficiency. Though the flapping pattern differs from one mode of flight to another, the direction of the net force still acts in a direction and can be resolved into horizontal and vertical components. Due to the limitations of time and costs a single fore wing is chosen for the experimental purpose. Hence the single forewing is considered for calculating the horizontal and vertical forces.

The objective is to design and develop a flapping mechanism that can be used to test the 3D model wing for its aerodynamic properties like lift thrust and drag. This chapter explains how it is achieved.

Design of linkages

The linkages for the flapping mechanism are designed based upon the flapping amplitude. It consists of two main linkages, the leading link and a rare link. The leading link is a U channel shaped which has a slot that holds the root of the 3D model wing. The other end of the link is connected to a smart servo Herculex motor. This link with the servo helps in changing the angle of attack by rotating the wing in clock and anti-clockwise directions. The rear link consists of an L shaped structure which holds the smart servo motor from the second end of the leading linkage. The other end of the L shaped sub link is connected to a second smart servo Herculex motor. All the

linkages connecting and holding the servo motors are designed in a way that the centreline axis from the centre of the servo motor gear till the wing tip is inline.

The following figure shows the linkages that are designed for the flapping mechanism.

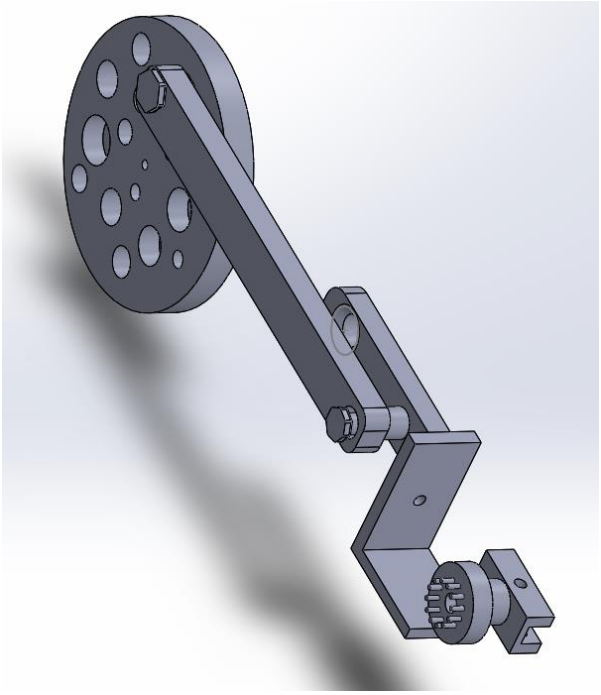

Figure 31: Flapping linkages[54]

Test rig

The test rig stand consists of a V shaped base made of aluminium. To one end of the V base a vertical aluminium square cross section bar is fixed. A horizontal bar which has a similar cross section like the vertical bar, is fixed to the top end of the vertical bar making the setup as an inverted L shape on a V base. Two 1N load cells

[54] Authors own resource.

are fixed onto the end of the horizontal bar. The load cells are attached end to end in a way that the bottom cell detects the vertical loads and the top cell detects the horizontal loads. The rear link from the linkage mechanism is fixed onto the end of the top load cell. Rear end of the leading link is fixed to the rear link completing a whole link chain. As the whole linkage mechanism is connected to the load cells, any change in loads upon the wing is directly transmitted to the load cells. The two Herculex smart servo motors are connected to Arduino Mini micro controller. A flapping program is written based on the flapping angle, torsion angle, amplitude and frequency in Arduino®[55] .The twist for changing the angle of attack is also considered while programming.

The two load cells are connected to a lab view software using an electronic circuit board. For data acquisition from the cells a lab view circuit diagram is drawn. The circuit diagram enables the user to analyse the data from the cells in a live graphical format and the data can also be saved in a notepad format for every cycle as per the user requirement. The load cells are zeroed and calibrated with applied weights. The following figure explains the LabView® circuit and the different windows of data collection within the program.

[55] Appendix 1, page XIV

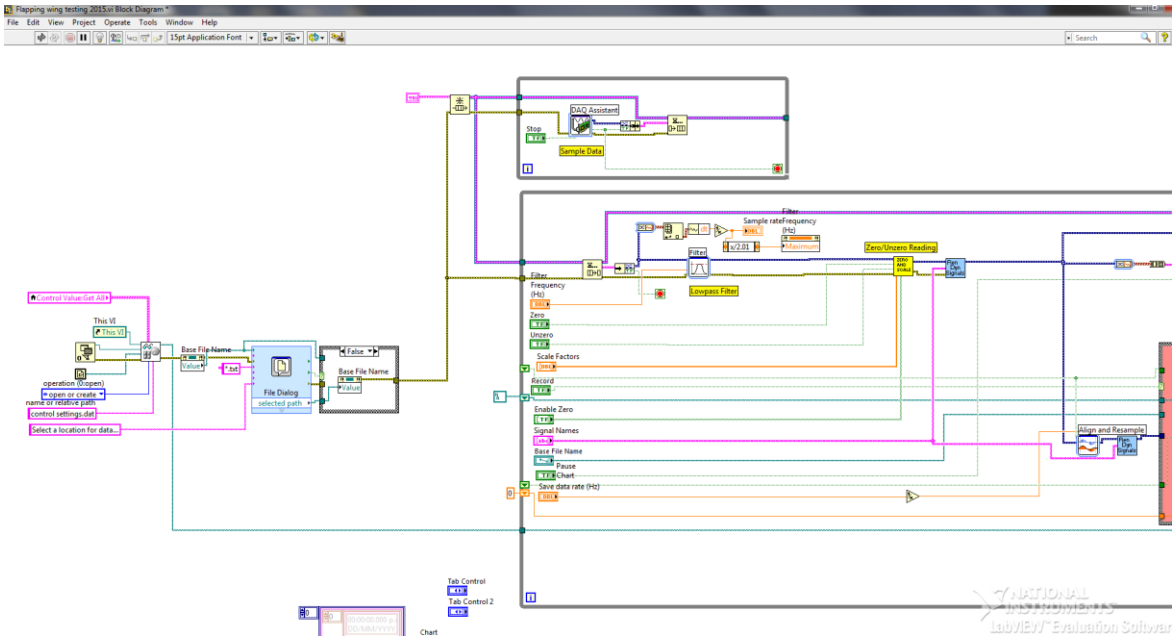

Figure 32: LabView block diagram for data collection from load cells[56]

[56] Authors own resource.

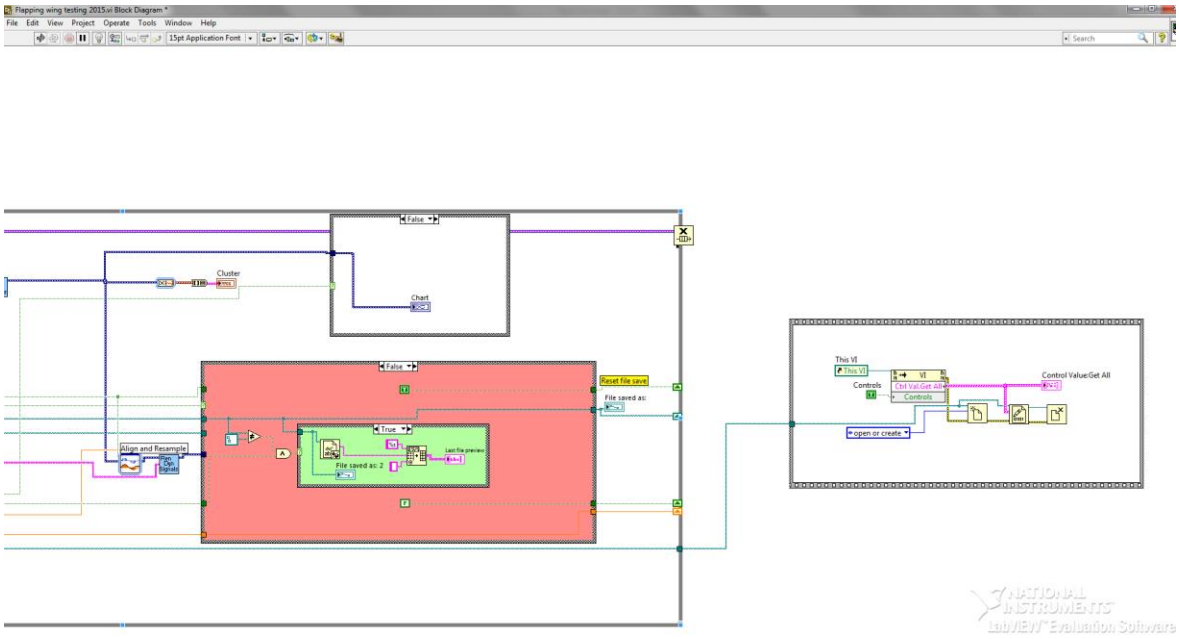

Figure 33: LabView block diagram for data collection from load cells[57]

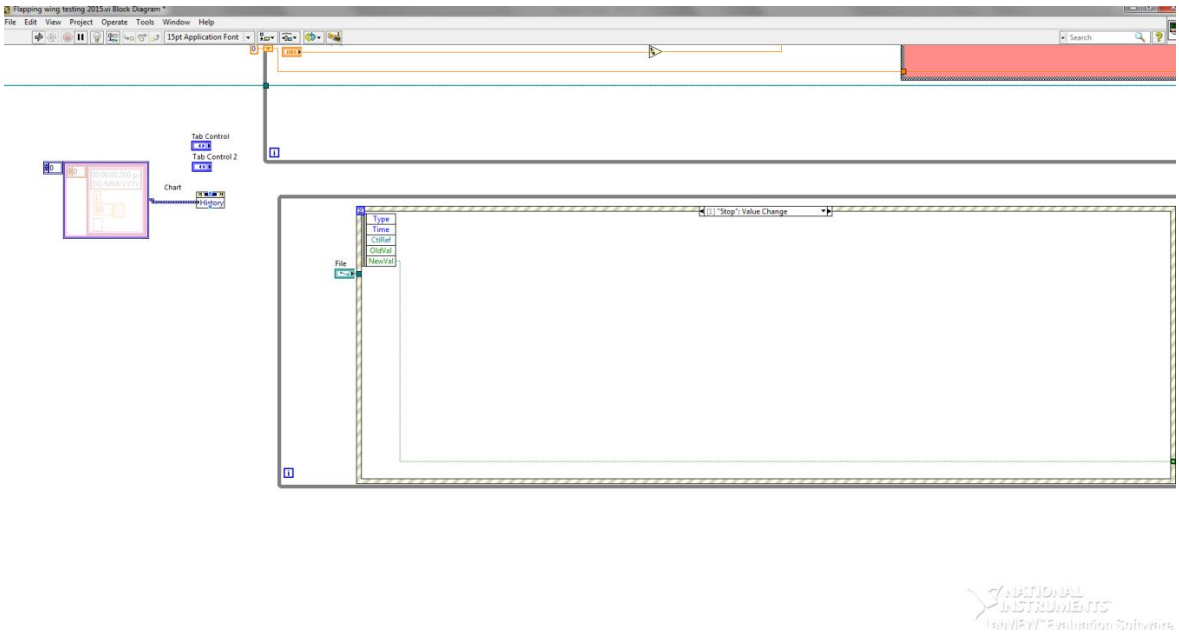

Figure 34: LabView block diagram for data collection from load cells[58]

[57] Authors own resource.
[58] Authors own resource.

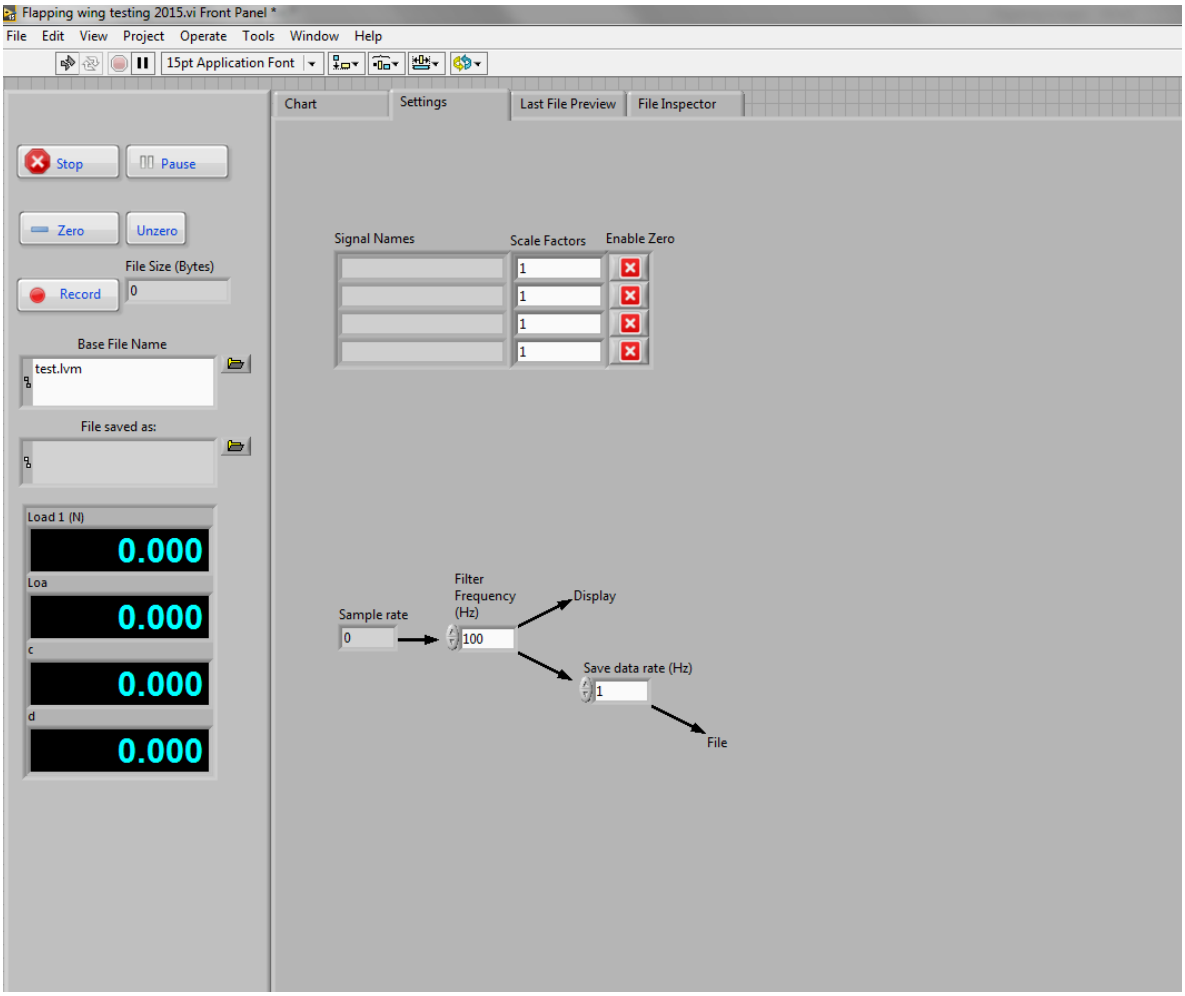

Figure 35: Frequency filter in LabView[59]

[59] Authors own resource.

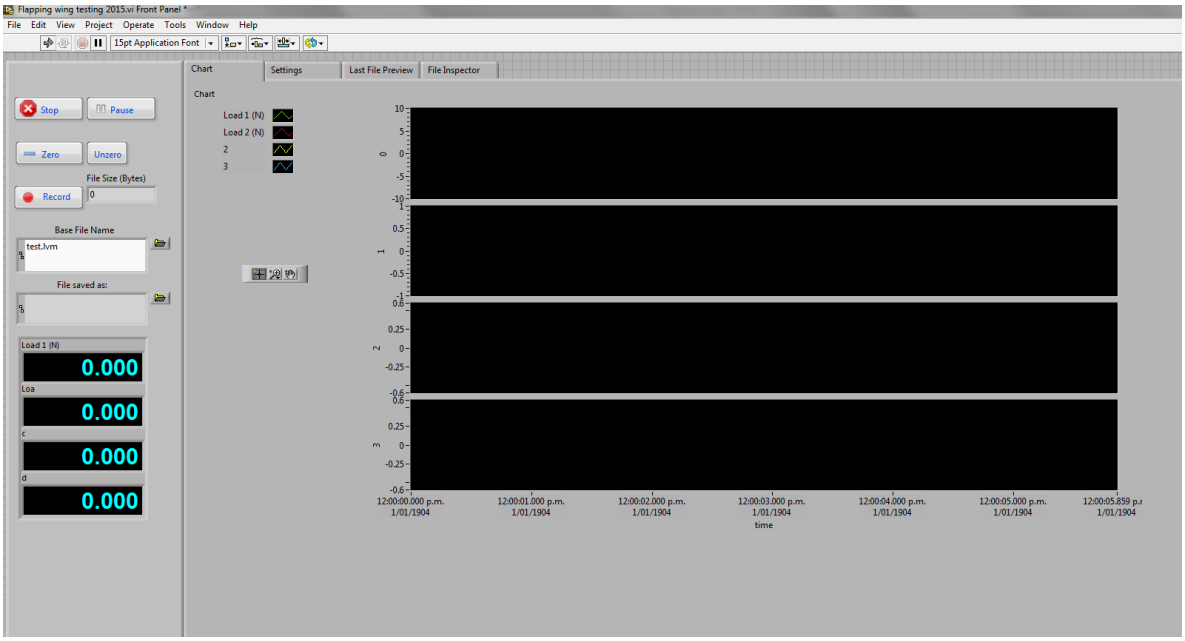

Figure 36: LabView showing the signal windows, load in N[60]

[60] Authors own resource.

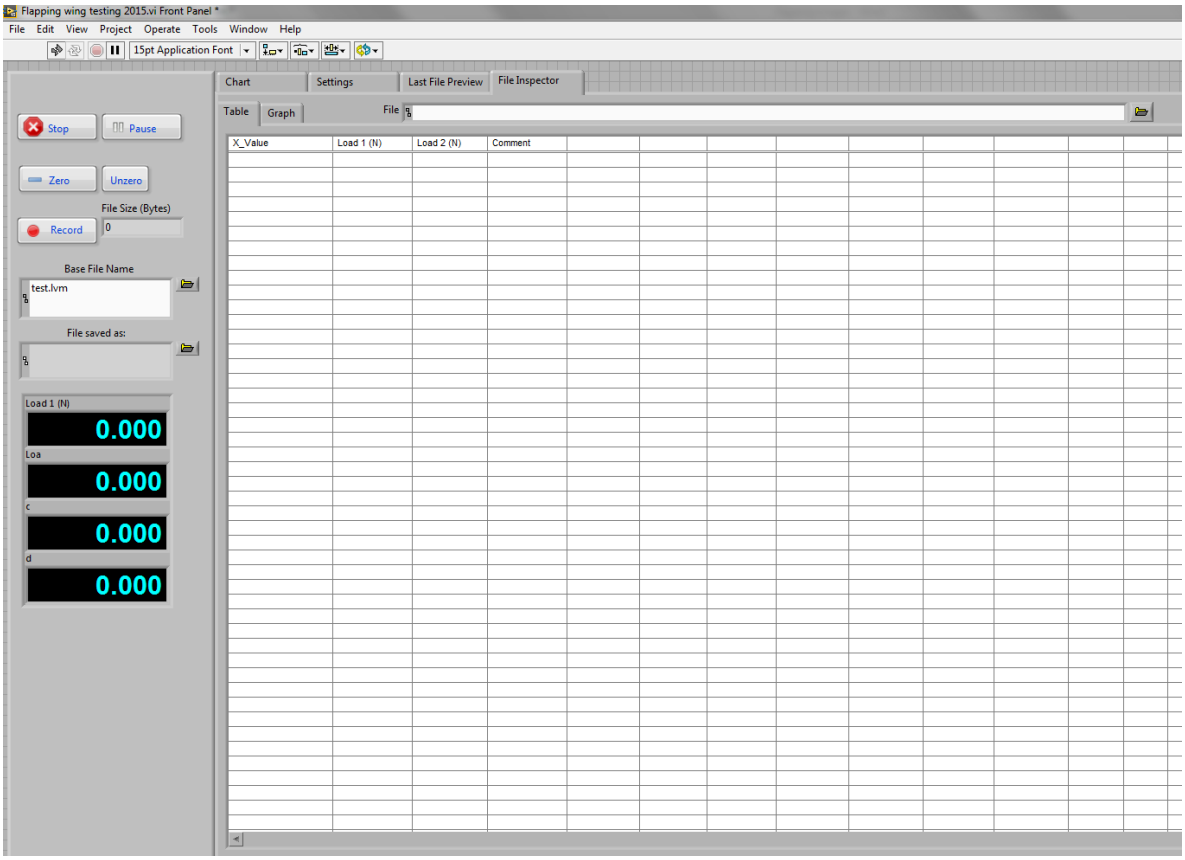

Figure 37: Lab view showing the data collection window[61]

3.3 Testing of the dragonfly wing

The corrugated structure of the dragonfly wing spars possesses great resistance to bending, but is compliant in torsion. Twisting of the leading or trailing edge results in torsion and relative movement of the remaining spars. As result camber will automatically change and sets in the wing as it twists. In flight the aerodynamic forces produced during the wing strokes will result in bending and twisting changing the camber that will help improving the aerodynamic efficiency. This chapter explains

[61] Authors own resource.

how the bending and torsional stiffness values are determined for the dragonfly 3D model wing.

3.3.1 Experimental test rig

The aim for the design of test rig is to facilitate the cantilever position for the 3D wing. A U shaped wooden frame is constructed with the following dimensions:

Dimension	Value
Length	350mm
Width	350mm
Height	450mm

Table 4: Dimensions of the test rig frame[62]

The 3D model wing is suspended in a cantilever position onto one side of the frame and a measuring scale is fixed close to the tip of the 3D wing. Thin copper pointer of length 15mm is attached at the tip of the 3D wing so that the pointer slides over the scale giving a reading in deflection upon loading. A light weight wire with a base is hanged from the wing tip to suspend weights. Mercury thermometer is placed within the U frame to note the changes in temperature near the wing.

[62] Authors own resource.

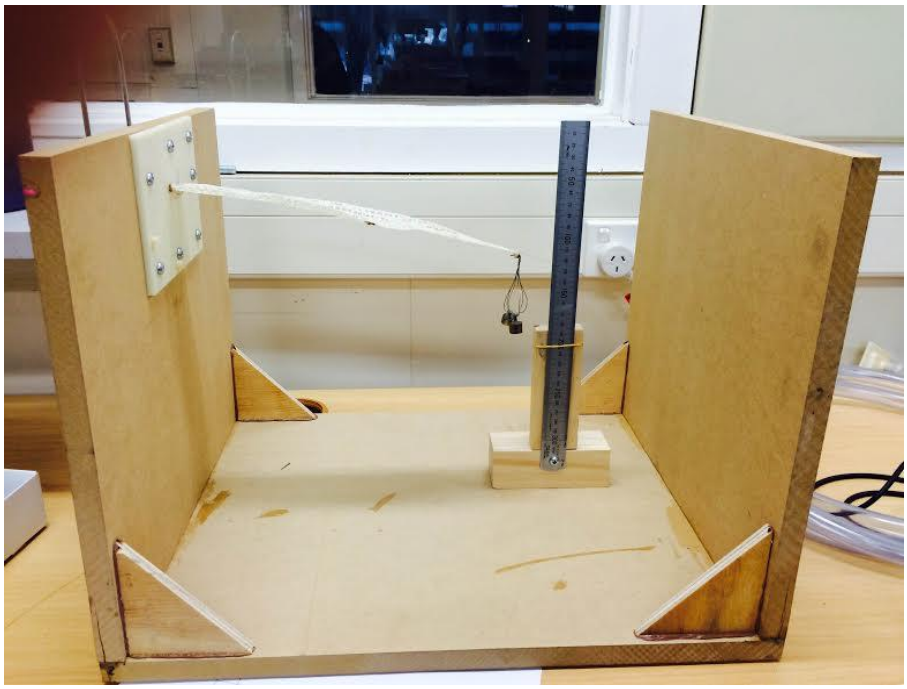

Figure 38: Experimental test bench showing the cantilever suspension of the wing[63]

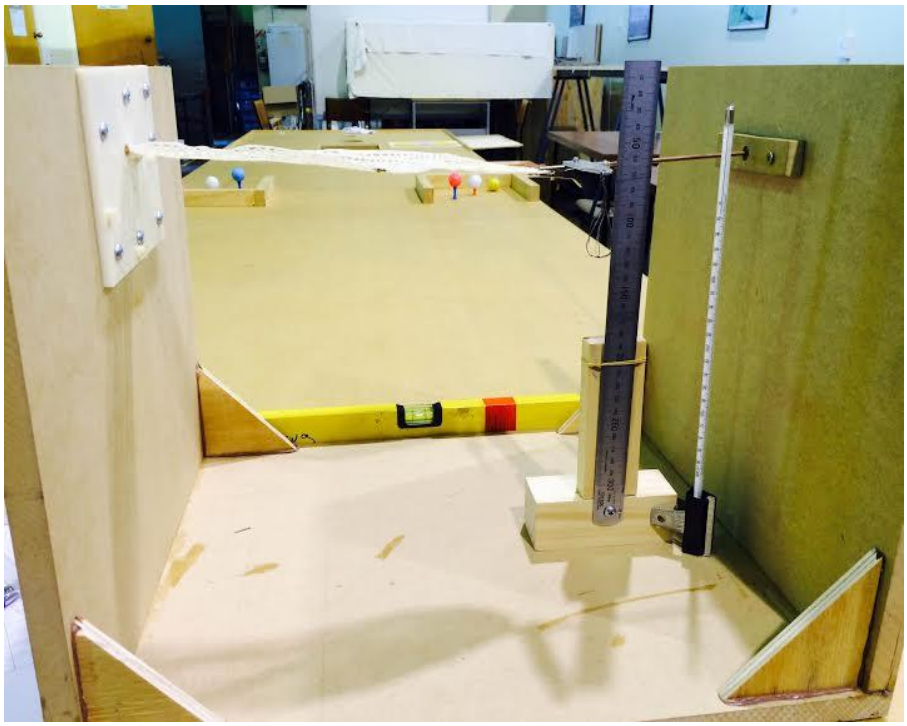

Figure 39: Experimental test bench showing the attachment of offset loading on the wing[64]

[63] Authors own resource.
[64] Authors own resource.

3.3.2 Bending stiffness experiment

The test is carried out at three different room temperature circumstances whereby the temperature is kept constantly. The zero load values of deflection are 76mm, 76mm and 76mm depending on the room temperature during testing, to achieve significant values concerning the bending stiffness changes, are noted. All other settings like force applied weight, force applied in Newton and deflection scales vary during the test. Table 5 shows the values of deflection obtained from the respective loads applied on the 3D model wing at 18°C. The average bending stiffness values for the model wing at 18°C is determined as 0.3258 in test 1.

Serial number	Room temperature in °C	Force applied weights in gm	Force applied in Newton	Deflection in mm Default = 76 mm +/0.5mm	Bending stiffness P/W
1	18	1.00	0.0098	79.0	0.3332
2	18	2.00	0.0196	82.5	0.3070
3	18	5.01	0.0490	91.5	0.3232
4	18	10.00	0.0980	106.0	0.3333
5	18	12.00	0.1176	112.5	0.3287
6	18	15.00	0.1470	121.5	0.3296

Table 5: Bending stiffness test 1[65]

Table 6 shows the values of deflection obtained from the respective loads applied on the 3D model wing at 26°C. The average bending stiffness value for the model wing at this temperature is determined as 0.3266 in test 2.

[65] Authors own resource.

Serial number	Room temperature in °C	Force applied weights in gm	Force applied in Newton	Deflection in mm Default = 76 mm +/0.5mm	Bending stiffness P/W
1	26	1.00	0.0098	79.0	0.3333
2	26	2.00	0.0196	82.0	0.3333
3	26	5.01	0.0490	91.5	0.3232
4	26	10.00	0.0980	106.5	0.3278
5	26	12.00	0.1176	113.5	0.3200
6	26	15.00	0.1470	122.5	0.3225

Table 6: Bending stiffness test 2[66]

In table 7 the values of deflection obtained from the respective loads applied on the 3D model wing at 11°C is shown. The average bending stiffness values for the model wing at 11°C is determined as 0.3166 in test 3.

Serial number	Room temperature in °C	Force applied weights in gm	Force applied in Newton	Deflection in mm Default = 76 mm +/0.5mm	Bending stiffness P/W
1	11	1.00	0.0098	80.5	0.2857
2	11	2.00	0.0196	83.5	0.3076
3	11	5.01	0.0490	93.0	0.3131
4	11	10.00	0.0980	107.5	0.3278
5	11	12.00	0.1176	113.5	0.3287
6	11	15.00	0.1470	121.5	0.3370

Table 7: Bending stiffness test 3[67]

[66] Authors own resource.
[67] Authors own resource.

In the above tables, the temperature does not have any major influences on the deflection and stiffness. Graph 1 shows the deflection of the 3D model wing upon the forces applied on it. It depicts that the final average value of the deflection is nearly constant in every test.

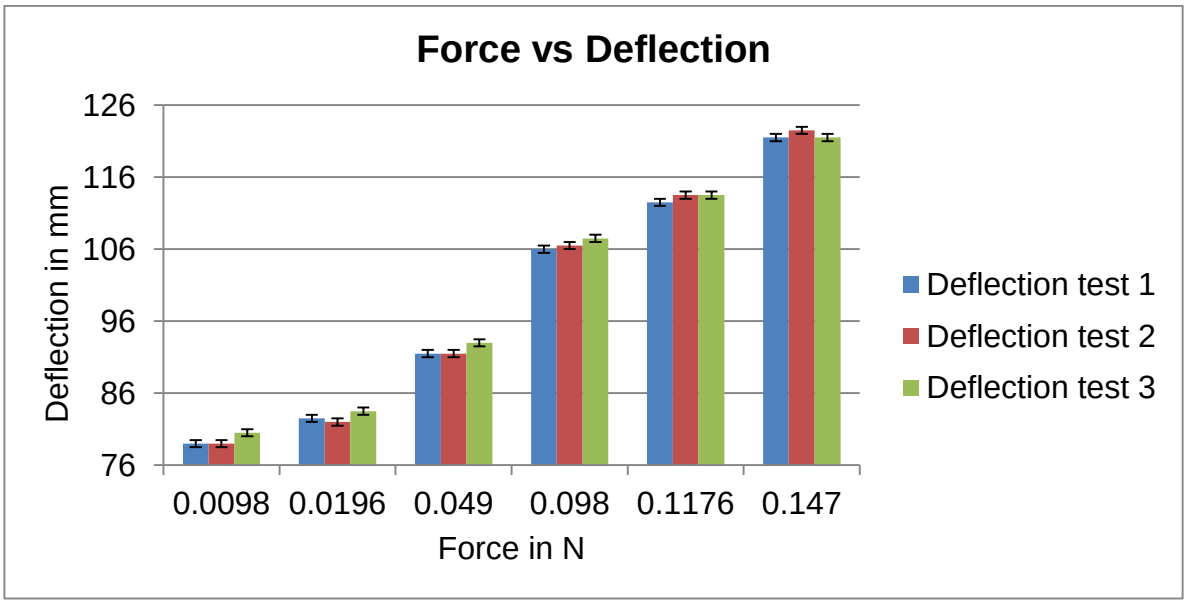

Graph 1: Force vs Deflection[68]

Graph 2 shows the plot for bending stiffness of three different room temperatures. It clearly depicts that the temperature does not have any major influence on the bending stiffness values of the model wing.

[68] Authors own resource.

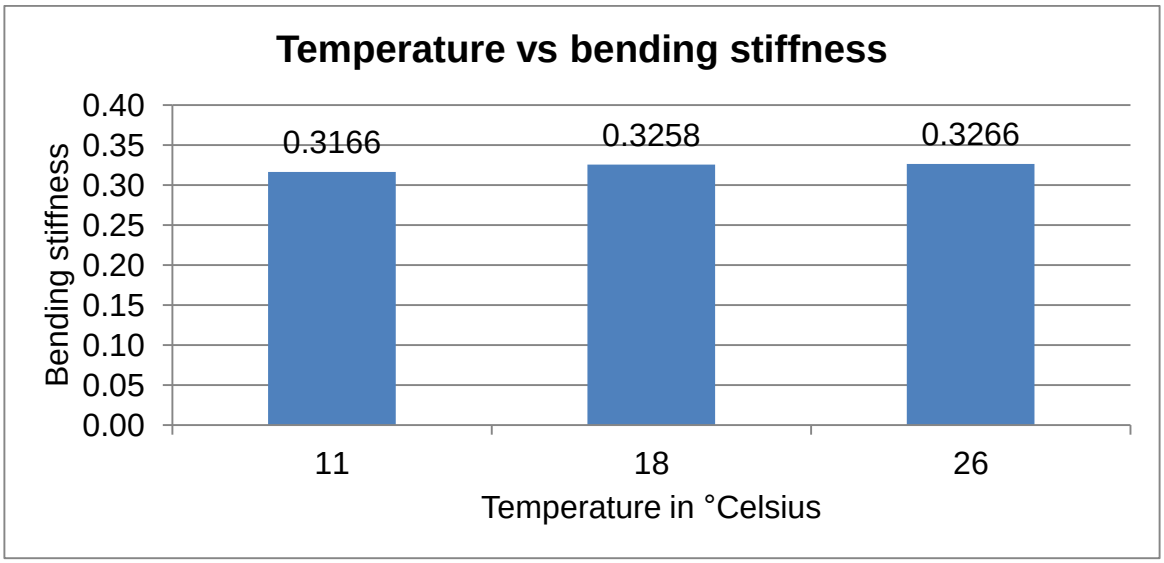

Graph 2: Temperature vs bending stiffness[69]

3.3.3 Torsional stiffness Experiment

For determining the torsional stiffness of the wing, an extra attachment is fixed onto the wing at offset close to the wing tip whereas the other end a thin copper wire is fixed to which the weights are suspended.

This experiment is carried out in two sets i.e., clockwise torsion and anti-clockwise torsion, with two different points of loading on the wing. The two points of loading are colour coded as red and black. The red point is on the leading edge whereas the black point is on the trailing edge. Similar to the bending stiffness experiment, the initial readings on the scale are noted and increasing weights are gradually suspended while change in deflections is noted. Any changes in temperatures are also noted during the experiments. Here in after the determined values shown.

[69] Authors own resource.

Table 8 shows the anti-clockwise torsion at point 1 on the model wing:

Serial number	Force Applied (P) Weights (gm) +/- 0.01gm	Force Applied in Newton	Deflection (W) Scale Reading(mm) Default=63 +/- 0.5mm	Deflection in Degrees	Room Temperature (°Celsius)	Tortional Stiffness =P/W
1	1.00	0.0098	63.0	0.00	14	0.0000
2	2.00	0.0196	63.5	0.45	14	0.0392
3	5.01	0.0490	64.5	1.36	14	0.0326
4	10.00	0.0980	67.0	3.64	14	0.0245
5	12.00	0.1176	68.0	4.55	14	0.0235
6	15.00	0.1470	69.0	5.46	14	0.0245
7	20.00	0.1961	71.0	7.29	14	0.0245
8	21.00	0.2451	73.0	9.13	14	0.0245

Table 8: Anti-clockwise torsion at point 1 on the model wing[70]

Table 9 shows the anti-clockwise torsion at point 2 on the model wing:

Serial number	Force Applied (P) Weights (gm) +/- 0.01gm	Force Applied in Newton	Deflection (W) Scale Reading(mm) Default=64.5 +/- 0.5mm	Deflection in Degrees	Room Temperature (°Celsius)	Tortional Stiffness =P/W
1	1.00	0.0098	65.0	0.44	14	0.0196
2	2.00	0.0196	65.5	0.88	14	0.0196
3	5.01	0.0490	66.5	1.77	14	0.0245
4	10.00	0.0980	69.5	4.44	14	0.0196
5	12.00	0.1176	70.5	5.33	14	0.0196
6	15.00	0.1470	72.5	7.12	14	0.0183
7	20.00	0.1961	76.5	10.72	14	0.0163
8	21.00	0.2451	82.0	15.74	14	0.0140

Table 9: Anti-clockwise torsion at point 2 on the model wing[71]

[70] Authors own resource.
[71] Authors own resource.

Graph 3 shows the plot of angular deflection of the 3D model wing upon the application of the loads respectively. It clearly depicts that the deflection at point 2 is higher than at point 1 during the anti-clockwise torsion. The determined deflection values of the wing during the clockwise torsion are ranging from maximum of 9° to 15°.

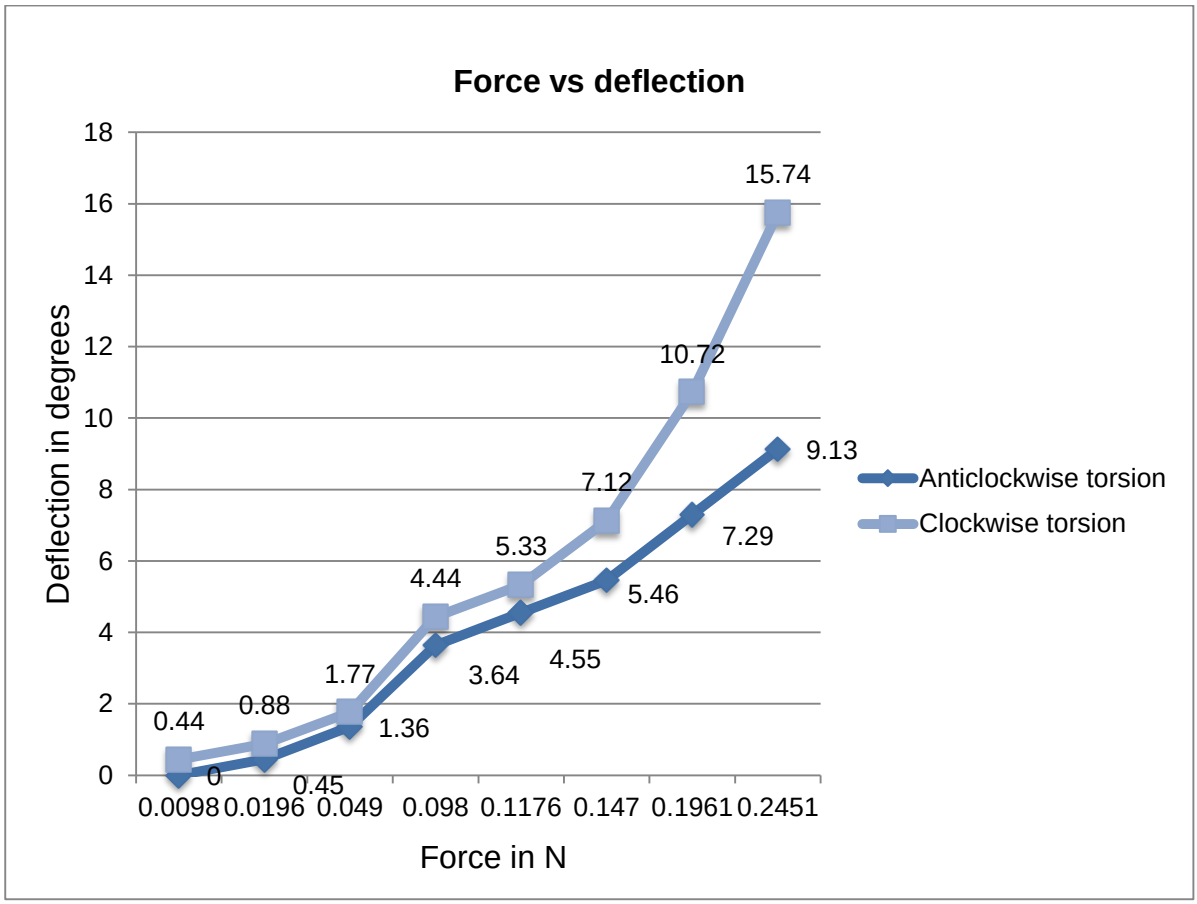

Graph 3: Anti clockwise torsion[72]

[72] Authors own resource.

Table 10 shows the clockwise torsion at point 1 on the model wing:

Serial number	Force Applied (P) Weights (gm) +/- 0.01gm	Force Applied in Newton-N	Deflection (W) Scale Reading(mm) Default=63 +/- 0.5mm	Deflection in Degrees.	Room Temperature (deg-Celsius)	Tortional Stiffness =P/W
1	1.00	0.0098	63.5	0.45	18	0.0196
2	2.00	0.0196	64.0	0.90	18	0.0196
3	5.01	0.0490	65.5	2.27	18	0.0326
4	10.00	0.0980	68.5	5.00	18	0.0178
5	12.00	0.1176	69.5	5.92	18	0.0180
6	15.00	0.1470	71.5	7.75	18	0.0172
7	20.00	0.1961	74.0	10.05	18	0.0178
8	21.00	0.2451	76.5	12.37	18	0.0181

Table 10: Clockwise torsion at point 1 on the model wing[73]

In table 11 the clockwise torsion at point 2 on the model wing is shown.

Serial number	Force Applied (P) Weights (gm) +/- 0.01gm	Force Applied in Newton-N	Deflection (W) Scale Reading(mm) Default=64.5 +/- 0.5mm	Deflection in Degrees	Room Temperature (deg-Celsius)	Tortional Stiffness =P/W
1	1.00	0.0098	65.0	0.44	16	0.0196
2	2.00	0.0196	65.5	0.88	16	0.0196
3	5.01	0.0490	66.5	1.77	16	0.0245
4	10.00	0.0980	68.5	3.55	16	0.0245
5	12.00	0.1176	69.5	4.44	16	0.0235
6	15.00	0.1470	70.5	5.33	16	0.0245
7	20.00	0.1961	73.5	8.02	16	0.0217
8	21.00	0.2451	76.5	10.72	16	0.0204

Table 11: Clockwise torsion at point 2 on the model wing[74]

[73] Authors own resource.
[74] Authors own resource.

Graph 4 shows the plot of angular deflection of the 3D model wing upon the application of the loads respectively. It clearly depicts that the deflection at point 1 is higher than at point 1 during the clockwise torsion. The determined deflection values of the wing during the clockwise torsion are ranging from maximum of 10° to 12°.

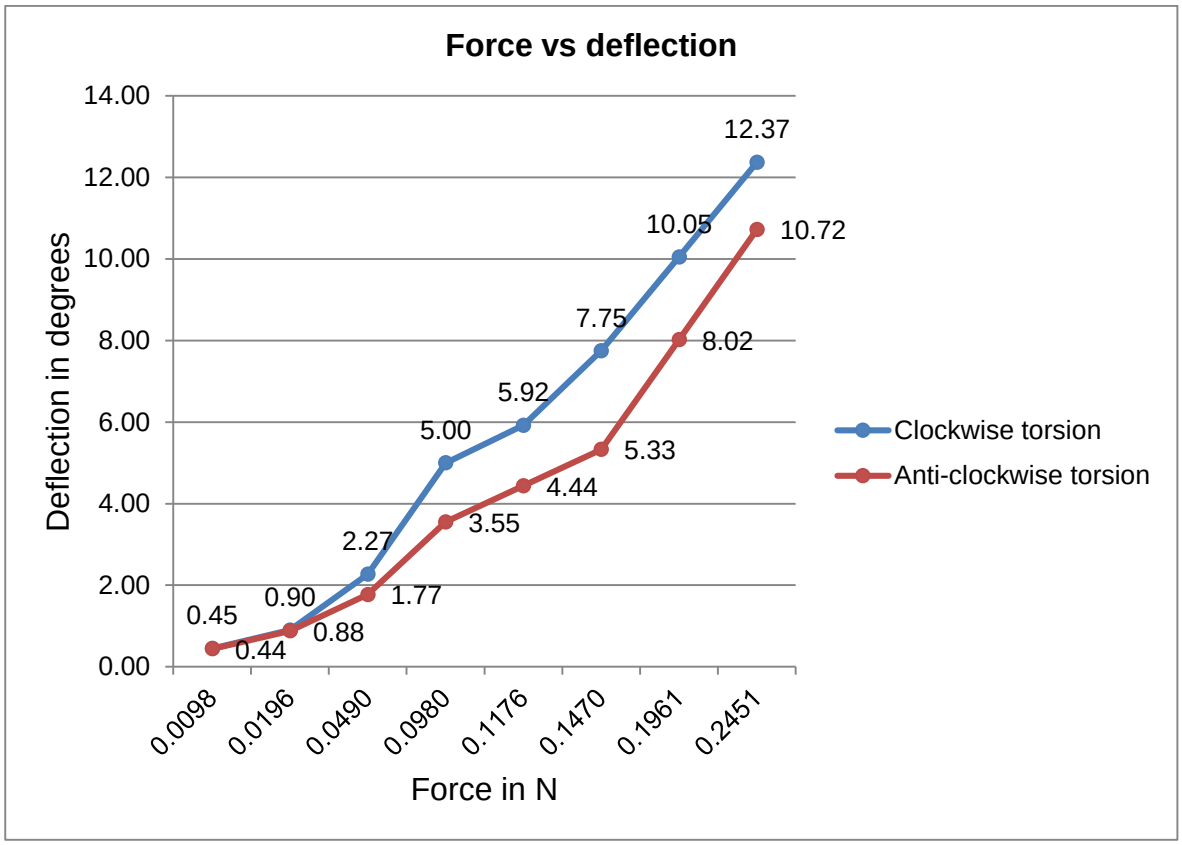

Graph 4: Clockwise torsion[75]

The torsional stiffness of the 3D wing is calculated and a mean average value of it is determined. The deflection values obtained are compared with the literature data.

[75] Authors own resource.

3.3.4 Determination of forces using flapping test

Experimentation

The flapping experiment is carried out for seven times for obtaining the values for seven different flapping patterns. The first test is based on a flapping frequency of 0.6Hz with set flapping and torsional angles maintaining a phase difference of 180 degrees. The required flapping pattern is obtained by making changes in the Arduino program for the servos. The load cells are calibrated to zero value, then the flapping program is loaded onto the Arduino board to start the servos for flapping. As soon as the flapping starts the load cells measure the changes in the loading and give an output which can be seen in LabView®. The data is collected for every eight continuous flapping cycles, so as to gather a continuous data and it will be clear to investigate the collected data. The collected data is saved in a note pad file which is further studied. The same procedure is followed for the remaining six tests and the corresponding data is collected for each. Following frequencies, flapping and torsion angles are the values which are used for the remaining tests. Next the frequency is changed to 0.3Hz and by varying the flapping angle for further four more readings are taken.

Test number	Flapping Frequency-Hz	Flapping Angle	Torsion Angle	Phase difference
1	0.68	60°	60°	180°
2	0.68	90°	60°	180°
3	0.34	60°	60°	180°
4	0.34	90°	60°	180°
5	0.68	90°	60°	0°
6	0.68	90°	60°	90°
7	0.68	90°	60°	270°

Table 12: Stages of flapping experiment [76]

Test 1

The below graphs show the force vs time graphs for the flapping experiment conducted with 0.68Hz of frequency, flapping angle 60° and torsion angle 60° with a phase difference of 180° between them replicating a sinusoidal flapping motion.

Graph 5 depicts that the lift force of 0.4N and a weight component of force 0.2N is generated during this flapping pattern, whereas graph 6 clearly points out that 0.09N of thrust is being generated along with 0.1N of drag.

[76] Authors own resource.

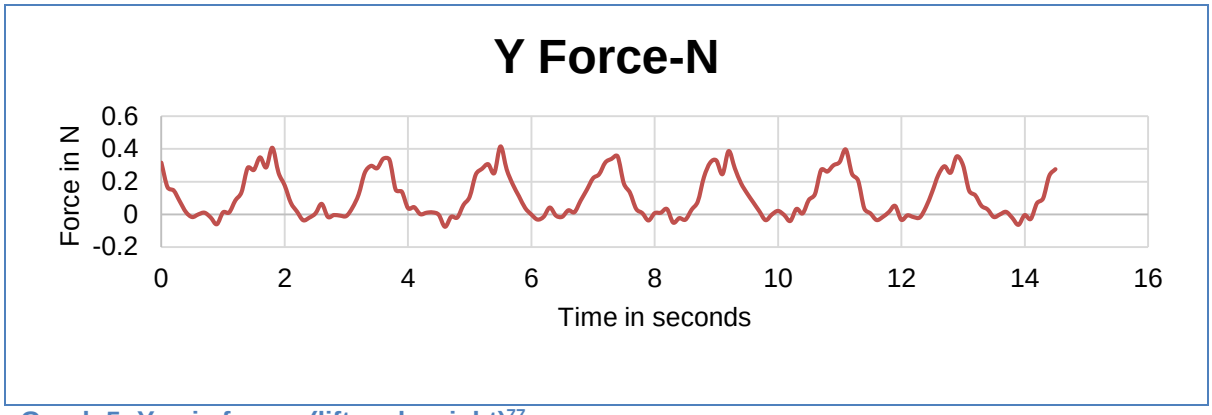

Graph 5: Y axis forces (lift and weight)[77]

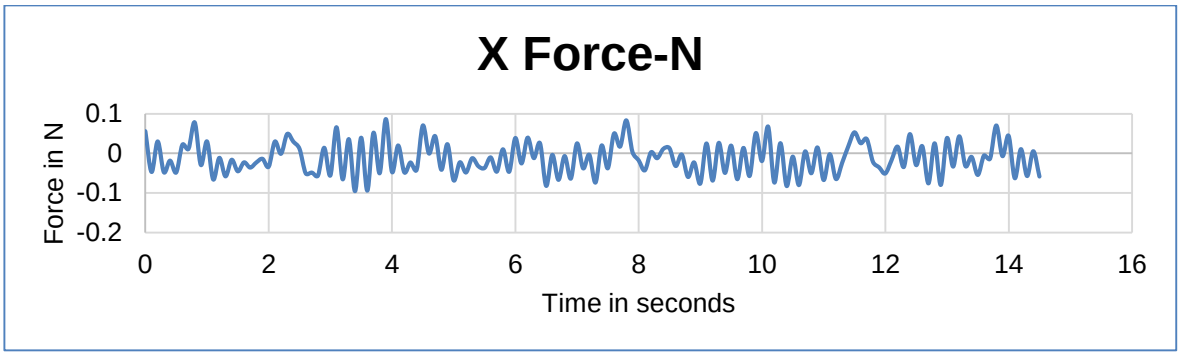

Graph 6: X axis forces (thrust and drag)[78]

The following graph 7 shows the plot of coefficient of lift and coefficient of drag with respect to time. It depicts that the coefficient of lift is at a lower point and gradually reducing with respect to time; this explains that the lift is gradually generated during the first half phase of the stroke while it tends to decrease for the next half. The coefficient of drag plot is behaving the same instead it is understood that during a hovering flight in stable air the drag value is consistently low.

[77] Authors own resource.
[78] Authors own resource.

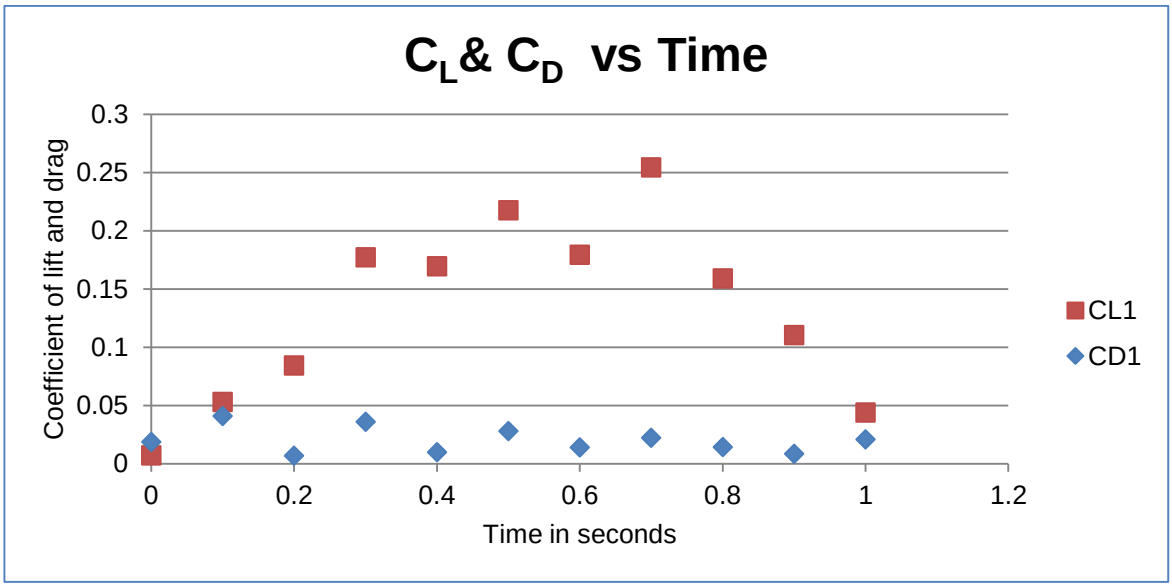

Graph 7: Coefficient of lift and drag[79]

Test 2

The below graphs show the force vs time graphs for the flapping experiment conducted with 0.68Hz of frequency, flapping angle 90° and torsion angle 60° with a phase difference of 180° between them replicating a sinusoidal flapping motion.

Graph 8 shows that the lift force of 0.39N and a weight component of force 0.25N is generated during this flapping pattern whereas graph 9 clearly shows that 0.09N of thrust is being generated along with 0.08 N of drag significantly.

[79] Authors own resource.

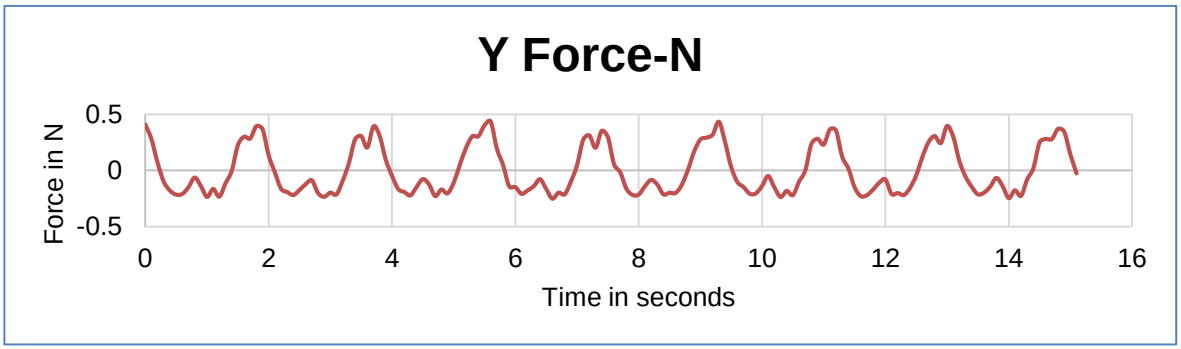

Graph 8: Y axis forces (lift and weight)[80]

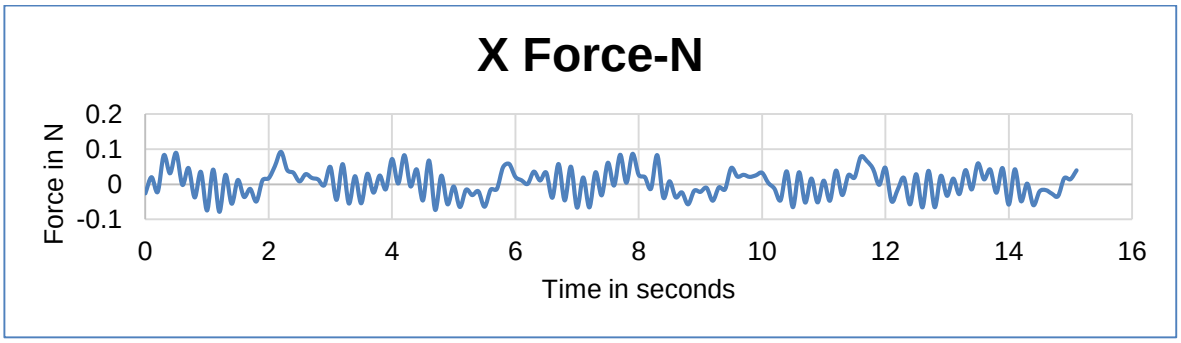

Graph 9: X axis forces (thrust and drag)[81]

The following graph 10 shows the plot of coefficient of lift and coefficient of drag with respect to time. It depicts that the coefficient of lift is at a lower point and gradually increasing with respect to time, this explains that the lift is gradually generated and reached a higher point at two different intervals during the first half phase of the stroke while it tends to decrease for the next half. The coefficient of drag plot is behaving the same instead it is understood that during a hovering flight in stable air the drag value is consistently low.

[80] Authors own resource.
[81] Authors own resource.

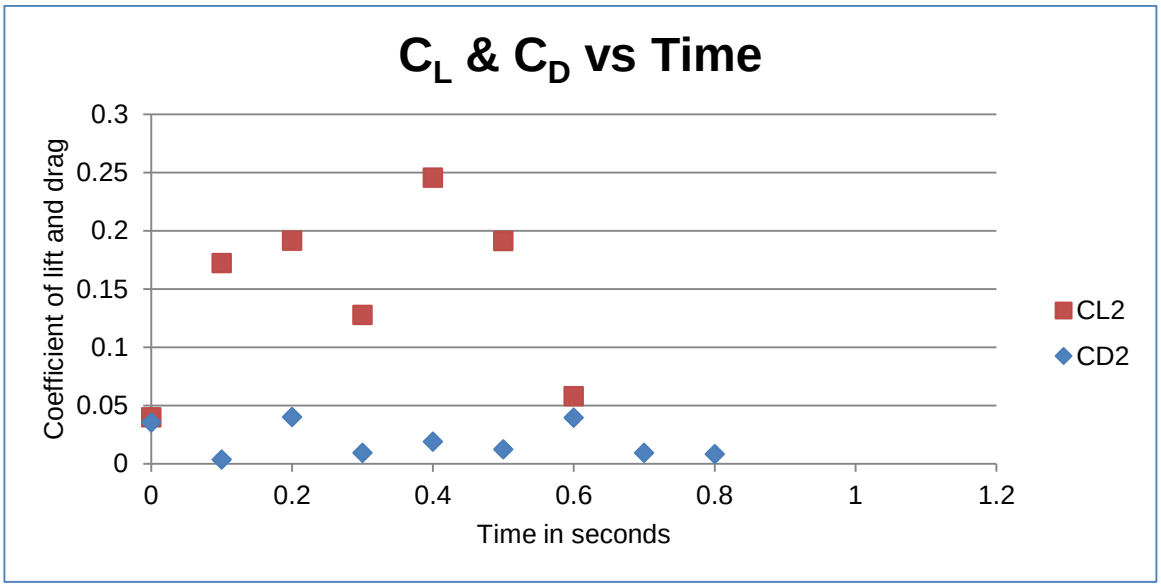

Graph 10: Coefficient of lift and drag[82]

The Highest points in the coefficient of lift vs time indicates that the C_L value is maximum at 0.25 for both the plots. That depicts that C_L -max is remaining constant at flapping angle of 60°,90° while frequency and torsion angle are maintained constant. The C_D is observed to be consistently low and reaching a maximum of 0.048 in both the experiments.

Test 3

The below graphs 11 and 12 show the force vs time graphs for the flapping experiment conducted with 0.3Hz of frequency, flapping angle 60° and torsion angle 60° with a phase difference of 180° between them replicating a sinusoidal flapping motion.

[82] Authors own resource.

Graph 11 shows that the lift force of 0.3N and a weight component of force 0.1N is generated during this flapping pattern, whereas graph 12 clearly shows that 0.04N of thrust is being generated along with 0.06N of drag significantly.

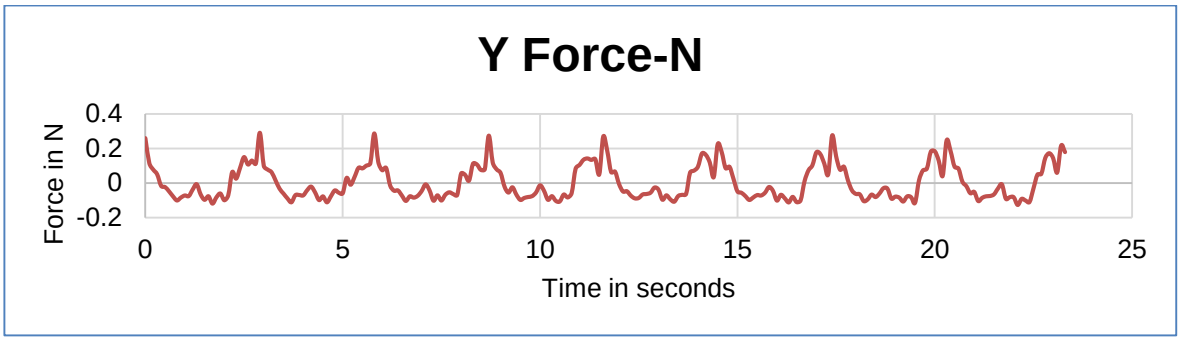

Graph 11: Y axis forces (lift and weight)[83]

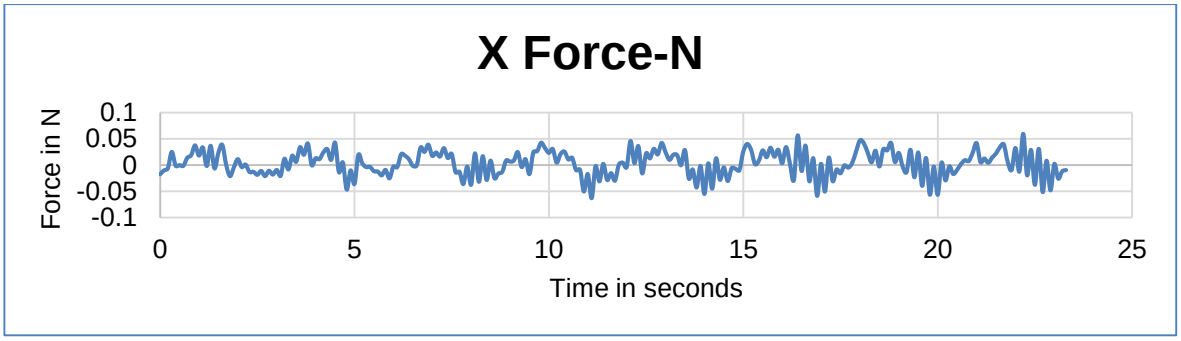

Graph 12: X axis forces (thrust and drag)[84]

The following graph 13 shows the plot of coefficient of lift and coefficient of drag with respect to time. It depicts that the coefficient of lift is at a lower point and gradually

[83] Authors own resource.
[84] Authors own resource.

increasing with respect to time, this explains that the lift is gradually generated during the first half phase and reaches at maximum at the end of the stroke while it tends to decrease for the next half. The coefficient of drag plot is relatively consistent instead it is understood that during a hovering flight in stable air the drag value is going to be consistently low.

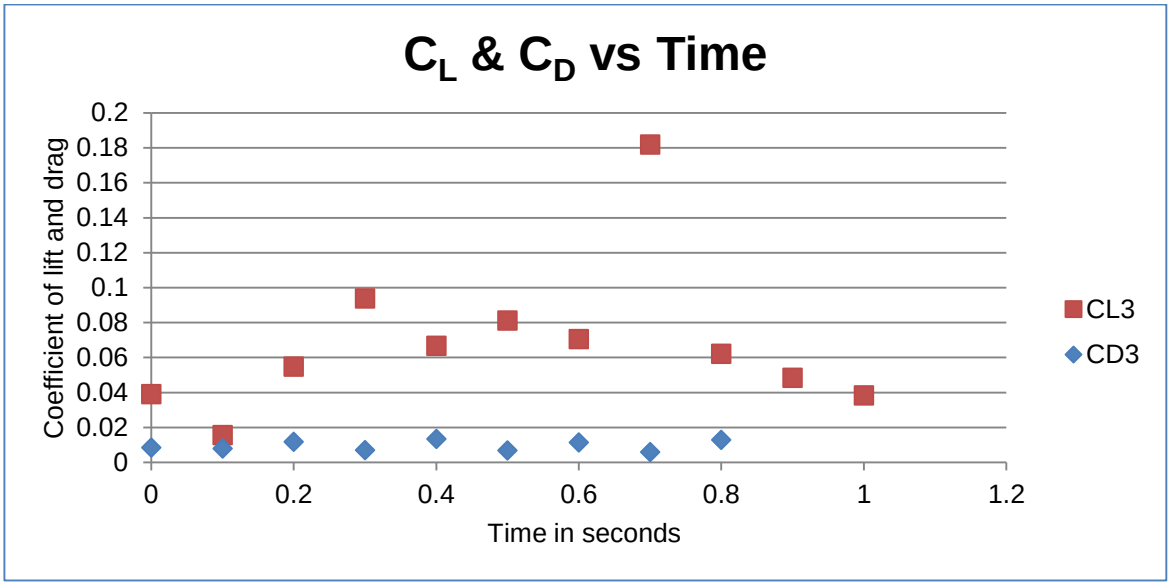

Graph 13: Coefficient of lift and drag[85]

Test 4

The below graphs 14 and 15 show the force vs time graphs for the flapping experiment conducted with 0.3Hz of frequency, flapping angle 90° and torsion angle 60° with a phase difference of 180° between them replicating a sinusoidal flapping motion.

[85] Authors own resource.

Graph 14 shows that the lift force of 0.4N and a weight component of force 0.24N is generated during this flapping pattern, whereas graph 15 clearly shows that 0.09N of thrust is being generated along with 0.07N of drag significantly.

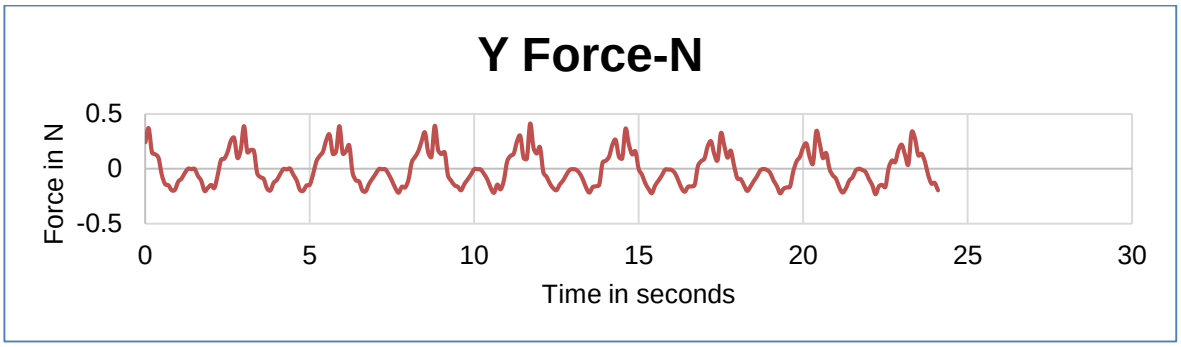

Graph 14: Y axis forces (lift and weight)[86]

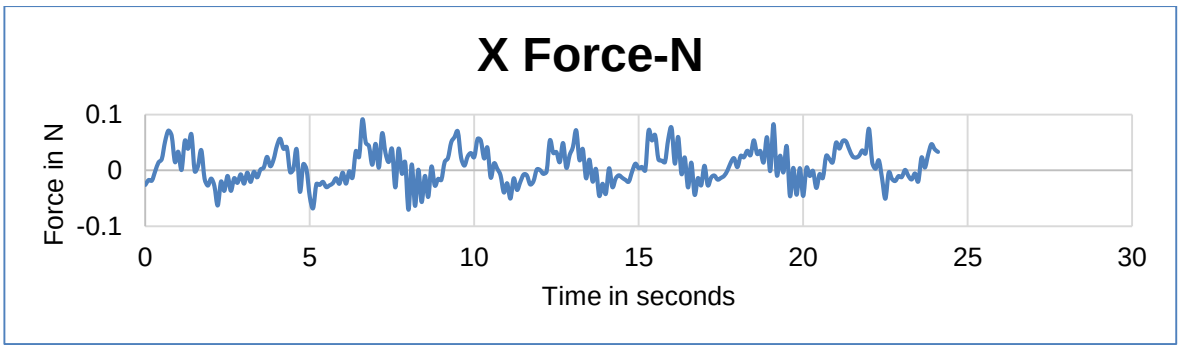

Graph 15: X axis forces (thrust and drag)[87]

The following graph 16 shows the plot of coefficient of lift and coefficient of drag with respect to time. It depicts that the coefficient of lift is at a lower point and gradually

[86] Authors own resource.
[87] Authors own resource.

increasing with respect to time, this explains that the lift is gradually generated and reached at it maximum at two intervals during the first half phase of the stroke while it tends to decrease at the end. The coefficient of drag plot is consistently smooth with a minor increase at two intervals instead it is understood that during a hovering flight in stable air the drag value is consistently low.

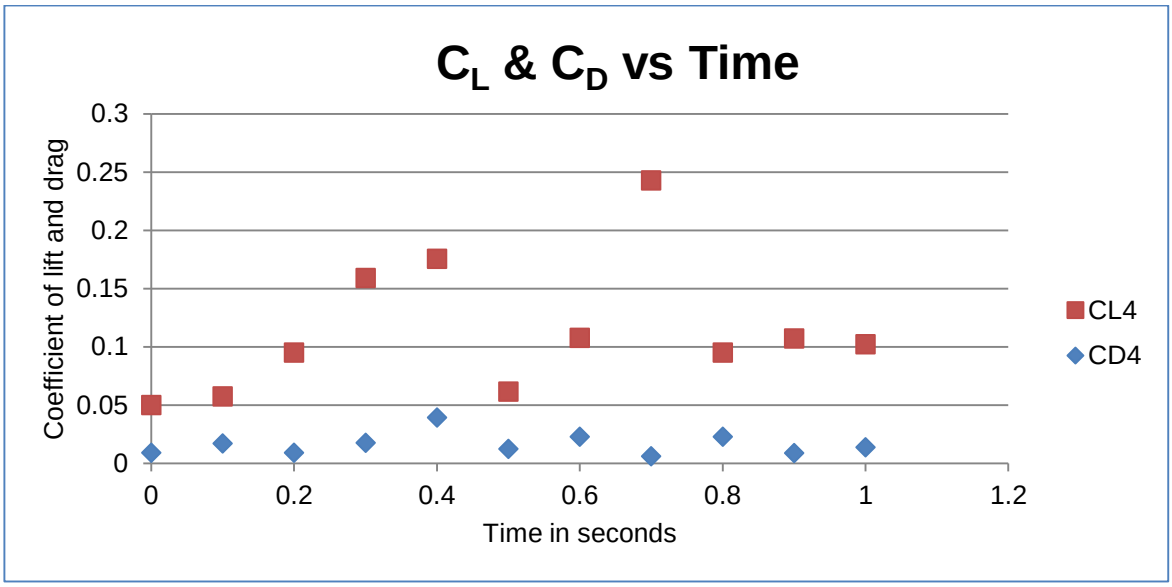

Graph 16: Coefficient of lift and drag[88]

From the C_L & C_D vs time plots it is observed that the C_L is reaching a maximum of 0.18 for flapping angle of 60°, whereas for 90° flapping angle the C_L value is maximum at 0.25 which is equal to the first experimental values of C_L for a frequency of 0.68Hz. Whereas for this frequency the C_D is relatively low for 60° flapping angle and for 90° flapping angle, it is consistent compared to the first experiment.

A conclusion can be drawn from these two experimental results that for the flapping frequencies of 0.68Hz and 0.3Hz the lift generated is maximum and average

[88] Authors own resource.

of C_L is the same for 90° flapping angle when the torsion angle and the phase difference between the torsion angle, flapping angle is maintained constant.

Phase difference experimental results

Test 5

The below graphs 17 and 18 show the force vs time graphs for the flapping experiment conducted with 0.68Hz of frequency, flapping angle 60° and torsion angle 60° with a phase difference of 0° between them replicating a sinusoidal flapping motion.

The graph 17 shows that the lift force of 0.6N and a weight component of force 0.1N is generated during this flapping pattern, whereas graph 18 clearly shows that 0.02N of thrust is being generated along with 0.1N of drag significantly.

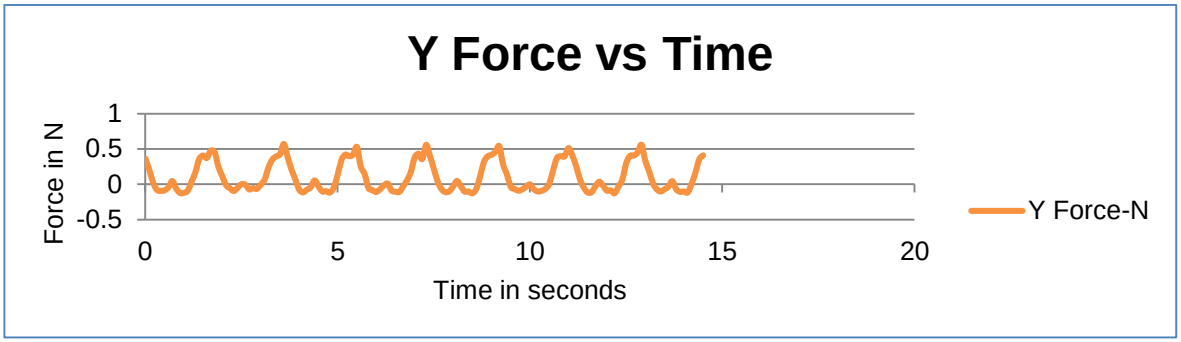

Graph 17: Y axis forces (lift and weight)[89]

[89] Authors own resource.

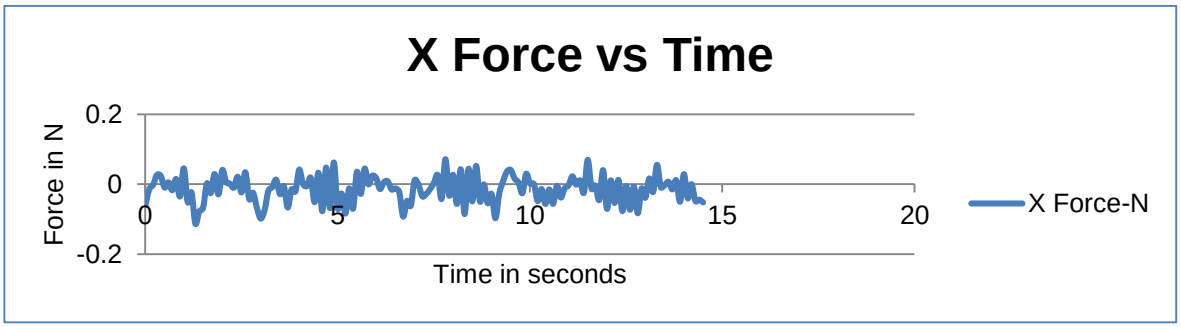

Graph 18: X axis forces (thrust and drag)[90]

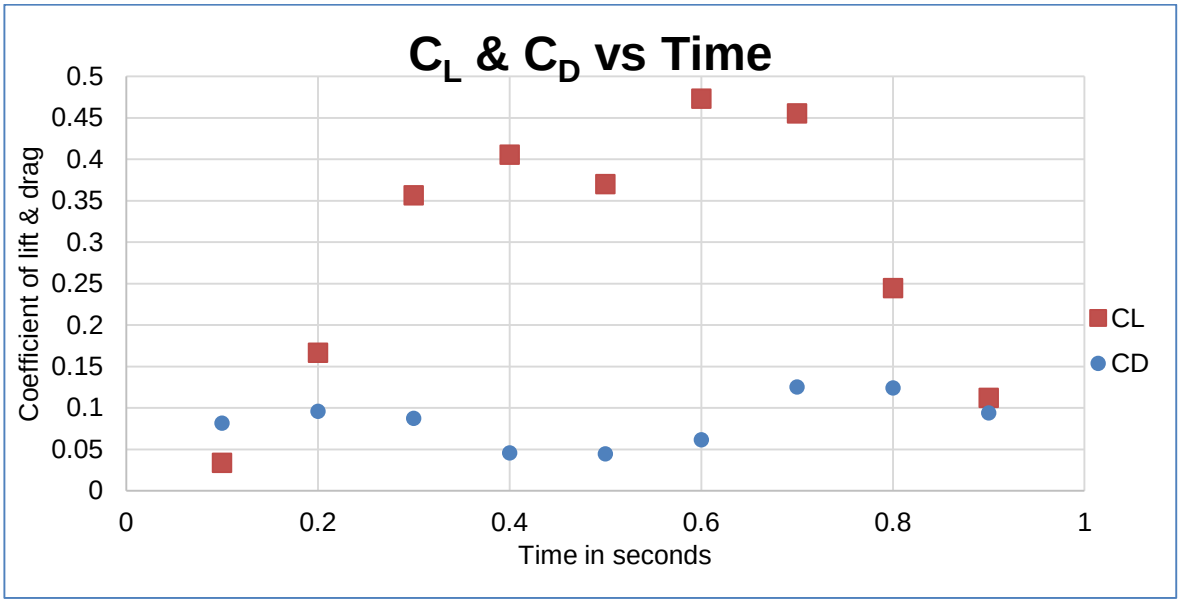

Graph 19: Coefficient of lift and drag[91]

The above graph 19 shows the C_L & C_D vs time of frequency 0.68Hz, flapping angle of 90°, torsion angle of 60° and the phase difference of 0° between the flapping angle and the torsion angle. In this C_L -max is observed as 0.47 whereas the C_D-max is of 0.125 which is relatively low in range.

[90] Authors own resource.
[91] Authors own resource.

Test 6

The below graphs 20 and 21 show the force vs time graphs for the flapping experiment conducted with 0.68Hz of frequency, flapping angle 60° and torsion angle 60° with a phase difference of 90° between them replicating a sinusoidal flapping motion.

Graph 20 shows that the lift force of 0.5N and a weight component of force 0.15N is generated during this flapping pattern, whereas graph 21 clearly shows that 0.05N of thrust is being generated along with 0.1N of drag significantly.

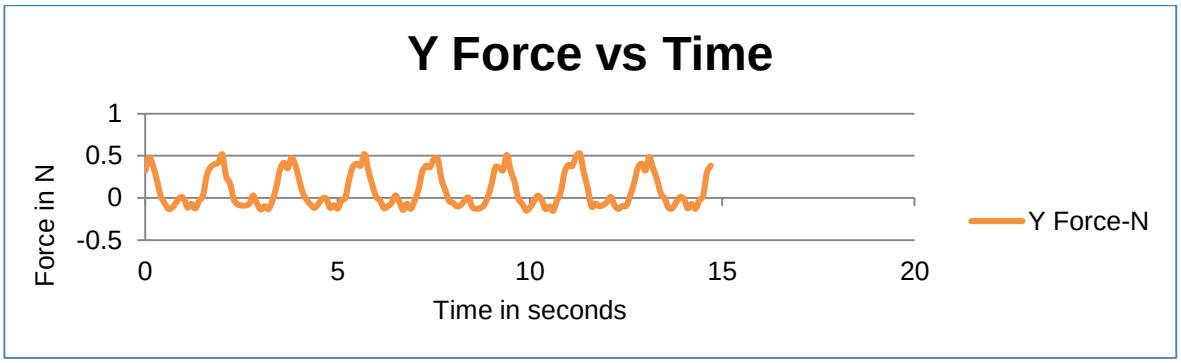

Graph 20: Y axis forces (lift and weight)[92]

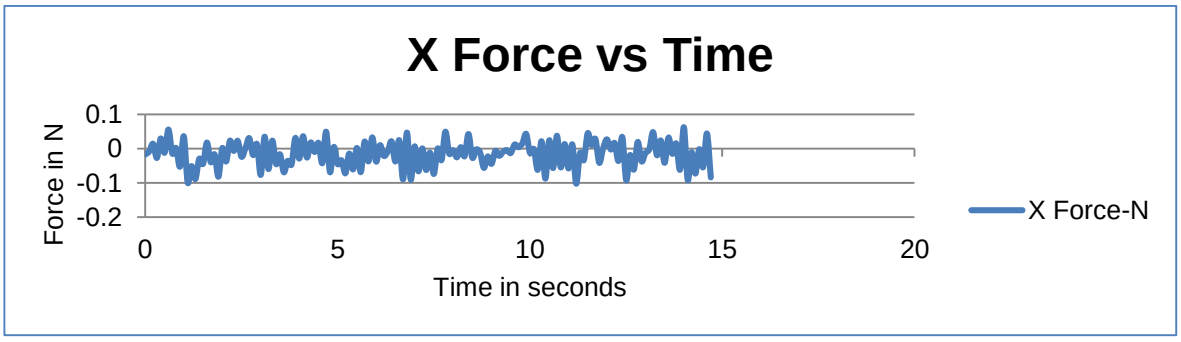

Graph 21: X axis forces (thrust and drag)[93]

[92] Authors own resource.
[93] Authors own resource.

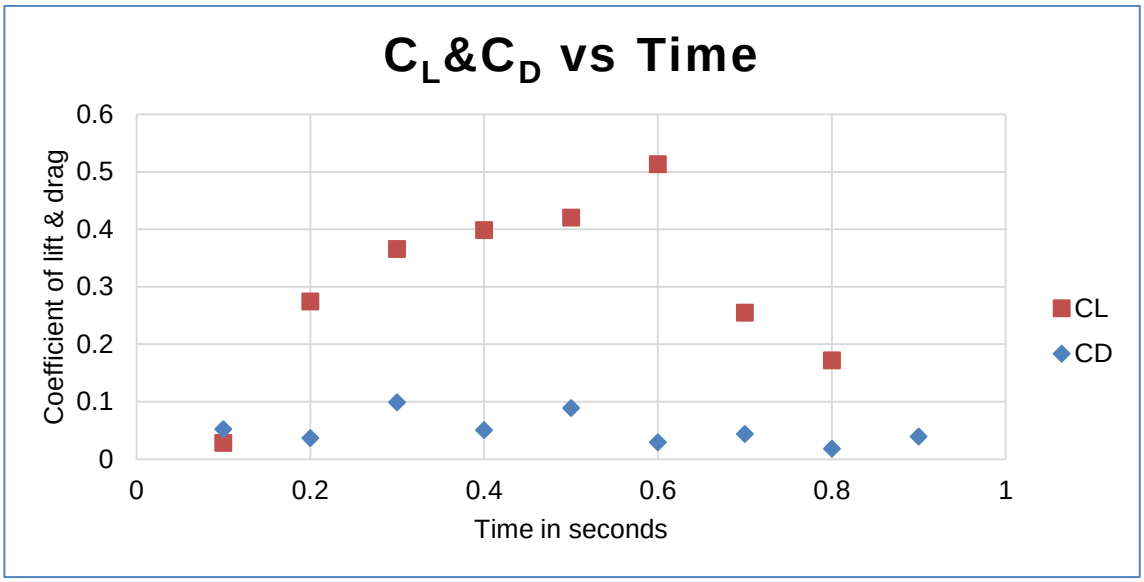

Graph 22: Coefficient of lift and drag[94]

The above graph 22 shows the C_L & C_D vs time of frequency 0.68Hz, flapping angle of 90°, torsion angle of 60° and the phase difference of 90° between the flapping angle and the torsion angle. In this C_L -max is observed as 0.52 whereas the C_D -max is of 0.1 which is relatively low than the flapping condition with a phase difference of 0°.

Test 7

The below graphs 23 and 24 shows the force vs time graphs for the flapping experiment conducted with 0.68Hz of frequency, flapping angle 60° and torsion angle 60° with a phase difference of 270° between them replicating a sinusoidal flapping motion.

[94] Authors own resource.

Graph 23 shows that the lift force of 0.5N and a weight component of force 0.15N is generated during this flapping pattern, whereas graph 24 clearly shows that 0.04N of thrust is being generated along with 0.1N of drag significantly.

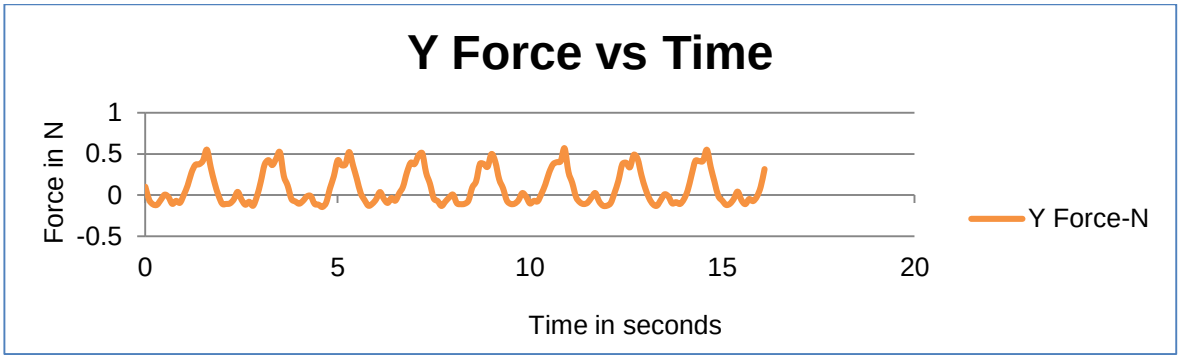

Graph 23: Y axis forces (lift and weight)[95]

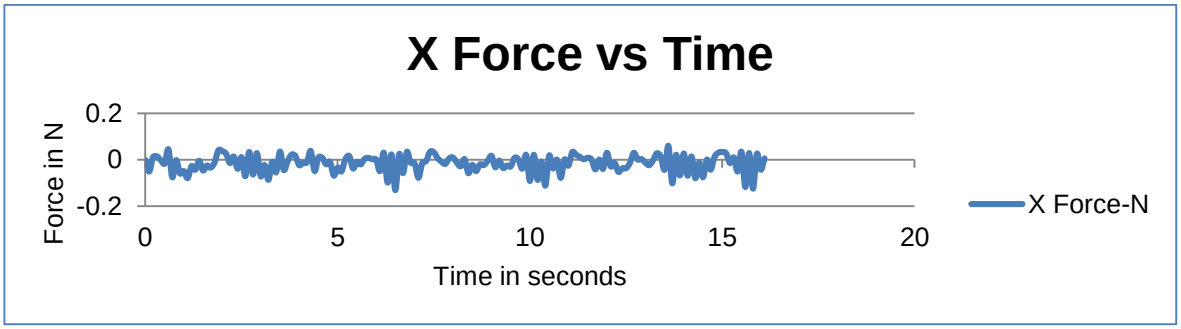

Graph 24: X axis forces (thrust and drag)[96]

[95] Authors own resource.
[96] Authors own resource.

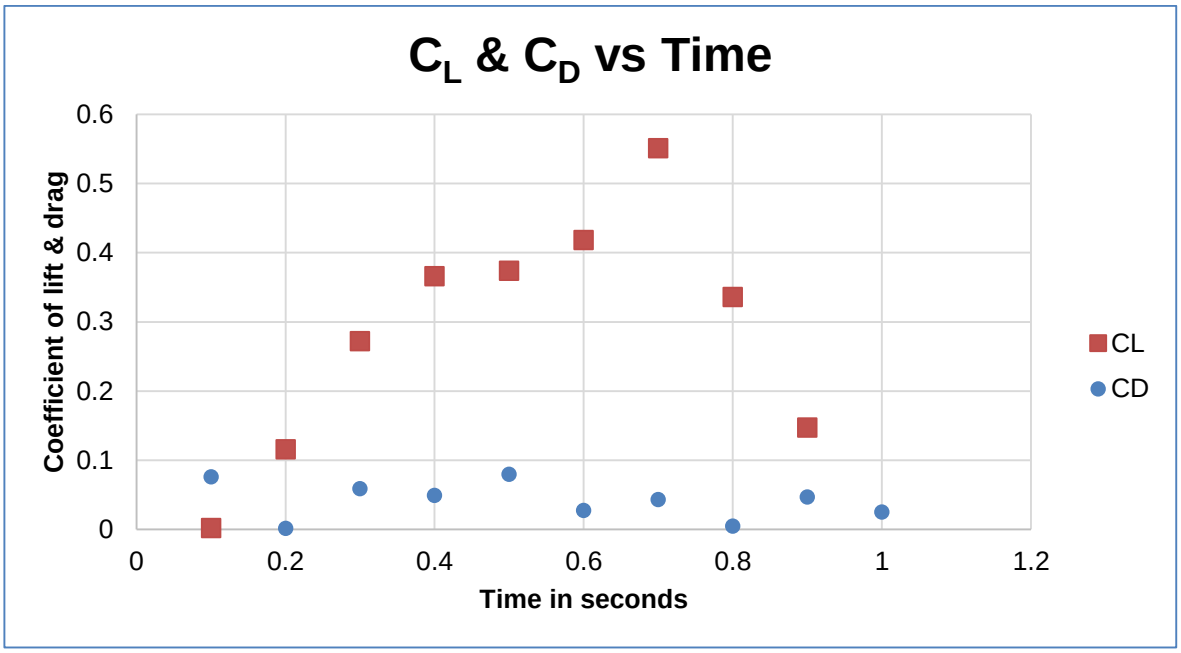

Graph 25: Coefficient of lift and drag [97]

The above graph 25 shows the C_L & C_D vs time of frequency 0.68Hz, flapping angle of 90°, torsion angle of 60° and the phase difference of 270° between the flapping angle and the torsion angle. In this C_L -max is observed as 0.55 whereas the C_D -max is of 0.1 which is lower than the flapping conditions with a phase difference of 0° and 90°.

The conclusions are drawn from the above plots such as the C_L is maximum when the phase difference between the flapping angle and the torsion angle is maintained as 270°and is reducing for lower phase differences of 90° and 0°. From this we can also say that lift generated is increasing when the phase difference is increased from 0° and 270°.While the C_D value is lower for higher phase difference values. It is also understood that the drag force generated on the wing during the

[97] Authors own resource.

flapping can be reduced by maintaining higher phase difference between the flapping angle and the torsion angle.

Fourier Transform

Fourier transform is a function that breaks a signal into an alternative representation which is characterized either by sine or cosines. It shows that any function can be re-written as the sum of sinusoidal functions. It is also called as the frequency domain representation of the original signal. The Fourier Transform finds the recipe for a signal:

- Start with a time-based signal
- It breaks the signal into a set of sines and cosines of different amplitudes, which when assumed gives the original signal
- Collect the full recipe, listing the amount of each signal

The data obtained from the flapping test is large. Hence in order to filter the large data for a clear signal, the Fourier Transform is used at this stage of the project. Fourier Transform Analysis is carried out using a programming software called Matlab®. This is a proprietary programming language that allows matrix manipulations, data plotting, functions plotting, user interface and implementing algorithms. It also helps in the interfacing of programmes written in the other coding languages like C, C++, Python, Java, etc.

Fourier analysis using Matlab:

The Fourier transform code used in filtering the data is show in figures 40 to 43.

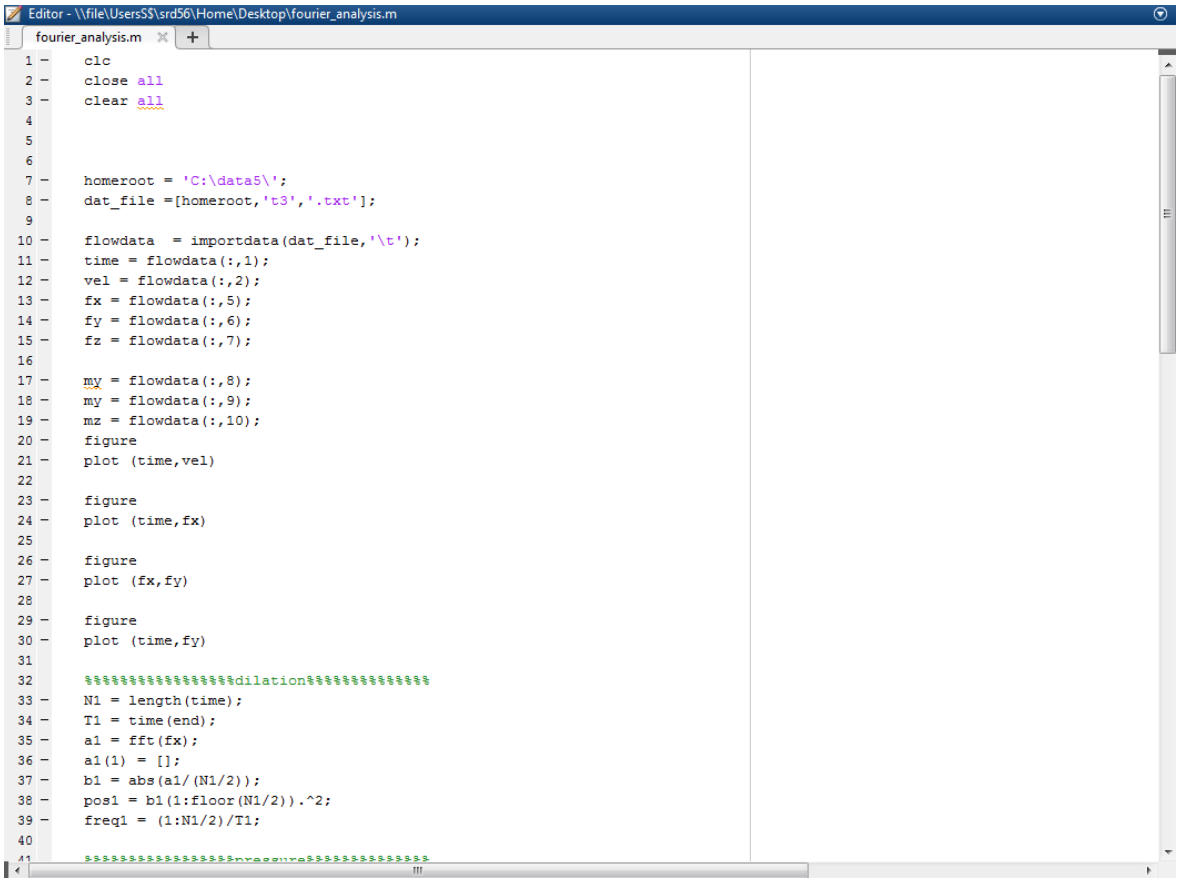

Figure 40: Fourier Transform program in Matlab (1)[98]

[98] Authors own resource.

Editor - \\file\Users$$\srd56\Home\Desktop\fourier_analysis.m

fourier_analysis.m

```
%%%%%%%%%%%%%%%%%pressure%%%%%%%%%%%%%%%
N2 = length(time);
T2 = time(end);
a2 = fft(fy);
a2(1) = [];
b2 = abs(a2/(N2/2));
pos2 = b2(1:floor(N2/2)).^2;
freq2 = (1:N2/2)/T2;


%%%%%%%%%%%%%%%%%flow%%%%%%%%%%%%%%%
N3 = length(time);
T3 = time(end);
a3 = fft(fz);
a3(1) = [];
b3 = abs(a3/(N3/2));
pos3 = b3(1:floor(N3/2)).^2;
freq3 = [1:N3/2]/T3;

figure ('name','fx')
hold on
% set(gcf, 'PaperPositionMode', 'auto');
% set(gcf,'Color',[1 1 1],'OuterPosition',[350 300 282 350])
% set(gca,'Position',[0.21 0.15 0.75 0.75])
title('fx')
plot (freq1,pos1,'color','k')
ylabel('Power','FontName','Arial'), xlabel('Frequency Hz','FontName','Arial')
% set(gca,'XLim',[0 4.5],'YLim',[0 0.3],'YColor',[0 0 0],'XTickLabel',[],'YTickLabel',[],'YTick',[0 0.1 0.2 0.3],'XMinorT
box on
hold off

figure ('name','fy')
hold on
% set(gcf, 'PaperPositionMode', 'auto');
% set(gcf,'Color',[1 1 1],'OuterPosition',[350 300 282 350])
% set(gca,'Position',[0.21 0.15 0.75 0.75])
plot (freq2,pos2,'color','k')
title('fy')
ylabel('Power','FontName','Arial'), xlabel('Frequency Hz','FontName','Arial')
% set(gca,'XLim',[0 4.5],'YLim',[0 0.3],'YColor',[0 0 0],'XTickLabel',[],'YTick',[0 0.1 0.2 0.3],'XMinorTick','off', 'YMi
```

Figure 41: Fourier Transform program in Matlab (2)[99]

[99] Authors own resource.

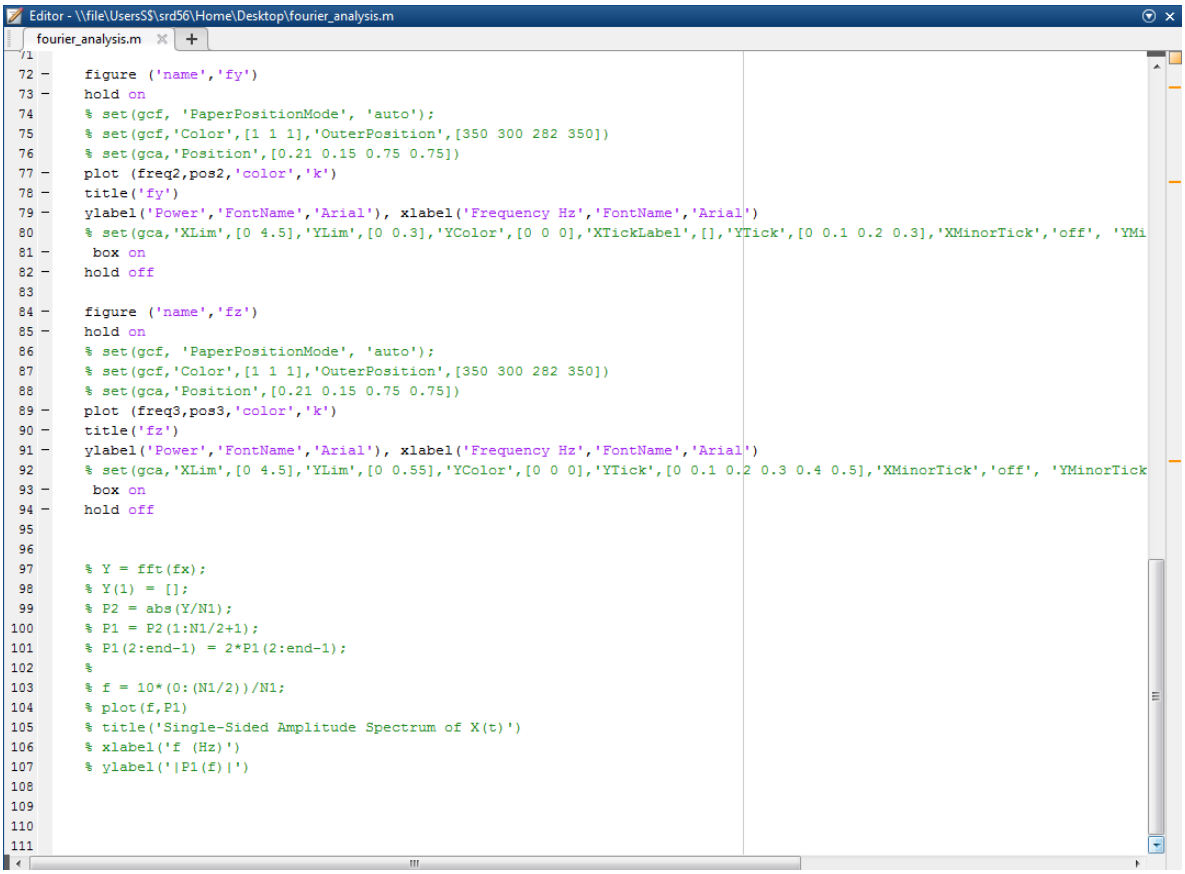

Figure 42: Fourier Transform program in Matlab (3)[100]

[100] Authors own resource.

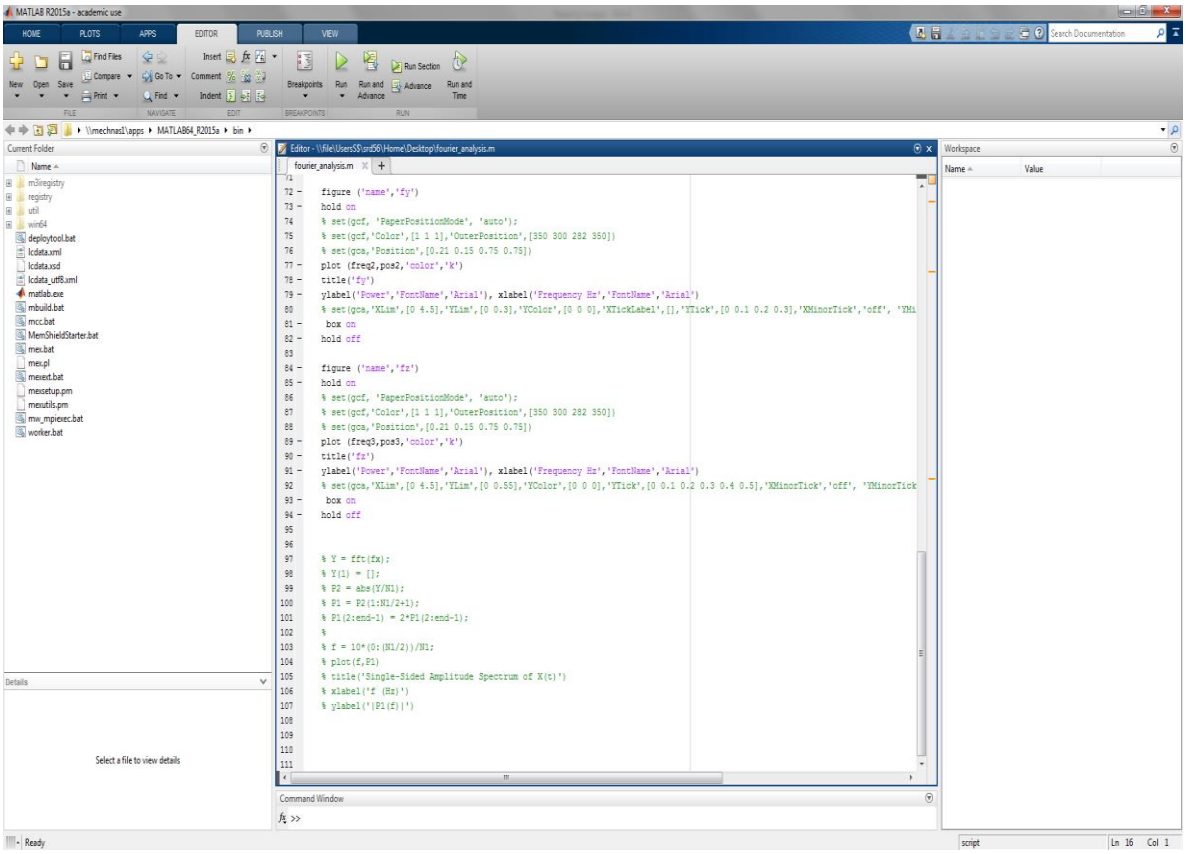

Figure 43: Fourier Transform program in Matlab (4)[101]

Fourier spectrum analysis:

When the raw data obtained from the experiment is arranged according to the coding of the program, then it is run through the Fourier Transform in Matlab. The algorithm gives the output as graphs which consist of a power spectrum. These spectrums are obtained for the forces in all directions. The spectrum graphs obtained from the Fourier Transform analysis in Matlab are as follows:

[101] Authors own resource.

Natural Frequency spectrum

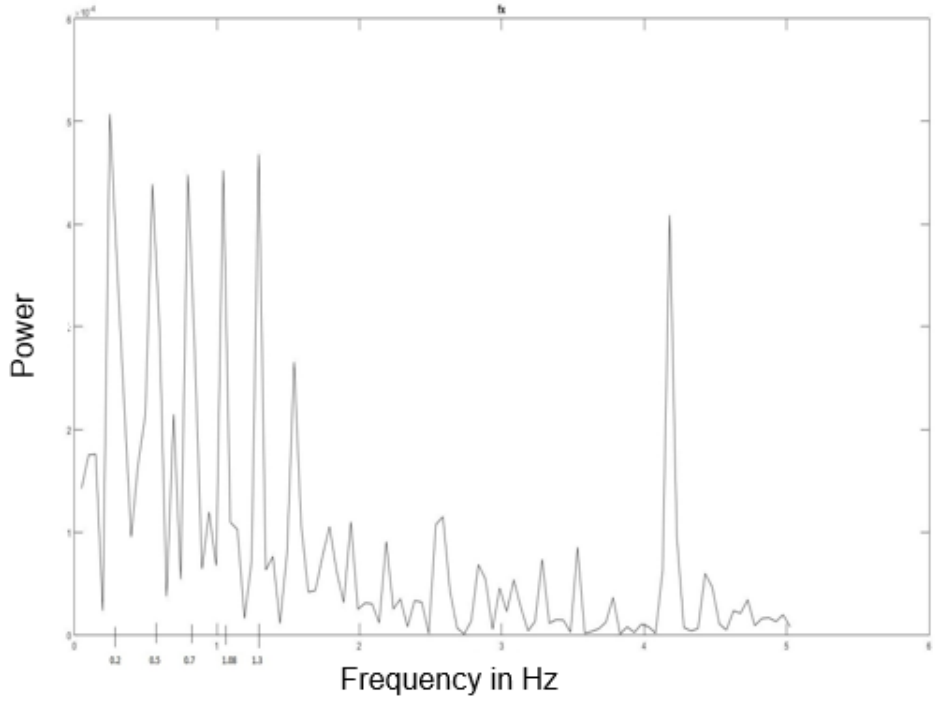

Graph 26: Natural Frequency-Fx1[102]

[102] Authors own resource.

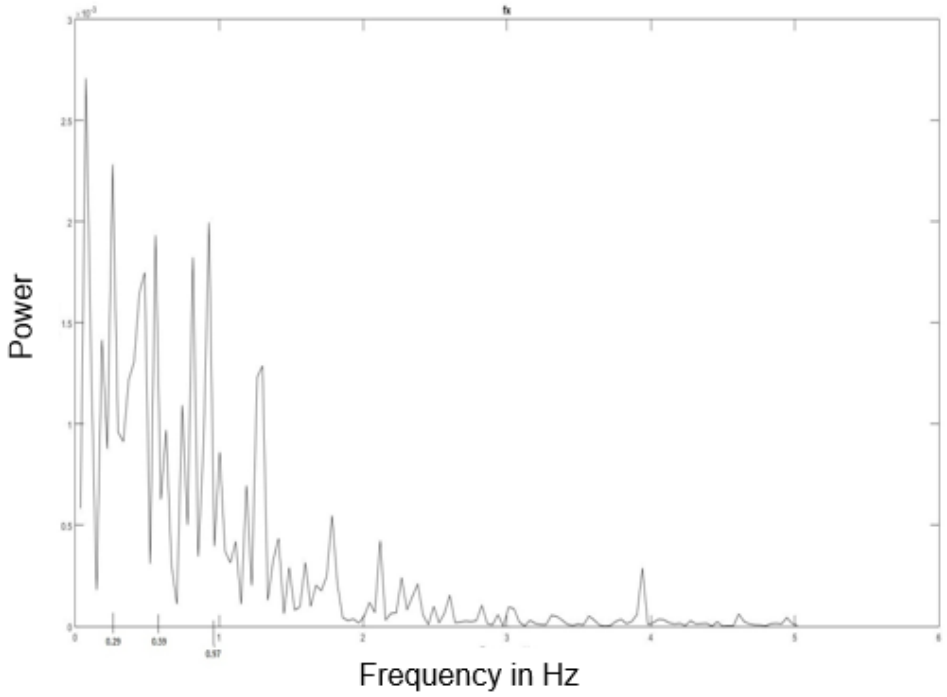

Graph 27: Natural Frequency-Fx2[103]

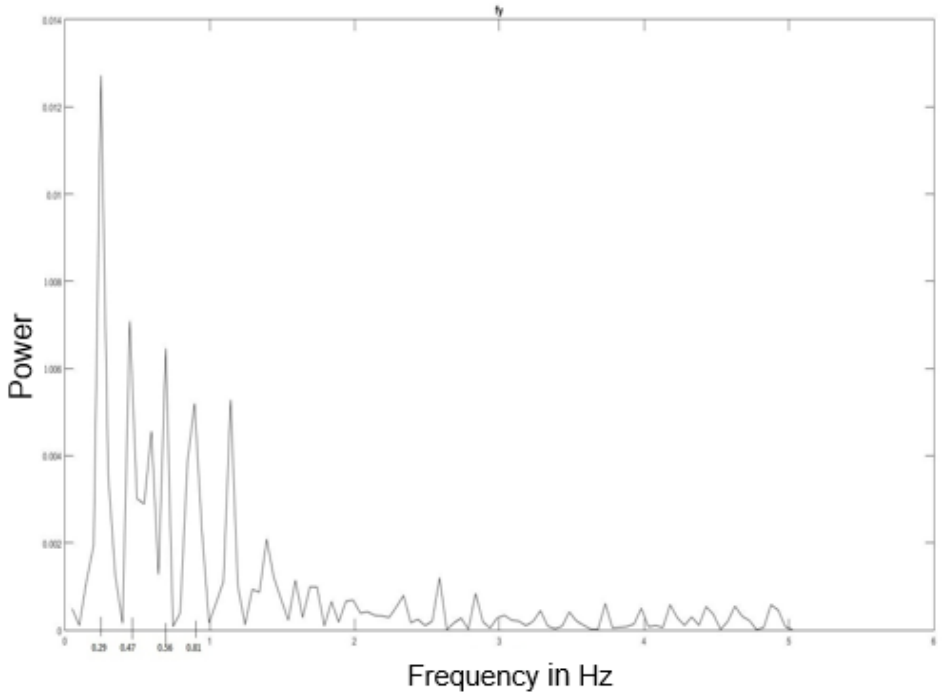

Graph 28: Natural Frequency-Fy1[104]

[103] Authors own resource.
[104] Authors own resource.

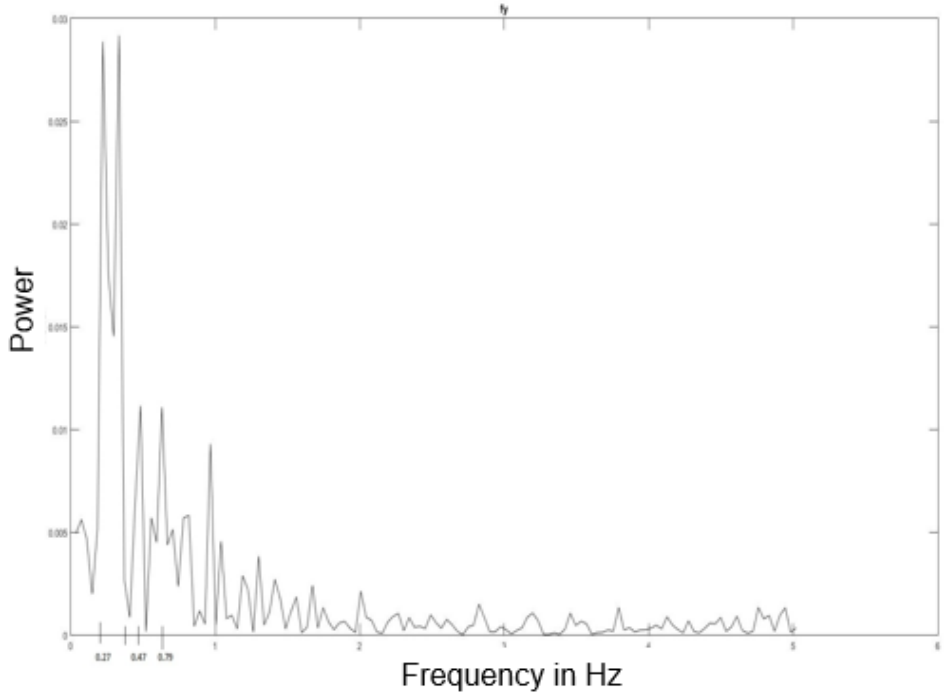

Graph 29: Natural Frequency-Fy2[105]

The Natural frequency spectrum is derived to investigate the natural frequency of the wing which helps in eliminating it from the other frequency signals for a clear result. The X axis force spectrum shows a signal at 0.2 Hz and 0.5 Hz in both the experiments showing a consistency in natural frequency of the wing. The Y axis force spectrum also shows a strong signal at 0.2 Hz and 0.7 Hz in both the experiments showing its consistency.

[105] Authors own resource.

Force spectrum in Vertical axis at flapping angle 60°, torsion angle 60° and flapping frequency -0.68 Hz

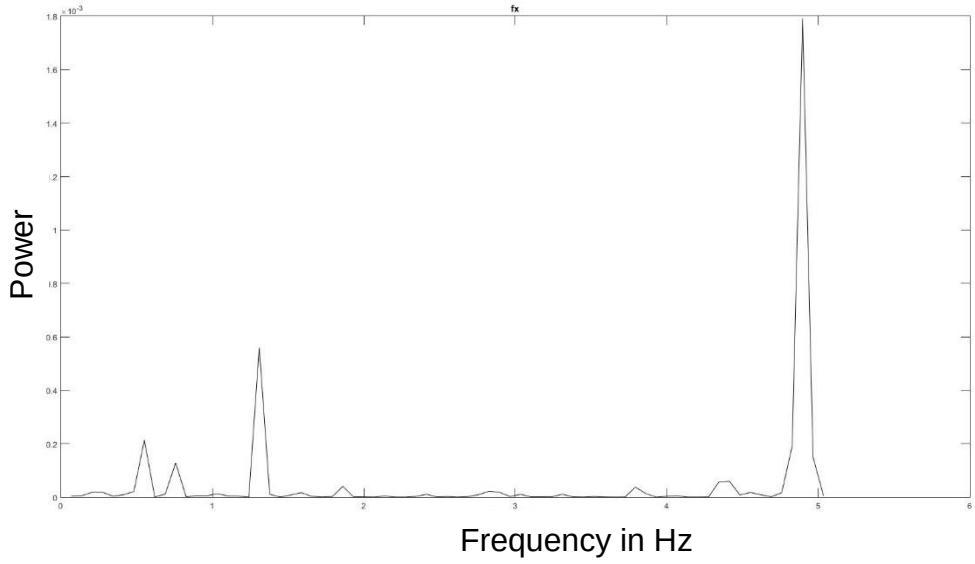

Graph 30: Test 1 Fx[106]

[106] Authors own resource.

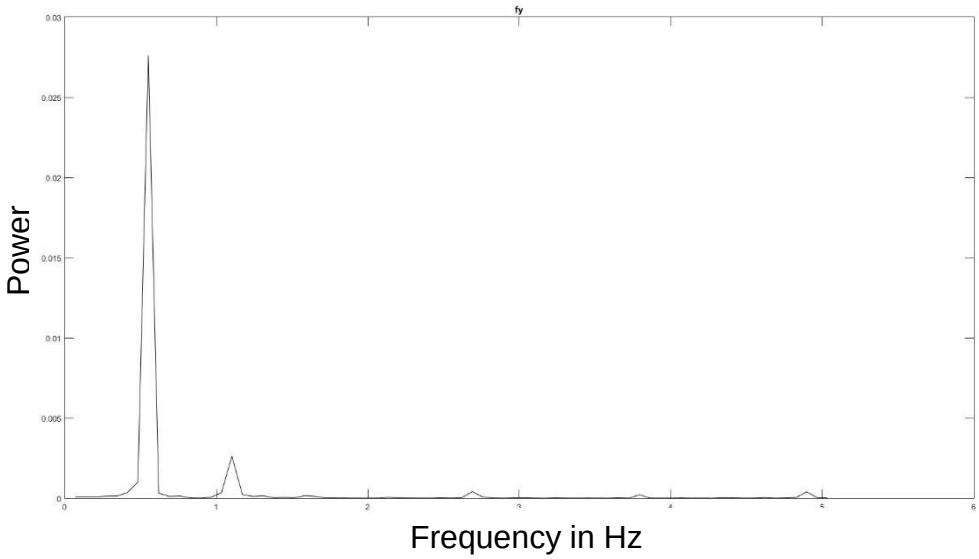

Graph 31: Test 1 Fy[107]

Tests 1 show a spectrum of 0.68 Hz flapping with flapping angle of 60°, torsion angle 60°. It depicts a high signal of much power than any of the peak in the frequency spectrum at 4.9 Hz - 0.6 Hz which indicates that vertical and horizontal forces are being generated during the flapping. The high power signal is observed at the flapping frequency of 0.6 Hz which is equal to a frequency of 0.68 Hz

[107] Authors own resource.

Force spectrum in Vertical axis at flapping angle 90°, torsion angle 60° and frequency of 0.68 Hz

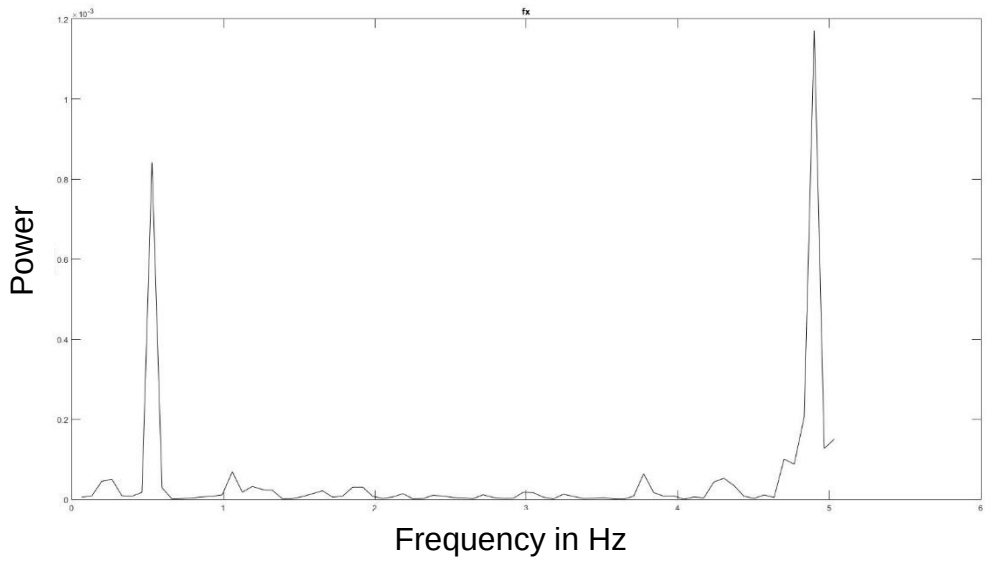

Graph 32: Test 2 Fx[108]

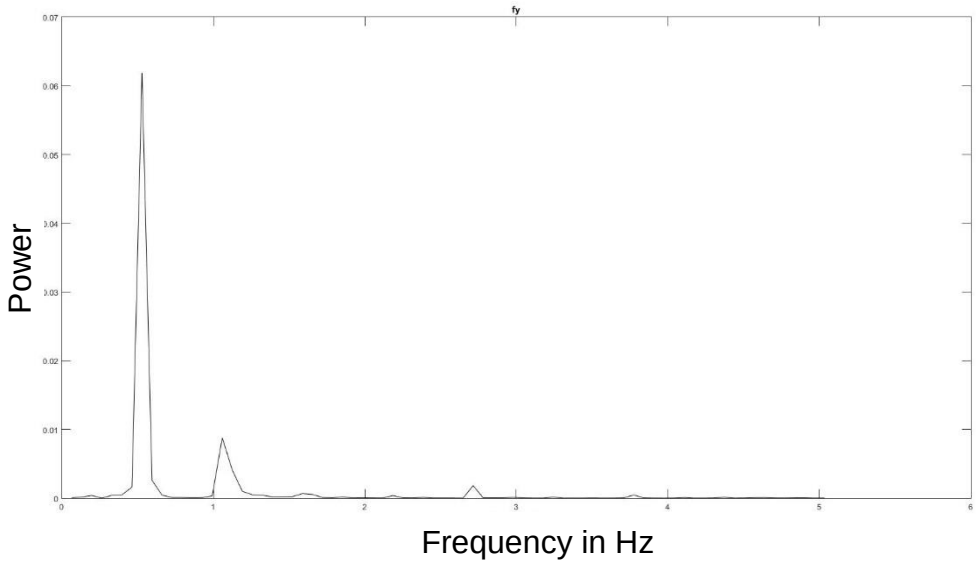

Graph 33: Test 2 Fy

[108] Authors own resource.

Tests 2 show a spectrum of 0.68 Hz frequency flapping with flapping angle of 90°, torsion angle 60°. It depicts a high signal of much power than any of the peak in the frequency spectrum at 0.5 Hz - 0.5 Hz which indicates that vertical and horizontal forces are being generated during the flapping. Similar to the previous experiment the high peak signals are also observed at the flapping frequency.

Force spectrum in Vertical axis at flapping angle 60°, torsion angle 60° and frequency of 0.3 Hz

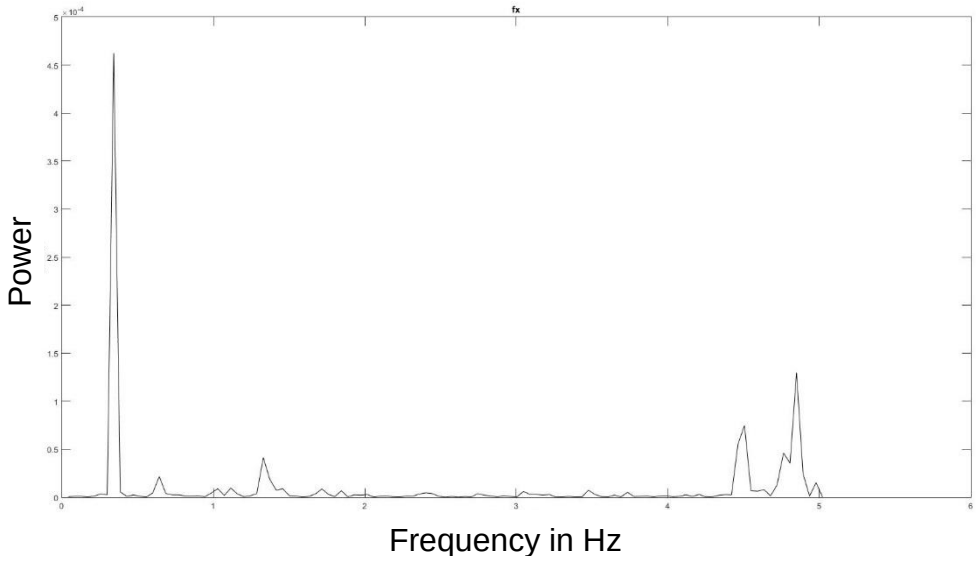

Graph 34: Test 3 Fx[109]

[109] Authors own resource.

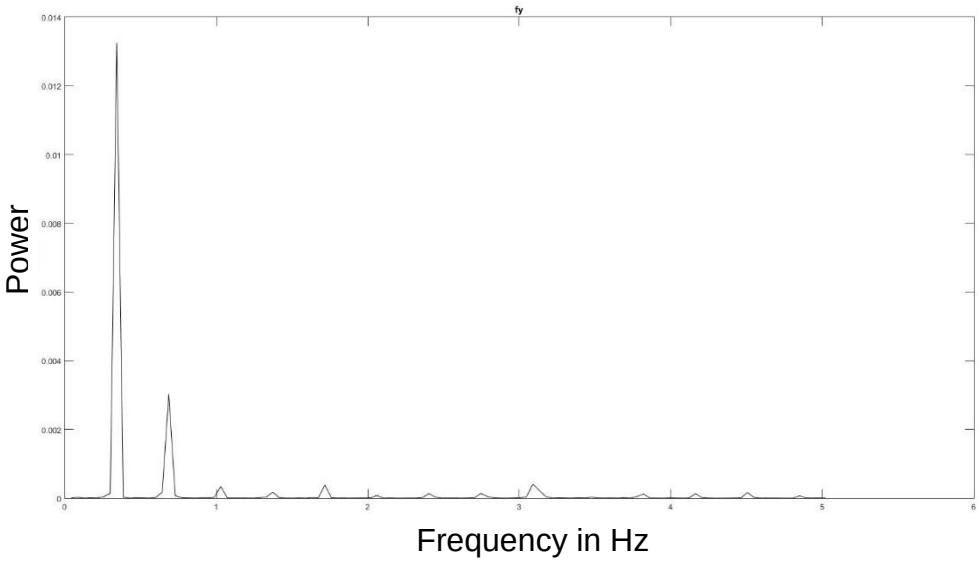

Graph 35: Test 3 Fy[110]

Tests 3 show a spectrum of 0.3 Hz frequency flapping with flapping angle of 60°, torsion angle 60°. It depicts a high signal of much power than any of the peak in the frequency spectrum at 0.3 Hz -0.29 Hz which indicates that vertical and horizontal forces are being generated during the flapping. High power signals are observed in the spectrum at the desired flapping frequency.

[110]Authors own resource.

Force spectrum in Vertical axis at flapping angle 90°, torsion angle 60° and frequency of 0.3 Hz

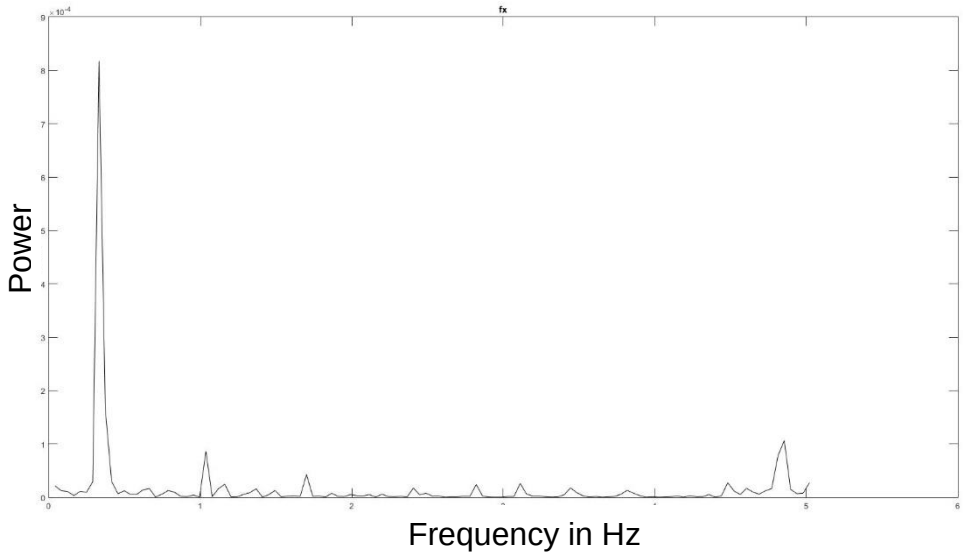

Graph 36: Test 4 Fx[111]

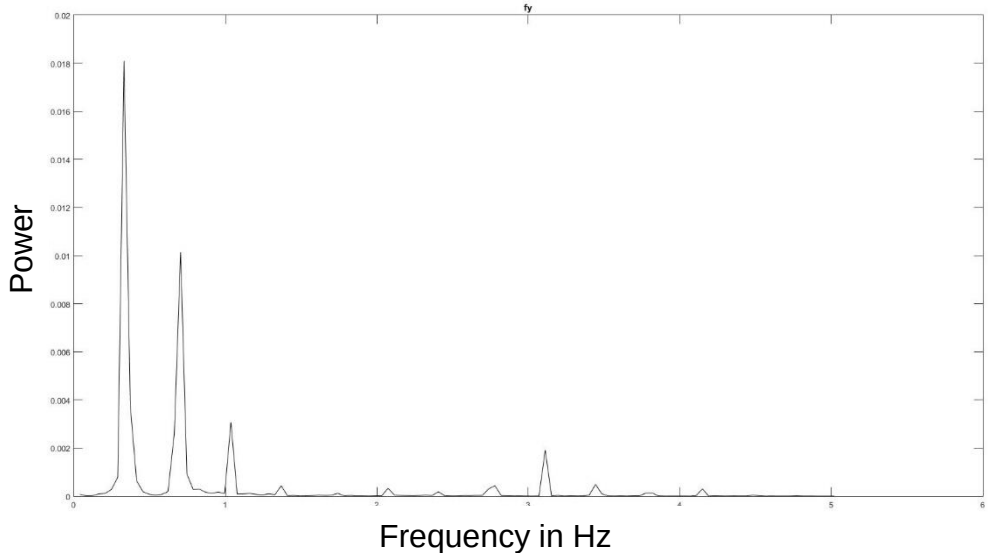

Graph 37: Test 4 Fy[112]

[111] Authors own resource.
[112] Authors own resource.

Tests 4 show a spectrum of 0.3 Hz frequency flapping with flapping angle of 90°, torsion angle 60°. It depicts a high signal of much power than any of the peak in the frequency spectrum at 0.28 Hz -0.3 Hz which indicates that vertical and horizontal forces are being generated during the flapping.

3.3.5 High speed video analysis of flapping wing

The flapping motion is captured using a high speed video camera for a better understanding of the flex, twist and bending of the wing during a single flapping stroke. The setup consists of a *Photron*® high speed camera, to which a Canon® lens is attached for a better aperture. Two high focus led lights are arranged to focus in a conical pattern for a better lighting and to eliminate multiple shadows, created behind the wing. Behind the wing two scales are fixed onto a wall right angle to each other which help in determining the deflection during the flapping.

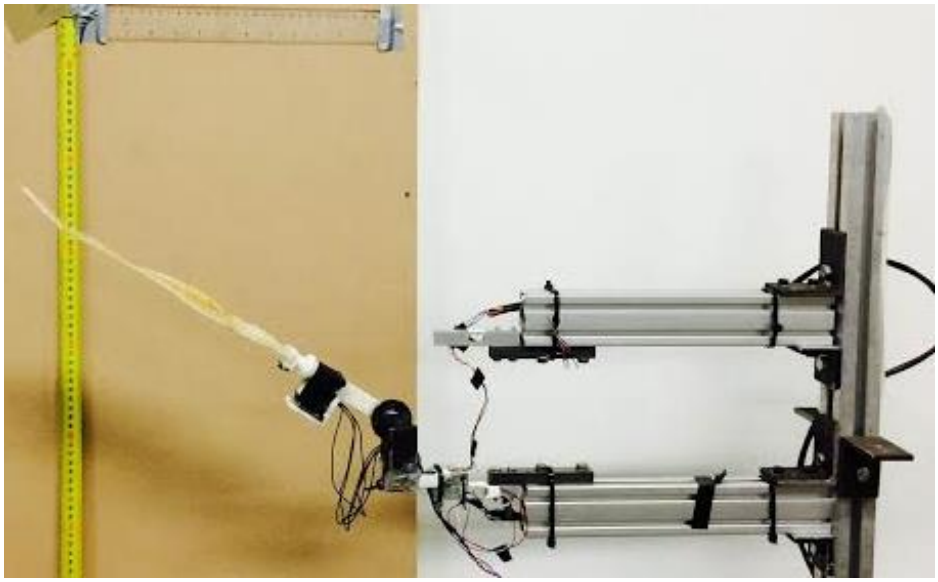

Figure 44: High speed video setup[113]

[113] Authors own resource.

The high speed video is taken for five continuous strokes and is analysed using the *Photron* fast cam Viewer (PFV). Figure 45 shows the default wing tip position of straight hovering flapping pattern with zero torsion angle at the bottom of the flapping stroke. The value is determined by calculating as pixels between two points for a corresponding distance of one millimetre and the position value is 52.03mm.

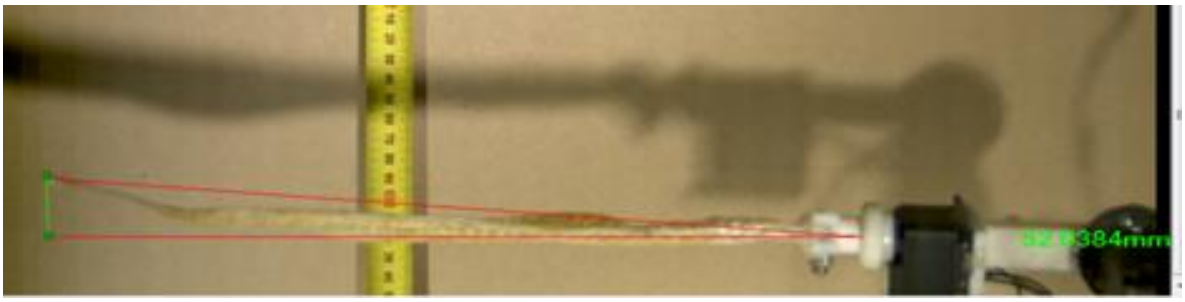

Figure 45: Default position of the wing tip at bottom stroke[114]

In the below figure 46 the wing tip deflection due to its flex is determined as 62.00mm. By reverse engineering method, the forces acting on the wing tip to deflect it by 10mm is calculated as 0.03N from the previously determined bending stiffness experimental values. The similar procedure is followed to calculate the wing tip deflection at the top end of the stroke and the force acting on the wingtip is identified as 0.02N. No significant twist is observed in the wing during this flapping pattern, hence the change in camber is estimated to be zero.

[114] Authors own resource.

Figure 46: Deflected position of the wing tip[115]

3.4 Numerical analysis

Due to the scaling of the dragon fly wing all the static and dynamic properties of the wing change. The changes in the properties need to be either derived or calculated as per the scaling factor. The unknown forces and parameters are also calculated in this process. This chapter explains how these objectives are achieved.

3.4.1 Advance ratio

Advance ratio in aeronautics is defined as the advancement or the distance travelled by the tip of the propeller for one complete rotation of it. Whereas in case of the flapping flight it is defined as the distance travelled by the wingtip for one complete flap of the wing.

$$\text{Advance Ratio (J)} = \frac{V_{cruise}}{2\,\emptyset n R}$$

While studying the model wing for its flapping or aerodynamic properties it is a primary objective to preserve the Reynolds number (R_e) constant irrespective of any changes that are to be made on the other parameters.

[115] Authors own resource.

Real wing:

Vertical tip speed = v * t = $(\frac{b}{2} * 2\ sin\emptyset * 2f)$= 3.6 m/s

Advance ratio =$\frac{V}{V_t} = 0.54$

Model wing:

Vertical tip speed = v * t = $(\frac{b}{2} * 2\ sin\emptyset * 2f)$= 0.825 m/s

Advance ratio = $\frac{V}{V_t} = 2.42$

3.4.2 Relation between the advance ratios of two wings

The advance ratio for the model wing and the real wing are equated to obtain the relation between them keeping the Reynolds number constant.

Advance ratio of the real wing$(J_{fly}) = \frac{V_{cruise}}{2\ \emptyset\ n_{fly} R_{fly}}$

Advance ratio of the Model Wing$(J_{model}) = \frac{V_{tunnel}}{2\ \emptyset\ n_{model} R_{model}}$

$$\frac{(J_{fly})}{(J_{model})} = \frac{\frac{V_{cruise}}{2\ \emptyset\ n_{fly}\ R_{fly}}}{\frac{V_{tunnel}}{2\ \emptyset\ n_{model}\ R_{model}}}$$

When the flapping amplitude (Ø) is kept constant the following relations are obtained:

Based upon the scaling ratio 1: 4.48, the span length $R_{model} = (4.48)R_{fly}$

$$V_{tunnel} = \frac{1}{4.48} V_{fly}$$

$$\frac{(J_{fly})}{(J_{model})} = \frac{V_{cruise}}{V_{tunnel}} * \frac{n_{model}}{n_{fly}} * \frac{R_{model}}{R_{fly}}$$

$$=4.48 * \frac{n_{model}}{n_{fly}} * 4.48$$

$$n_{fly} = 20 * n_{model} \qquad (n_{fly} = 32.3Hz)$$

$$n_{model} = 1.6Hz$$

While determining the relation between the advance ratios of the real wing and the model wing, the flapping frequency of the 3D model wing is determined as 1.6Hz.

3.4.3 Length and frequency calculation

By equating the Reynolds number formulae for both of the wings, a relation between the velocities is obtained from which the flapping frequency of the model wing is obtained.

Reynolds number of the real wing $R_{e_{fly}} = \frac{V L_{fly}}{\mu}$

Reynolds number of the model wing $R_{e_{model}} = \frac{V_{tunnel} L_{model}}{\mu}$

$$\frac{R_{e_{fly}}}{R_{e_{model}}} = \frac{\frac{V\ L_{fly}}{\mu}}{\frac{V_{tunnel}\ L_{model}}{\mu}}$$

$$\frac{L_{span_{model}}}{L_{span_{fly}}} = \frac{4.48}{1}$$

$$V_{cruise} * L_{fly} = V_{tunnel} * L_{model}$$

$$V_{tunnel} = \frac{1}{4.48} V_{fly}$$

$$V_{tunnel} = \frac{1}{4.48} V_{fly}$$

$$\frac{(J_{fly})}{(J_{model})} = \frac{V_{cruise}}{V_{tunnel}} * \frac{n_{model}}{n_{fly}} * \frac{R_{model}}{R_{fly}}$$

$$=4.48 * \frac{n_{model}}{n_{fly}} * 4.48$$

$$n_{fly} = 20 * n_{model} \qquad (n_{fly} = 32.3Hz)$$

$$n_{model} = 1.6Hz$$

3.4.4 Tabulation

The following tabulation gives the brief picture of all the forces, parameters for unknown and determined values for the real and model wing.

Forces &Parameters	Formulae Real wing	Formulae Model wing	Values Real wing	Values Model wing
Young's Modulus	$\frac{F\ L}{A\ \Delta L}$	$\frac{F\ L}{A\ \Delta L}$	1 GPA	0.5GPA
Reynolds number	$R_{e=\frac{U\ L}{\mu}}$	$R_{e=\frac{U\ L}{\mu}}$	3000-6000	3000-6000
Flapping Frequency	F_{fly}	F_{model}	32.3Hz	1.61Hz
Velocity	V_{fly}	V_{tunnel}	2 m/s	0.44m/s

Wing Density	ρ_{fly}	ρ_{model}	1.2 gm/cm^3	1.04gm/ cm^3
Flapping Amplitude	$\emptyset_{fly}$	$\emptyset_{model}$	100°	100°
Angular Frequency	w_{fly}	w_{model}	203 rad/s	10.15 rad/s
Mass	m_{fly}	m_{model}	3.4mg	264 mg
Advance Ratio	$(J_{fly}) = \frac{V_{cruise}}{2\,\emptyset\, n_{fly}\, R_{fly}}$	$(J_{model}) = \frac{V_{tunnel}}{2\,\emptyset\, n_{model}\, R_{model}}$	0@hovering 0.54	2.42
Linear Acceleration	$\frac{b}{2}(-w^2\theta_a \sin \omega t)$	4.48* $\frac{b}{2}(-\frac{1}{20}w^2\theta_a \sin \frac{\omega}{20}t)$	$2* 10^{-3}\ m/s^2$	$36* 10^{-3}\ m/s^2$
D'Alemberts Force	$(\rho\, V) *$ $\frac{b}{2}(-w^2\theta_a \sin \omega t)$	$(\rho\, V)$ *4.48* $\frac{b}{2}(-\frac{1}{20}w^2\theta_a \sin \frac{\omega}{20}t)$	$6.8* 10^{-6}$N	$9.5* 10^{-3}$N

Table 13: Forces and parameters for unknown and determined values for the real and model wing[116]

The D'Alemberts forces are calculated to verify its influence during the flapping motion. From the derived results it clearly shows that its effect it negligible and it is not considered in the calculation of the forces during flapping.

[116] Authors own resource.

4 Results and conclusions

Based on the experimental results determined using the developed synthetic 3D wing the following conclusions are drawn. The bending stiffness experiment gave the average value of the deflection range as 3mm-10mm. This range value is assumed to change for a sample wing that can constructed from the flexible PVC.

Whereas the torsional stiffness experimental results match the literature value range and it also depicts that the clockwise deflection is more than the anti-clockwise deflection. This supports the theory that the wing has a greater positive change in AOA than the negative change during the flapping flight.

The force graphs clearly depict that the lift force generated during the flapping experiment maintaining a phase difference of 180° between flapping angle and torsion angle is 0.4N at the maximum, whereas when the phase difference is changed to 90° and 270° the lift is raised up to 0.6N. C_L is maximum when the phase difference between the flapping angle and the torsion angle is maintained as 270°and is reducing for lower phase differences of 90° and 0°. Another conclusion can be drawn that, of the phases tested, a phase difference 270° gives the highest lift generated.

The forces like lift and drag for the single wing which are determined during this research is an initial step, resultant forces of all the four wings help in determining

the total forces produced during fight of a dragonfly which can be a contribution to the further research in developing a flapping UAV replicating dragonfly flight.

The most significant conclusion that can be drawn from this research is that this process of developing a 3D model for complex biological structures which are beyond the limitations of the current technologies like 3D scanning. For a reflective surface like a dragonfly wing the 3D scanners are ineffective to reproduce the model with a high detail. Although there is an alternative approach to the 3D model development using the Magnetic Resonance Imaging (MRI) scans, it still holds back due to the high costs that imply on each scan. This process is cost efficient and it also outputs a high detail which can be a major contribution for the future researchers in developing the 3D biological structures and replicating the nature.

5 Future research

The initial step of developing a dragonfly 3D wing opened a wide scope for the research of which a single fore wing is developed and tested. The next step is to develop the remaining wings and construct it using low density polyethylene to calculating the resultant forces of all the four wings. The four wings can be programmed as per the phase difference with the required frequency and the flapping motion can be tested in a wind tunnel using smoke to determine the flow over the wings. The flow analysis helps in understanding the interaction of the wing surface with the air moving over it which can be a contribution to the existing debate of flapping flight efficiency over non flapping flight. A prototype model can be constructed which might be a progressive step in development of flapping UAV's.

6 Bibliography

Carpenter, Frank M. (1947): Early insect life.

Chen, Mao Wei, Yan Lai Zhang, and Mao Sun (2013): Wing and body motion and aerodynamic and leg forces during take-off in droneflies.

Kesel, Antonia B. (2000): Aerodynamic characteristics of dragonfly wing sections compared with technical aerofoils.

Kreuz, P., W. Arnold, and A. B. Kesel. (2001): Acoustic microscopic analysis of the biological structure of insect wing membranes with emphasis on their waxy surface.

Magnan, A. (1934): La Locomotion chez les Animaux. I. Le Vol des Insectes. Paris: Hermann et Cie.

Norberg, R. Åke (1975): Hovering flight of the dragonfly Aeschnajuncea L., kinematics and aerodynamics. Swimming and flying in nature.

Rüppell, G. (1989): Kinematic analysis of symmetrical flight manoeuvres of Odonata.

Silsby, Jill. (2001): Dragonflies of the World.

Song, F., et al. (2007): Microstructure and nanomechanical properties of the wing membrane of dragonfly.

Wakeling, J. M., and C. P. Ellington. (1997): Dragonfly flight. II. Velocities, accelerations and kinematics of flapping flight.

Yahya 2002: 17, 20.

Internet sources

http://3dprintingindustry.com/3d-printing-basics-free-beginners-guide/processes.

http://www.ansys.stuba.sk/html/guide_55../graphics/GADV26.gif.

http://bioweb.uwlax.edu/bio203/s2007/cocchiol_matt/Anisoptera.htm.

http://www.delfly.nl/images/delfly12.jpg.

http://www.doitpoms.ac.uk/tlplib/beam_bending/twisting.php.

http://www.doitpoms.ac.uk/tlplib/thermal-expansion/images/cantilever.gif.http://scienceblogs.com/bioephemera/wp-content/blogs.dir/263/files/2012/04/i-182a4868c656367ae4778c96019c1424-Paulson1.jpg.

http://www.geometh.ethz.ch/uav_g/proceedings/hudzietz_presentation.

http://www.mat.uc.pt/~gil/downloads/IntroPhoto.pdf

http://www.meshmixer.com/.

https://techject.com/wp-content/uploads/2013/11/Picture11.png.

http://www.technologystudent.com/equip1/vacform1.htm.

http://theflightofbirdsandinsects.weebly.com/uploads/3/0/6/6/30665567/7329723_orig.png.

https://upload.wikimedia.org/wikipedia/commons/2/26/Meganeura_fossil_1.JPG

http://web.stratasys.com/APJ-ANZ-PPC-2015_PPC_ANZ_3DABC_WP_LP_v2.html?cid=70113000002F3w6&utm_ad=3D+Printer&utm_source=google&utm_term=3d%20printer&utm_campaign=AU+-+Search+-+3D&utm_medium=cpc&utm_content=sUUQbwN8X_dc|pcrid|90915388441|pkw|3d%20printer|pmt|p|.

http://www.wisegeek.com/what-is-beam-stiffness.htm.

Appendix

Appendix 1:

```
#include <Herkulex.h>

int n=1,m=2;
int x,xsine,ysine;
//motor ID - verify your ID !!!!

void setup()
{
  delay(2000);  //a delay to have time for serial monitor opening
  Serial.begin(115200);    // Open serial communications
  Serial.println("Begin");
  Herkulex.begin(57600,10,11); //open serial with rx=10 and tx=11
  Herkulex.reboot(n); //reboot first motor
  Herkulex.begin(57600,10,11); //open serial with rx=10 and tx=11
  Herkulex.reboot(m); //reboot second motor
  delay(500);
  Herkulex.initialize(); //initialize motors
  delay(200);
  x=0;
  x=x+(0.628);
  xsine=sin(x)*360;
  ysine=sin(x+3.14)*360;
}


void loop(){
  Serial.println("Move Angle: -100 degrees");
  Herkulex.moveOneAngle(n,xsine, 1000, LED_BLUE); //move motor with 300 speed
  Herkulex.moveOneAngle(m,ysine, 1000, LED_BLUE); //move motor with 300 speed
  delay(800);
  Serial.print("Get servo Angle:");
  Serial.println(Herkulex.getAngle(n));
  Serial.print("Get servo Angle:");
  Serial.println(Herkulex.getAngle(m));
```

Figure 47: Servo motors flapping program in Arduino[117]

[117] Authors own resource.